UNIVERSITY OF CALIFORNIA

SANTA CRUZ

MOLECULAR DYNAMICS SIMULATIONS OF CHARGE-TRANSFER REACTIONS AND SPECTRA AT LIQUID INTERFACES

A dissertation submitted in partial satisfaction
of the requirements for the degree of

DOCTOR OF PHILOSOPHY

in

CHEMISTRY

by

Katherine Vanessa Nelson

September 2013

The Dissertation of
Katherine Vanessa Nelson is approved:

Professor Ilan Benjamin, Chair

Professor Jin Zhang

Associate Professor Yat Li

Tyrus Miller
Vice Provost and Dean of Graduate Studies

Contents

List of Figures

Abstract

MOLECULAR DYNAMICS SIMULATIONS OF CHARGE-TRANSFER REACTIONS AND SPECTRA AT LIQUID INTERFACES

by

Katherine Vanessa Nelson

Using a recently developed empirical valence bond model for the nucleophilic substitution reaction S_N2 in solution, we examine microhydration effects on the benchmark $Cl^- + CH_3Cl \longrightarrow CH_3Cl + Cl^-$ reaction in liquid chloroform. Specifically, the effect of the hydration of the reactive system by one-to-five water molecules on the reaction free-energy profile and the rate constant is examined. We find that the activation free energy is highly sensitive to the number of water molecules hydrating the nucleophile, increasing the barrier by about 4 kcal/mol by the first water molecule. With five water molecules, the barrier height is 10 kcal/mol larger than the barrier in bulk chloroform and only 3 kcal/mol below the barrier in bulk water. A number of properties vary monotonically with the number of water molecules, including the rate of change in the system's electronic structure and the solvent stabilization of the transition state. These and other properties are a rapidly varying function of the reaction coordinate. Deviation from transition

state theory due to barrier recrossing is not large and falls between the behavior in bulk water and bulk chloroform

Using the same empirical valence bond (EVB) model for the nucleophilic substitution reaction (S_N2) in solution, we study the benchmark $Cl^- + CH_3Cl \longrightarrow CH_3Cl + Cl^-$ reaction at the water–chloroform liquid–liquid interface. The reaction free-energy profile is determined as a function of the reagents' location relative to the interface. We find that the activation free energy is very sensitive to the reagents' location and to the orientation of the nucleophilic attack. The barrier height at the interface is equal or slightly larger than the barrier in bulk water and approaches the value in bulk chloroform only when the solute is a few nanometers deep into the organic phase. We show that this is due to the ability of the nucleophile to keep part of its hydration shell. This suggests that for the catalytic effect of the nonpolar solvent to be appreciable, the nucleophile must be transferred away from the interface. The dynamical correction to the rate, the variation in the system's electronic structure and other system properties as a function of the location with respect to the interface, provide additional insight into the system's behavior.

The benchmark nucleophilic substitution reaction $Cl^- + CH_3Cl \longrightarrow CH_3Cl + Cl^-$ in water clusters of different sizes is studied using the previously developed empirical valence bond model. The reaction activation-free energy, the variation in the system's electronic structure and other system properties are determined as a

function of cluster size from 3 to 40 water molecules. The barrier height increases monotonically with the number of water molecules and reaches 90% of the value in bulk water with about 15 water molecules. The contribution of the water is analyzed utilizing a solvent coordinate and its coupling to the electronic state of the solute. The dynamical correction to the rate due to barrier recrossing is small.

The effect of a tetramethylammonium cation phase transfer catalyst on the benchmark $Cl^- + CH_3Cl \longrightarrow CH_3Cl + Cl^-$ reaction at the water–chloroform liquid–liquid interface is investigated by a molecular dynamics-empirical valence bond (EVB) model. The effect of the catalyst on the reaction free-energy profile at different interface locations and in bulk chloroform is examined. We find that, because of significant water pollution, activation of the nucleophilic attack is limited to the bulk organic region. The barrier height at the interface is equal to or slightly larger than the barrier in bulk water and is unaffected by the presence of the catalyst. In bulk chloroform, our calculations suggest that the barrier height, which is much lower than in bulk water, moderately increases when a few water molecules interact with the system and when the catalyst forms an ion pair with the nucleophile. Thus, the catalyst is most effective if its role is limited to bringing the nucleophile to the bulk organic phase.

Molecular dynamics calculations of the benchmark nucleophilic substitution reaction (S_N2) $Cl^- + CH_3Cl \longrightarrow CH_3Cl + Cl^-$ are carried out at the water liquid–vapor interface. The reaction free-energy profile and the activation free energy

are determined as a function of the reactants' location normal to the surface. The activation free energy remains almost constant relative to that in bulk water, despite the fact that the barrier is expected to significantly decrease as the reaction is carried out near the vapor phase. We show that this is due to the combined effects of a clustering of water molecules around the nucleophile and a relatively weak hydration of the transition state.

In order to investigate the factors that contribute to the electronic absorption line shape of a chromophore adsorbed at the water liquid–vapor interface, molecular dynamics simulations of a series of dipolar solutes undergoing various electronic transitions at various locations along the interface normal are studied. For electronic transitions that involve a change in the permanent dipole moment of the solute, the transition from the bulk water to the liquid–vapor interface involves a spectral shift consistent with the lower polarity of the interface. The change in the spectral width relative to that in the bulk is determined by several factors, which, depending on the nature of the transition and the dipole moment of the initial state, can result in a narrowing or broadening of the spectrum. These factors include the location of the interface region (which directly correlates with local polarity), the heterogeneity of the local solvation shell, and the width of the surface region. The contribution of the heterogeneity of the local solvation shell can be determined by comparing surface water with bulk methanol, whose polarity is comparable to one of the surface regions.

Acknowledgments

I would like to thank my research advisor Ilan Benjamin for guiding and supporting my doctoral studies, and for providing me with a solid background in computational physical chemistry. I would also like to thank my other dissertation committee members, Jin Zhang and Yat Li, for providing me with insightful and essential feedback on my work.

I would also like to thank other University of California, Santa Cruz chemistry faculty, especially Glenn Millhauser for giving me my first undergraduate research position in his lab as well as providing me with a solid foundation in statistical mechanics. In addition, Gene Switkes has given me much of his time and advice over the years as well as a strong base in chemical thermodynamics, both of which are greatly appreciated.

I am grateful to my fellow UCSC graduate student Jason Cooper, of the Zhang Lab, for major contributions he made to my work.

Finally, I must express my appreciation to my friends and family for their support throughout the course of my chemistry studies.

The text of this dissertation includes the following previously published material:

- K. V. Nelson and I. Benjamin. Microhydration effects on a model S_N2 reaction in a nonpolar solvent. *J. Chem. Phys.*, 130:194502, 2009
- K. V. Nelson and I. Benjamin. A molecular dynamics–empirical valence bond study of an S_N2 reaction at the water/chloroform interface. *J. Phys. Chem. C*, 114:1154, 2010
- K. V. Nelson and I. Benjamin. A molecular dynamics/EVB study of an S_N2 reaction in water clusters. *Chem. Phys. Lett.*, 492:220, 2010
- K. V. Nelson and I. Benjamin. Effect of a phase transfer catalyst on the dynamics of an S_N2 reaction. A molecular dynamics study. *J. Phys. Chem. C*, 115:2290, 2011
- K. V. Nelson and I. Benjamin. A model S_N2 reaction 'on water' does not show rate enhancement. *Chem. Phys. Lett.*, 508:59, 2011
- K. V. Nelson and I. Benjamin. Electronic absorption line shapes at the water liquid/vapor interface. *J. Phys. Chem. B*, 116:4286, 2012

Introduction

Many important chemical processes occur at the interface between a liquid and a second phase. As such, it is important to understand the influence of the interface region on the behavior of solute molecules and their chemical reactivity. The interface is a highly inhomogeneous environment, with a number of properties that differ significantly from those in bulk liquid as well as those of the gas phase. These unique solvent properties include asymmetry of intermolecular forces, steep variation in the density and dielectric properties, dynamics of molecular orientation and reorientation, and surface roughness. Each of these affects the solvation thermodynamics, dynamics of relaxation and transport processes, and reaction free energy of solutes in the interface region.[14] This dissertation describes molecular dynamics simulations of both nucleophilic substitution reactions at a number of interfaces, and spectra of a model chromophore at the water–vapor interface.

Molecular dynamics simulations provide a method for testing theoretical models and investigating interfacial solvent–solute phenomena at the molecular level.

The detailed molecular structure of the interfacial region, particularly of the solvation complex, may be of crucial importance for a quantitative account of the solvent effects on reactions at interfaces. While some experimental techniques, particularly nonlinear optical spectroscopies (sum frequency generation and second harmonic generation),[143] are able to provide molecular-level information about the interface, the greatest contribution to theoretical understanding of interfacial phenomena at the molecular level has come from computer simulations.[15] We employ molecular dynamics simulations, including a fully-molecular solvent model, to determine the solvent effects on the reactivity of an interfacial second-order nucleophilic substitution reaction (S_N2) and on the line shape of the spectrum of a simple dipolar model chromophore.

The first five chapters of this dissertation describe simulations of the benchmark symmetric S_N2 reaction $Cl^- + CH_3Cl \longrightarrow CH_3Cl + Cl^-$ as modeled by the empirical valence bond-molecular dynamics approach. Valence bond methods advantageously use configurations described by wavefunctions which have easily-understood chemical meaning, describing the reactants' changing electronic structure along the reaction coordinate. The empirical valence bond method makes it possible to simplify the treatment of the reaction by using a reduced number of resonance structures to describe the reactive system (we employ a two-state model), while still accurately describing the potential surfaces. This is achieved by parameterizing the model such that it reproduces known experimental or *ab*

initio data.[7,140] The obvious distribution of charge in each state also simplifies the treatment of the electrostatic coupling between the classical solvent and the valence bond configurations. The interactions between the solvent and solute charge distributions strongly influence the energetics and dynamics of charge-transfer reactions.[21,60] These chapters build understanding of the solvent effects, specifically those of water molecules, on the S_N2 reaction in bulk chloroform "polluted" with a few water molecules, in water clusters, at the water liquid–vapor interface, and at the water–chloroform interface, first without and then with a phase transfer catalyst.

Chapter 1 describes the effect of hydration of the Cl^- nucleophile by one to five water molecules on several energetic, structural, and dynamical characteristics of the S_N2 reaction $Cl^- + CH_3Cl \longrightarrow CH_3Cl + Cl^-$ in the bulk phase of liquid chloroform ($CHCl_3$). This study also establishes the reaction barrier, rate, and structure of the activated complex for comparison with later studies which include a phase transfer catalyst. In Chapter 2, the reaction free-energy profile and several structural and dynamical characteristics of the same S_N2 reaction are examined at eight different locations relative to the water–chloroform interface. All calculations are also repeated with the interface constrained to be molecularly sharp in order to examine the influence of surface roughness[23] on the reactivity. In Chapter 3 the S_N2 reaction is simulated in small water clusters composed of from 3 to 40 water molecules. For each cluster, as before, we calculate the reaction free-energy profile

and several structural and dynamical characteristics of the reaction, quantifying the influence of the water molecules on the electronic state of the solute as a function of the reaction coordinate.

Chapter 4 provides a detailed examination of the reactivity and thermodynamics of the $Cl^- + CH_3Cl \longrightarrow CH_3Cl + Cl^-$ S_N2 reaction at the water–chloroform interface in the presence of a tetramethylammonium (TMA^+) phase transfer catalyst. This is the first theoretical investigation of whether the role of the catalyst is limited to transport of the nucleophile across the interface into the organic phase or whether the catalyst also affects the reaction thermodynamics. In addition, we investigate the effect of hydration by a small number of water molecules on the stability, structure, thermodynamics and dynamics of the TMA^+Cl^- ion pair by repeating these calculations in bulk chloroform with the TMA^+Cl^- hydrated by from one to five water molecules. In Chapter 5 the S_N2 reaction is examined "on water" at three locations normal to the free water surface. Certain classes of organic reactions have been observed to proceed more rapidly at the water–air interface than in bulk water (for example, Diels-Alder, Claisen rearrangements, and allylic amination of olefins).[96] This kinetic effect is investigated in the context of the symmetric S_N2 reaction and these calculations are compared with previously published bulk water calculations.[21]

Chapter 6 examines the electronic absorption spectral width of a series of differently-charged simple dipolar models of a chromophore which is adsorbed at

various locations of the water liquid–vapor interface. Previous bulk studies have shown that spectral line widths could provide information about the orientational and translational distribution and fluctuation of solvent molecules around the solute. This is the first systematic investigation of what extent the observed line width is due either to the local heterogeneity of the interface region, or to the fact that the observed spectrum is a sum of differently shifted spectra.

Chapter 1

Microhydration Effects on a Model S_N2 Reaction in a Nonpolar Solvent

1.1 Introduction

The strong dependence of the activation free energy of S_N2 reactions on the solvent is well known.[38,60,62,64,83,110,134,141] This dependence has been studied in recent years by examining this reaction in environments other than bulk liquids, such as in water clusters,[105,109,146] organic liquid clusters,[91] supercritical water,[9,10,25,49,108] enzymes,[106,134] and vesicles.[73] One issue which has been the subject of much interest is the effect of a small amount of water impurity on S_N2 reactions taking

place in nonpolar solvents, and specifically noteworthy is the observation that the hydration state of the anion strongly influences its nucleophilicity in *bulk nonpolar solvents*.[76,79] This is of particular interest to the field of phase transfer catalysis (PTC)[3,4,47,80,119,123,135] where a water soluble anionic nucleophile is transferred from the aqueous phase to the organic phase by a catalyst (e.g., tetrabutylammonium cation), and this may give rise to a cotransfer of one or more water molecules per nucleophile.

A few theoretical studies have noted the marked influence that a few water molecules have on the S_N2 barrier height in gas-phase clusters.[31,109,147] Several other quantum mechanical studies with a continuum solvent model have examined the effect of a few water molecules on the barrier height.[56,107] These and other studies have demonstrated the sensitivity of the barrier height to the degree of hydration. Yet, no *molecularly detailed* theoretical examination of the influence of the hydration state of the nucleophilic anion on the energetics and *dynamics* of S_N2 reactions in a nonpolar solvent is available.

In this chapter, we examine in detail several energetic, structural, and dynamical characteristics of the simple benchmark symmetric S_N2 reaction $Cl^- + CH_3Cl \longrightarrow CH_3Cl + Cl^-$ in chloroform, $CHCl_3$, where the anion Cl^- is hydrated by N_w water molecules, with $N_w = 1, 2, \ldots, 5$. The choice of $\max(N_w) = 5$ is motivated, in part, by the observation that up to five water molecules are believed to be cotransferred from water to different organic liquids used in PTC reactions.[135]

We utilize a recently developed empirical valence bond (EVB) model for the above reaction. In addition to the intrinsic interest in hydration effects of a few water molecules, we are also motivated by the need to establish the reaction barrier, the rate, and the structure of the activated complex in the bulk organic solvent under conditions where the PTC catalyst is not present. In particular, while experimentally measured rate constants are typically interpreted in terms of the number of water molecules coextracted with the anion (N_w), this number is not generally well known, and thus it would be important to determine the sensitivity of the activation energy to N_w. In subsequent publications, we will examine this reaction at the water–$CHCl_3$ interface with and without the presence of a catalyst.

This chapter is organized as follows: In Section 1.2, we briefly review the main features of the EVB model and the methodology used to compute the free energy and the dynamical corrections to the rate. In Section 1.3, the results of the reaction free energy profile, the structural, and the time-dependent calculations are described and discussed. A summary and conclusions are given in Section 1.4.

1.2 Systems and Methods

1.2.1 The EVB approach and potential energy functions

Our approach is similar to the EVB model first developed by Warshel and coworkers,[60,141] and it also includes some features from the one-dimensional continuum model of Mathis et al.[83] Our model was discussed in detail in an earlier publication,[21] and here we summarize its main ingredients. For other approaches, the reader is referred to Refs. 10, 25, 27, 29, 38, 42, 49, 50, 59, 64, 91, 106, 108, 109, 116.

Briefly, we use the simplest approach that contains the basic component of the changing electronic structure along the reaction coordinate. We assume that only two valence states, $\psi_1 = \mathrm{Cl{-}CH_3\ Cl:^-}$ and $\psi_2 = \mathrm{Cl:^-\ CH_3{-}Cl}$, contribute to the total wave function:

$$\Psi = c_1\psi_1 + c_2\psi_2 \tag{1.1}$$

where ψ_1 and ψ_2 are assumed orthonormal ($\langle\psi_1 \,|\, \psi_2\rangle = \delta_{ij}$). See the original article[21] for a discussion of the two-state approximation and the orthonormality assumption.

The total Hamiltonian is written as

$$\hat{H} = \begin{pmatrix} H_{11}(\vec{r}_i, \vec{r}_d, \vec{r}_s) & H_{12}(r_1, r_2, \theta) \\ H_{12}(r_1, r_2, \theta) & H_{22}(\vec{r}_i, \vec{r}_d, \vec{r}_s) \end{pmatrix}, \tag{1.2}$$

$$H_{11} = E_k + H^0_{11}(r_1, r_2, \theta) + U_{ss}(\vec{r}_s) + U_{si}(\vec{r}_s, \vec{r}_i) + U_{sd}(\vec{r}_s, \vec{r}_d), \tag{1.3}$$

where H_{11} is the diabatic Hamiltonian, which includes from left to right: E_k—the kinetic energy of all atoms, $H^0_{11}(r_1, r_2, \theta)$—the gas phase interaction between the Cl^- ion and the CH_3Cl molecule (in which the CH_3 is treated as a united atom), $U_{ss}(\vec{r}_s)$—the solvent potential energy, $U_{si}(\vec{r}_s, \vec{r}_i)$—the solvent–ion potential energy and $U_{sd}(\vec{r}_s, \vec{r}_d)$—the solvent–$CH_3Cl$ potential energy. In Eqs. 1.2 and 1.3, $\vec{r}_i$ is the vector position of the Cl^- ion, $\vec{r}_d$ is the vector positions of the CH_3Cl atoms and the vector $\vec{r}_s$ stands for the positions of all the solvent atoms. r_1 is the distance between the Cl^- ion and the carbon atom, r_2 is the C−Cl bond distance in CH_3Cl and θ is the $Cl^-\cdots$C−Cl angle. Due to the symmetric nature of the reaction, H_{22} has the same functional form, but with r_1 and r_2 interchanged.

For the gas-phase potential energy, we generalize to noncollinear geometries the form suggested by Mathis *et al.*:[83]

$$H^0_{11} = V_M(r_2) + V_i(r_1, \theta) + V_{id}(r_1, r_2, \theta) + V_{bend}(r_1, r_2, \theta) + \Delta_{11}. \tag{1.4}$$

In this expression,

$$V_M(r_2) = De^{-2a(r_2 - r_{eq})} - 2De^{-a(r_2 - r_{eq})} \tag{1.5}$$

is a Morse potential for the CH_3Cl bond, in which D, r_{eq}, and a are the bond dissociation energy, the bond equilibrium distance (in the isolated molecule), and the Morse parameter, respectively.

$$V_i(r_1, \theta) = Ze^{\rho(1+cos\theta)}e^{-2a(r_1 - r*)} - EA, \tag{1.6}$$

is the repulsion energy between the Cl^- ion and the CH_3 radical, in which a is the Morse parameter from Eq. 1.5, r is the sum of the covalent carbon and the ionic chlorine radii, EA is the absolute value of the electron affinity of Cl^-, ρ determines the rate of increase of the ion–radical repulsion as a function of the bending angle θ, and Z is determined from the electron affinity of the CH_3Cl molecule and the Cl atom.[83]

$$V_{id}(r_1, r_2, \theta) = b\epsilon \left[\left(\frac{\sigma}{r_1 + r_2} \right)^n - \left(\frac{\sigma}{r_1 + r_2} \right)^2 \right] e^{-\gamma(1+cos\theta)} \tag{1.7}$$

is the ion–dipole term, in which ϵ is the well depth and σ determines the minimum of the ion–dipole complex. They are obtained from the *ab initio* calculations of Tucker and Truhlar.[83,131] The parameters n and b are selected to give the best agreement with the *ab initio* transition state geometry. The exponential θ-dependent term causes the ion–dipole well depth to decrease for noncollinear geometries.

$$V_{bend}(r_1, r_2, \theta) = k_b e^{-\lambda(r_1+r_2)}(\theta - \pi)^2 \tag{1.8}$$

is a bending term with an effective bending force constant that diminishes as $r_1 + r_2$ increases. The parameters k_b and λ, as well as γ and ρ mentioned earlier, were determined by a best fit to the *ab initio* values of the energy and location of the transition state, and the ion–dipole well depth as a function of θ. The final term in Eq. 1.4, $\Delta_{11} = EA + D$, is a constant that sets the energy of the separate reactants to zero. All the parameters involved in the expression for H_{11}^0 are given

in Ref. 21. Additional details about the different terms appearing in H_{11}^0 can be found in Ref. 83.

$U_{ss}(\vec{r}_s), U_{si}(\vec{r}_s, \vec{r}_i)$, and $U_{sd}(\vec{r}_s, \vec{r}_d)$ are all represented by the usual sum of Lennard-Jones plus Coulomb interactions between every two sites on different solute and solvent molecules:

$$u_{ij} = 4\epsilon_{ij}\left[\left(\frac{\sigma_{ij}}{r_{ij}}\right)^{12} - \left(\frac{\sigma_{ij}}{r_{ij}}\right)^{6}\right] + \frac{q_i q_j}{4\pi\epsilon_0 r_{ij}}, \tag{1.9}$$

where i and j are two sites on two different molecules, r_{ij} is the distance between the sites and ϵ_0 is the universal constant (vacuum permittivity). The Lennard-Jones parameters σ_{ij} and ϵ_{ij} are determined from the parameters for the individual sites on the solvent atoms and the reacting system atoms by the usual combination rules:[54]

$$\sigma_{ij} = (\sigma_{ii} + \sigma_{jj})/2, \qquad \epsilon_{ij} = \sqrt{\epsilon_{ii}\epsilon_{jj}}. \tag{1.10}$$

The partial charges on the CH_3Cl were selected to reproduce its experimental dipole moment of 1.94 D.[85] These parameters, together with the Lennard-Jones parameters for the Cl^- ion and the CH_3Cl molecule, are given in Ref. 21. The Lennard-Jones parameters and the charges for the different sites on the chloroform molecule were selected to reproduce a number of solvent bulk properties and structure. In addition, the chloroform potential energy function includes intramolecular stretching and bending terms. The solvent's Lennard-Jones parameters, intramolecular potential terms, and the corresponding intramolecular pa-

rameters can be found elsewhere.[13] The water model was selected to be the model previously used to study the bulk and interfacial properties of water. Although a more appropriate choice would have been a model that better describes the properties of water clusters, we kept the bulk model since we anticipated comparing the results to the interfacial simulations. Another approach, which is reserved for future studies (and requires reparameterization of the solvent and solute potential parameters), is to employ a many-body potential that reasonably describes both the cluster and the bulk limits.[39,40]

The off-diagonal electronic coupling term H_{12} in Eq. 1.2 is the one suggested by Hynes and coworkers:[83,130]

$$H_{12} = -QS(r_1)S(r_2), \tag{1.11}$$

where $S(r)$ is the overlap integral for the sigma orbital formed from the carbon 2p and chlorine 3p atomic orbitals. $S(r)$ is determined[83] using Slater-type orbitals and the approximation of Mulliken et al.[93] These expressions can also be found in Ref. 21. $Q = 678.0$ kcal/mol is a parameter which is fitted to obtain the correct activation energy.

Diagonalization of Eq. 1.2 yields the electronic ground state adiabatic Hamiltonian as a function of all nuclear coordinates:

$$H_{ad} = \tfrac{1}{2}(H_{11} + H_{22}) - \tfrac{1}{2}[(H_{11} - H_{22})^2 + 4H_{12}^2]^{1/2}. \tag{1.12}$$

This Hamiltonian is used for the classical propagation of the system. The gas-phase adiabatic ground state potential energy is given by

$$U_{ad}^0 = \tfrac{1}{2}(H_{11}^0 + H_{22}^0) - \tfrac{1}{2}[(\Delta H^0)^2 + 4H_{12}^2]^{1/2}, \tag{1.13}$$

where

$$\Delta H^0 = H_{11}^0 - H_{22}^0 = V_M(r_2) + V_i(r_1, \theta) - V_M(r_1) - V_i(r_2, \theta), \tag{1.14}$$

and where we used the symmetry of the reaction to simplify the expression for ΔH^0.

The reaction coordinate is defined by

$$\xi = r_2 - r_1, \tag{1.15}$$

so the reactants and products correspond to $\xi \ll 0$ and $\xi \gg 0$, respectively. (They are, of course, identical for this symmetric reaction). The minimum energy path along ξ for the collinear geometry is shown as the dotted curve in Fig. 1. The transition state is located at $r_1 = r_2 = 2.19$ Å and has an energy of 2.74 kcal/mol above the energy of the separate reactants, and an activation energy of 13.72 kcal/mol above the ion–dipole minimum energy.

The total wave function is given by the solution for c_1 and c_2:

$$c_1^2 = \frac{1}{2 + \chi^2/2 + \chi(1 + \chi^2/4)^{1/2}}, \qquad c_2^2 = 1 - c_1^2, \tag{1.16}$$

where $\chi = \Delta H^0 / H_{12}$. At the transition state, $r_1 = r_2$, so $\chi = 0$ (in a vacuum) and $c_1^2 = c_2^2 = 1/2$. Since the coupling H_{12} falls off rapidly to zero as $|\xi|$ increases,

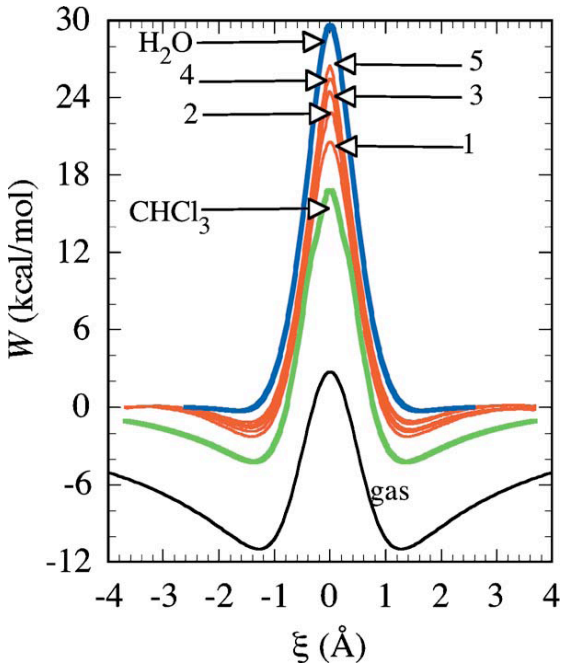

Figure 1.1: Reaction free energy along the reaction coordinate for $Cl^- + CH_3Cl \longrightarrow CH_3Cl + Cl^-$ in bulk chloroform, with the presence of one-to-five water molecules (lines labeled by the number of water molecules). Also shown are the reaction free energy in bulk water and bulk chloroform and the minimum energy path for the collinear geometry in the gas phase. The temperature is T=298 K.

$\chi \to \pm\infty$ and $c_1^2(\chi \to \infty) = 0, c_1^2(\chi \to -\infty) = 1$. Thus, as ξ varies from $-\infty$ to $+\infty$, the ground state varies from $\psi_2(c_1 = 0, c_2 = 1)$ to $\psi_1(c_1 = 1, c_2 = 0)$. In fact, the limiting values of 0 and 1 for c_1 and c_2 are reached for $|\xi|$ near 1 Å. In solution, Eq. 1.16 still holds, except that $\chi = (H_{11} - H_{22})/H_{12}$.

1.2.2 Reaction free energy profile

The reaction free energy profile along the reaction coordinate $\xi = r_2 - r_1$ is calculated using umbrella sampling with overlapping windows and a biasing potential[36]

according to

$$W(\xi) = -\beta^{-1} ln \frac{\int \delta(r_1 - r_2 - \xi) exp[-\beta(H_{ad} + U_b(\xi)] d\Gamma}{\int exp(-\beta H_{ad}) d\Gamma} - U_b(\xi), \qquad (1.17)$$

where $\beta = 1/kT$ with k being the Boltzmann constant, T is the temperature, and $U_b(\xi)$ is a biasing potential. This is an arbitrary analytic function approximating $-W(\xi)$ which is useful for accelerating the convergence of the ensemble average in Eq. 1.17. We chose for the biasing potential an approximate Gaussian fit of the transition state region of the free energy profile in bulk chloroform:[21]

$$U_b(\xi) = 20.6928 e^{-2.63322\xi^2} \quad \text{kcal/mol.} \qquad (1.18)$$

$W(\xi)$ is determined in the interval $[\xi_0, \xi_N]$ by dividing the interval into N overlapping subintervals, running the trajectories using the Hamiltonian $H_{ad} + U_b(\xi)$ and binning $r_2 - r_1$ in the subinterval j by constraining the system to be in the region $[\xi_{j-1}, \xi_j]$ using a window potential. The set of N overlapping $W_j(\xi)$ is "stitched" together by adding to $W_j(\xi)$ a constant C_j that minimizes the difference between the overlapping portion of $W_j(\xi)$ and $W_{j-1}(\xi)$. Using intervals of 0.5 Å width gave a good sampling of each interval, except near the transition state, where an additional 0.2 Å wide window was added. ξ_N is selected so that $W(|\xi_N|)$ reaches a plateau.

At each value of the reaction coordinate ξ, the solvent is at equilibrium with the solute electronic state (as determined by the charge distribution and the values of c_1 or c_2). One can approximately characterize any solvent configuration using

(by analogy to electron transfer simulations[71]) the "solvent coordinate" s by the solvent contribution to the energy gap $\Delta H = H_{11} - H_{22}$:

$$H_{11} - H_{22} = \Delta H^0 + s. \tag{1.19}$$

For future reference, we denote by $s_{eq}(\xi)$ the equilibrium value of s when the reaction coordinate is equal to ξ. By symmetry, if $\xi = 0$ we must have $s_{eq}(0) = 0$.

1.2.3 Reactive flux calculations

The activation free energy E_a obtained from the reaction free energy profile $W(\xi)$ can be used to compute the transition state theory (TST) approximation of the rate constant $k_{\mathrm{TST}} = Ae^{-\beta E_a}$, where A is the pre-exponential factor. The actual rate is reduced by the value of the transmission coefficient $\kappa < 1$, due to the fact that not every trajectory that reaches the transition state and heads toward the products ends as products. κ can be calculated using the reactive flux correlation function formalism.[28,52,142] Starting from the solute molecules constrained to the transition state ($\xi = 0$), random velocities are assigned from a flux-weighted Maxwell-Boltzmann distribution, and the constraint is released. The value of the reaction coordinate is followed for a long enough time for the solvent-induced recrossings of the transition state to cease and for the system to reach the stable reactant state. The normalized flux correlation function can be calculated using[52]

$$\kappa(t) = N_+^{-1} \sum_{i=1}^{N_+} \theta[\xi_i^+(t)] - N_-^{-1} \sum_{i=1}^{N_-} \theta[\xi_i^-(t)], \tag{1.20}$$

where $\xi_i^{\pm}$ is the value of the reaction coordinate for the ith trajectory at time t, given that at $t = 0, d\xi/dt$ was positive (negative), $N_+(N_-)$ is the corresponding number of trajectories, and θ is the unit step function.

1.2.4 Simulation details

We consider five different systems, obtained by inserting into a cavity at the center of a bulk chloroform box the reactive system constrained to the transition state, with $N_w = 1, 2, ..., 5$ water molecules. The configurations $[Cl^{\delta-}-CH_3-Cl^{\delta-}](H_2O)_{N_w}$ ($\delta \approx 0.5$) were selected from equilibrated transition state configurations in bulk water. The cavity was prepared by removing a number of chloroform molecules from a pure chloroform truncated octahedron box enclosed in a cube of size 38.68 $Å^3$ containing 215 molecules. The system was first equilibrated at a constant temperature (298 K) and pressure (1 atm), with the water and solute molecules frozen. Then all constraints, except for $\xi = 0$, (the system remains at the transition state) were removed and the system equilibrated for 1 ns, saving 100 independent configurations for the reactive flux correlation function dynamic calculations.

The reaction free energy calculations are done using windows that are each 0.5 Å wide and have a 0.2 Å overlap with the two neighboring windows. The number of windows is selected until the free energy profile reaches a plateau. Calculations are done for both the $\xi > 0$ and $\xi < 0$ regions, despite the symmetry of the reaction,

as an additional check for convergence. In each window, the total simulation time is 1 ns. This allows for a determination of the free energy profile, with a statistical error that is less than 0.2 kcal/mol.

A number of properties, including solvent–solute radial distribution functions, solvent coordinate equilibrium values, location of water molecules, and solute electronic structure (values of c_1^2) are dependent on the reaction coordinate. These are calculated by fixing the reaction coordinate at different values of ξ, starting from $\xi = 0$ and continuing with increments of 0.1 Å up to $\xi = 1$ Å. At larger values of ξ, the above properties vary much more slowly with ξ, so they are calculated at $\xi = 1.5$, 2.0 Å, etc. These calculations are done using a 1 ns trajectory at each value of ξ.

The reactive flux calculations are done by using the 100 equilibrated independent transition state configurations, saved earlier, to run 1000 constant-energy trajectories using ten different selections of flux-weighted initial velocities per configuration. Each trajectory is 0.2 ps long, which is long enough for $\kappa(t)$ to reach its plateau value.

The integration time step is 0.5 fs for all systems, using the velocity version of the Verlet algorithm.[5]

1.3 Results and Discussion

1.3.1 Reaction free energy profiles

The results of the umbrella sampling calculations of the free energy profile $W(\xi)$ for the $Cl^- + CH_3Cl \longrightarrow CH_3Cl + Cl^-$ reaction in bulk chloroform with $N_w = 1$, 2, ..., 5 are shown in Figure 1.1. As a comparison, the gas-phase potential energy along the minimum energy path and the free energy profiles in bulk chloroform and in bulk water are also shown. Due to the extended charge distribution of the reactant and product states compared to the less polar transition state, as the number of the water molecules increases, the reactants and products experience a much greater lowering of their free energy than does the transition state. This gives rise to a marked increase in the activation free energy E_a and to a gradual diminishing of the ion–dipole minimum. The calculated activation free energy (relative to the separated reactants or products) as a function of the number of water molecules is shown in Fig. 1.2. While the first water molecule increases the barrier height (relative to the barrier in bulk chloroform) by 3.7 kcal/mol, each additional water molecule contributes a smaller amount to the increase. With five water molecules, the total increase in the barrier height is about 10 kcal/mol and is only 3 kcal/mol below the value in bulk water.

Another important characterization of the free energy profile of the reaction is its curvature (second derivative) at the transition state, which we express using

the effective mass μ and the (equilibrium) barrier frequency ω_b by

$$\mu\omega_b^2 = -\left(\frac{\partial^2 W(\xi)}{\partial \xi^2}\right)_{\xi=0}. \tag{1.21}$$

This quantity determines the average acceleration experienced by the reaction coordinate as ξ varies from 0. The curvature is depicted in Fig. 1.2 as a function of the number of water molecules. As a comparison, we also show the values in bulk chloroform ($N_w = 0$) and in bulk water (BW). As the number of water molecules is increased, the effective barrier gets sharper. It is interesting to note that the effective bulk value is essentially reached with $N_w = 5$.

1.3.2 Electronic state variation

The change in the electronic state of the system as a function fo the reaction coordinate may be characterized by the quantum weight of one of the diabatic states, e.g., c_1^2. Combining Eqs. 1.16 and 1.19 and the relation $\chi = (H_{11} - H_{22})/H_{12}$ gives in solution:

$$c_1^2 = \frac{1}{2 + \chi^2/2 + \chi(1 + \chi^2/4)^{1/2}}, \qquad \chi = \frac{\Delta H^0 + s}{H_{12}}. \tag{1.22}$$

The top panel of Fig. 1.3 shows $c_1^2(\xi)$ versus ξ for the systems with different numbers of water molecules, as well as in the gas phase, in bulk chloroform and in bulk water. As c_1^2 varies from 0 to 1, the charge distribution on the solute atoms varies from that of the products to the reactants. All the curves pass through (0,

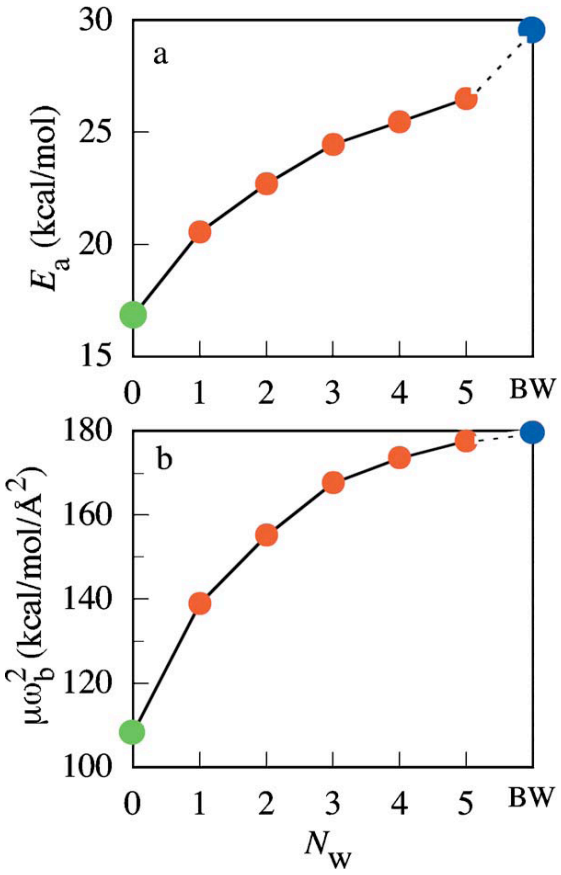

Figure 1.2: (a) The activation free energy of the reaction $Cl^- + CH_3Cl \longrightarrow CH_3Cl + Cl^-$ as a function of the number of water molecules present in bulk chloroform. Also shown is the result in bulk water (BW) and bulk chloroform ($N_w = 0$). (b) The corresponding barrier curvature [Eq. 1.21].

1/2), since at the transition state ($\xi = 0$), where $\Delta H^0 = 0$ and $\langle s \rangle = s_{eq}(\xi = 0) = 0$ (see Section 1.3.4 below), we have $\xi = 0$, and so $\langle c_1^2 \rangle \approx 1/2$. Since H_{12} decays exponentially as $|\xi|$ increases, c_1^2 varies rapidly near the transition state.

As the polarity of the medium is increased from the gas phase to bulk chloroform, and with the addition of water molecules, there is an increase in the solvation energy of the nonsymmetric charge distribution that is produced as soon as ξ varies

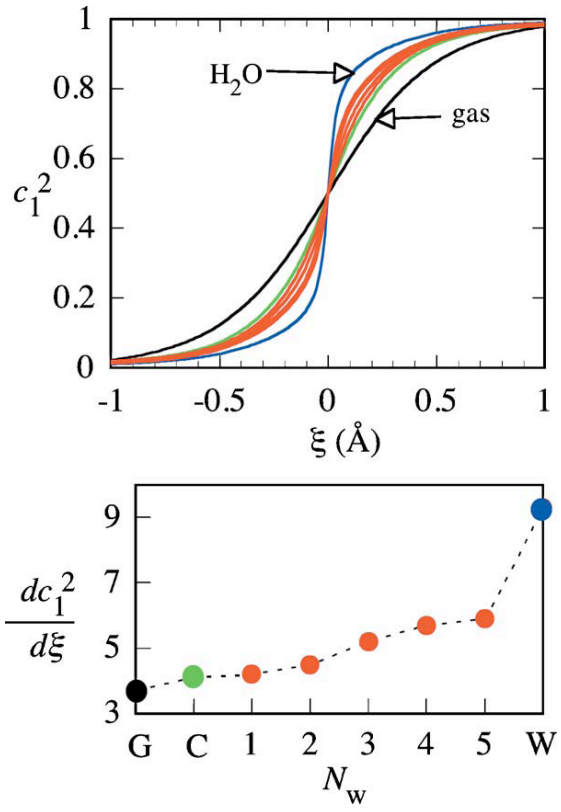

Figure 1.3: Top panel: Equilibrium average quantum population of one of the diabatic states as a function of the reaction coordinate. The red (unlabeled) lines are for the reaction in bulk chloroform with one to five water molecules, and the blue, green, and black are in bulk water, bulk chloroform, and the gas phase, respectively. Bottom panel: The rate of change in the quantum population at the transition state as a function of the number of water molecules in bulk chloroform. The circles corresponding to the labels G, C, and W are the results in the gas phase, bulk chloroform, and bulk water, respectively.

from zero. This explains the significant dependence of $c_1^2(\xi)$ on the polarity of the solvent. The rate of the stabilization of the nonsymmetric charge distribution can be quantified by calculating $d\langle c_1^2(\xi)\rangle/d\xi$ at $\xi = 0$. This "electronic state switching rate" is closely related to the charge switching rate in the phenomenological description of the S_N2 reaction by several groups.[9,27,38,42,59,109] This is shown in the bottom panel of Fig. 1.3. The rate of change in $\langle c_1^2(\xi)\rangle$ varies monotonically with the solvent polarity and with the increase in the number of water molecules, changing from 3.7 Å^{-1} in vacuum to 4.1 Å^{-1} in chloroform, and increases slowly as water molecules are added. Unlike the barrier frequency and the barrier height, by the time five water molecules are added, the rate of change in $\langle c_1^2(\xi)\rangle$ is still quite far from the asymptotic value of 9.3 Å^{-1} in bulk water.

1.3.3 Hydration structure

The contribution of the water molecules to the different aspects of the equilibrium hydration discussed in Secs. 1.3.1 and 1.3.2 can be correlated with the gradual development of the hydration structure as a function of the number of water molecules and of the reaction coordinate. This can be clearly demonstrated by examining the oxygen(water)–chlorine(nucleophile) radial distribution function $g_{O-Cl}(r)$. Specifically, in Fig. 1.4 the peak value of $g_{O-Cl}(r)$ is plotted against ξ for the reaction taking place in bulk chloroform with the presence of one-to-five

water molecules. As a comparison, we also show the results in bulk water.

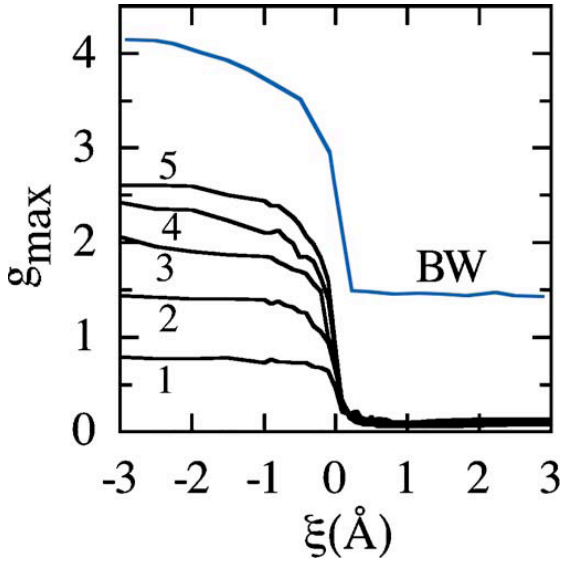

Figure 1.4: The peak value of the oxygen(water)–Cl^-(nucleophile) radial distribution function as a function of the reaction coordinate in bulk water, and in bulk chloroform in the presence of the indicated number of water molecules.

The peak value of $g_{O-Cl}(r)$ has its largest value for large negative values of ξ, reflecting the hydration of the free nucleophile Cl^-. As the number of water molecules increases, the peak value at large negative ξ increases as expected toward the value in bulk water. The peak value remains nearly constant as the nucleophile approaches the CH_3 group, and rapidly decreases as the system gets near the transition state ($\xi = 0$) and the charge on the nucleophile diminishes. This clearly correlates with the changes in the electronic structure described earlier. For positive ξ, the peak value is near zero for all systems except bulk water, as the water molecules now exclusively hydrate the leaving anion. In bulk water, the finite small nonzero value for $\xi > 0$ reflects the weak hydration of the Cl atom

in the CH_3Cl product.

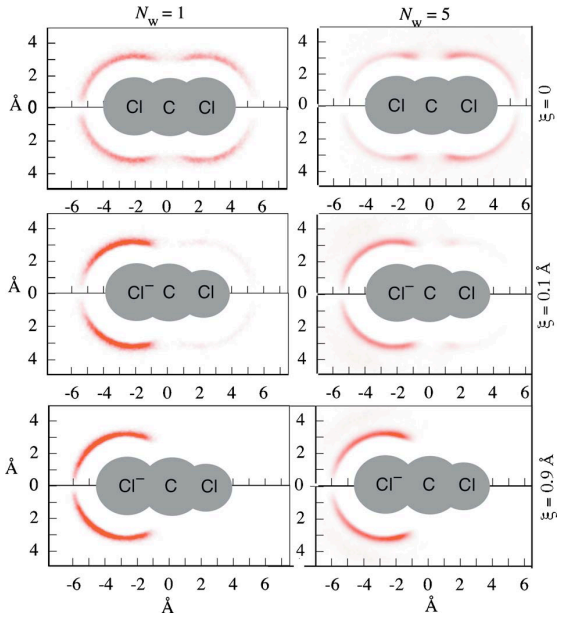

Figure 1.5: The probability distribution of finding an oxygen water atom around the reactive system atoms at a fixed value of the reaction coordinate ξ. The panels on the left (right) are for the systems with one (five) water molecules in bulk chloroform.

Another demonstration of the variation in the water structure around the reactive system is provided in Fig. 1.5, which shows, as contour plots, the probability of finding the water oxygen near the reacting system's atoms. It is interesting to note that the completely symmetric oxygen distribution around the $Cl^{0.5-}{-}CH_3{-}Cl^{0.5-}$ transition state configuration ($\xi = 0$) already shows marked asymmetry when $\xi = 0.1$ Å. The plots for larger ξ are essentially the same (we show as an example the one at $\xi = 0.9$ Å). Also note that except for less sharply defined distributions, the contour plots for one and five water molecules (and all

the cases in between) are very similar.

1.3.4 Solvent coordinate and solvent free energy

As the reactive system moves along the reaction coordinate, the variations in the hydration structure, as well as in the interaction with the chloroform molecules, can be described more conveniently using the concept of the solvent coordinate s introduced in Eq. 1.19. This is simply the solvent contribution to the energy difference between the two diabatic states at a given nuclear configuration. This quantity is analogous to the definition used in simulations of electron transfer reactions.[71] Figure 1.6 shows the equilibrium average $s_{eq}(\xi) = \langle s(\xi) \rangle$ as a function of the reaction coordinate ξ, as well as the separate contributions of the water and the chloroform molecules:

$$s_{eq}(\xi) = s^{w}_{eq}(\xi) + s^{c}_{eq}(\xi). \tag{1.23}$$

Because of the symmetrical nature of the transition state, $s_{eq}(\xi = 0) = 0$. As soon as an asymmetric charge distribution is developed, there is a significant shift toward more favorable interactions with the localized charge of the anion than with the dipolar CH_3Cl molecule, reflected by the large increase in $|s_{eq}|$. The rate at which s_{eq} varies with ξ reflects the strength of the interaction of the solvent molecules with the localized charge distribution of the products (or reactants) relative to the weaker interaction with the delocalized charge distribution

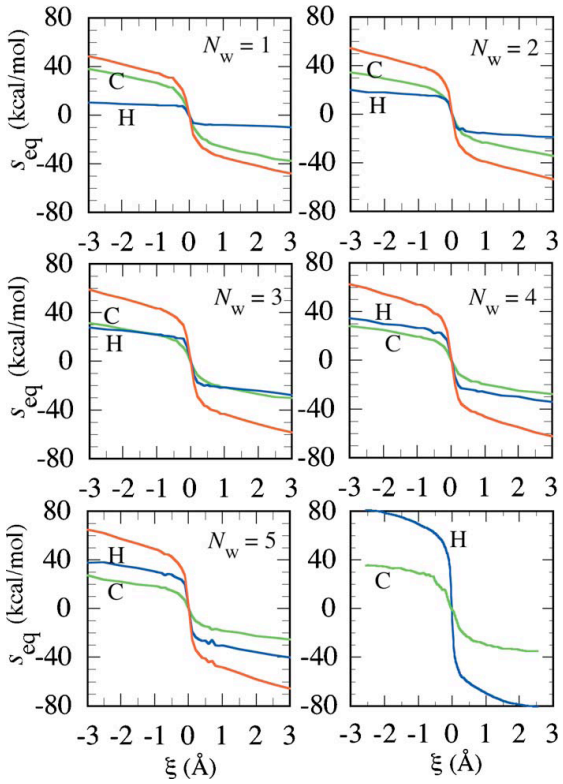

Figure 1.6: The equilibrium values of the solvent coordinate as a function of the reaction coordinate. Different panels correspond to different numbers of water molecules, as indicated. In each panel, the lines labeled H (blue) and C (green) correspond to the water contribution and the chloroform contribution to the solvent coordinate, respectively, while the unlabeled (red) lines show the total. The bottom-right panel gives the result in the bulk of the two solvents.

of the transition state. It is not surprising, therefore, that as the number of water molecules increases, the water contribution shown in blue increases more rapidly and to larger final values, (as $\xi \to \pm\infty$), while the chloroform contribution (shown in green) remains fixed and is quite similar to that in bulk chloroform. it is interesting to note that with five water molecules, the water contribution to s is only about half of the contribution in bulk water. However, the total solvent coordi-

nate, which includes the (nearly full) bulk contribution of chloroform, is about 80% of the contribution in bulk water. This is consistent with the rate of change in the activation-free energy with the number of water molecules discussed in the top of Section 1.3.1.

While $s_{eq}(\xi)$ represents the equilibrium (and most probable) value of the solvent coordinate when the reaction coordinate is fixed at a value of ξ, solvent orientational and translational fluctuations will cause fluctuations in the value of s. The probability of observing a given value of $\delta s = s - s_{eq}$ is, to a good approximation, a Gaussian, which suggests that the free energy associated with a given solvent fluctuation s is a quadratic in δs:

$$G(s;\xi) \approx \tfrac{1}{2} k_s(\xi)[s - s_{eq}(\xi)]^2, \tag{1.24}$$

where $k_s(\xi)$ is referred to as the solvent force constant.[51] This quantity expresses the resistance of the solvent to a change in its orientational and translational polarization and is expected to increase as the solute charge distribution gets more localized.

One can easily determine $k_s(\xi)$ by binning the value of δs from an equilibrium simulation at a fixed ξ, obtaining the probability distribution $P(s;\xi)$ from which $G(s;\xi) = -kT\, ln\, P(s;\xi)$ can be determined. A 1 ns simulation at each value of ξ gives a smooth curve that can be accurately fitted to a parabola in the range $|\delta s| < 5kT$.

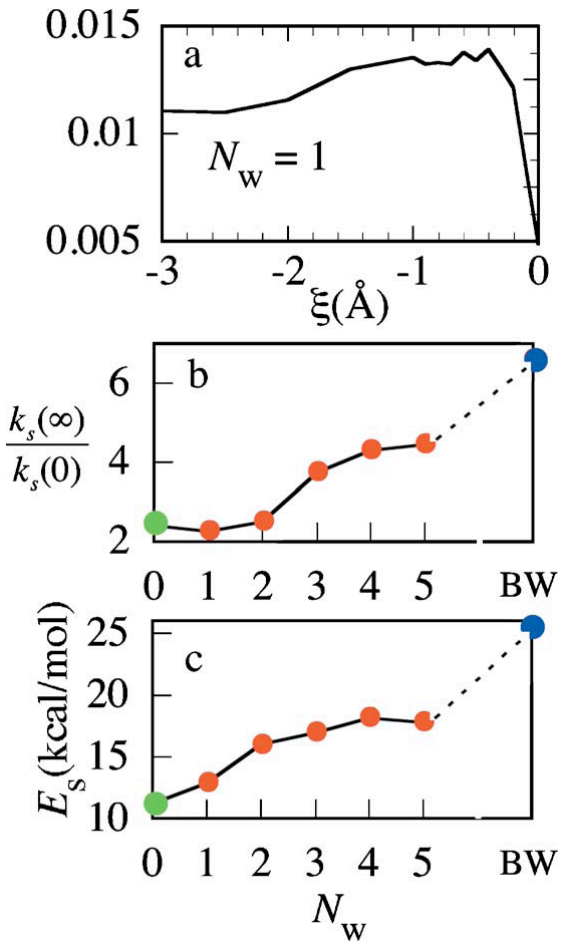

Figure 1.7: (a) The solvent force constant vs. the reaction coordinate for the $N_w = 1$ case. (b) The solvent force constant on the product (or reactant) side relative to the force constant at the transition state, as a function of the number of water molecules. Blue and green circles correspond to the ratio in bulk water and chloroform ($N_w = 0$), respectively. (c) Approximate solvent activation-free energy $E_s \approx (1/2)k_s(\infty)[s_{eq}(\infty)]^2$ as a function of the number of water molecules.

The top panel of Fig. 1.7 shows as an example the variation of $k_s(\xi)$ with ξ for the case of $N_w = 1$ (the plots for other values of N_w are similar). As expected, $k_s(\xi)$ varies with the reaction coordinate ξ and, as in the case of other properties discussed above, the variation is most rapid near the transition state ($|\xi| < 0.5$ Å). The values of $k_s(0)$ are in the range of $5.0 \times 10^{-3}(\text{kcal/mol})^{-1}$, increasing by about a factor of 5 when the system is on the reactant or the product side. The middle panel of Fig. 1.7 shows how the ratio $k_s(\infty)/k_s(0)$ varies with the change in the number of water molecules, with results in bulk chloroform and bulk water shown as a comparison. As the number of water molecules increases, the relative tightness of the hydration shell around the localized charge distribution (when $\xi = \pm\infty$), compared with that at the transition state, increases.

Another approximate measure of the work required to change the solvent configuration from that of the product to that of the transition state can be found from Eq. 1.24, by analogy with electron transfer, by substituting the values $s = 0$ and $\xi = \infty$: $E_s \approx \frac{1}{2}\, k_s(\infty)\, [s_{eq}(\infty)]^2$. This is shown in the bottom panel of Fig. 1.7. Of course in reality, as the transition state is approached k_s becomes smaller by a factor of 5, so the actual free energy required is much less. The exact value is given by the solvent contribution to the reaction free-energy barrier discussed earlier. However, the concept of E_s is still a useful measure of the relative contribution of the water molecules to the barrier.

1.3.5 Reaction dynamics

The activation barrier of the reaction can be used to estimate the transition state theory rate constant k_{TST}. This value assumes that every trajectory that reaches the transition state continues unhindered to form the products. This assumption may fail due to interaction with the solvent molecules, which may reverse the trajectory and induce it to recross the top of the barrier.[28,61] Specifically, as has been discussed extensively for this reaction in bulk water,[27] and as is clear from the discussion in Section 1.3.4, the solvent nuclear polarization which is equilibrated to the transition state charge distribution is typically not the proper polarization necessary to solvate the product charge distribution. This may give rise to an additional barrier that prevents the system from directly proceeding to the product side.[51]

As a result, the actual rate constant is reduced by the transmission coefficient factor κ. The reactive flux correlation function $\kappa(t)$, defined in Section 1.2.3, enables one to study the time scale of the recrossing and obtain the transmission coefficient from the plateau values of $\kappa(t)$. Figure 1.8 shows the flux correlation functions for the reaction in the presence of one-to-five water molecules, as well as in the bulk of water and chloroform. The correlation functions reach their plateau values in less than 50 fs. The reaction dynamics at the barrier top is controlled by the barrier frequency, which gives rise to a crossing time scale on the order of

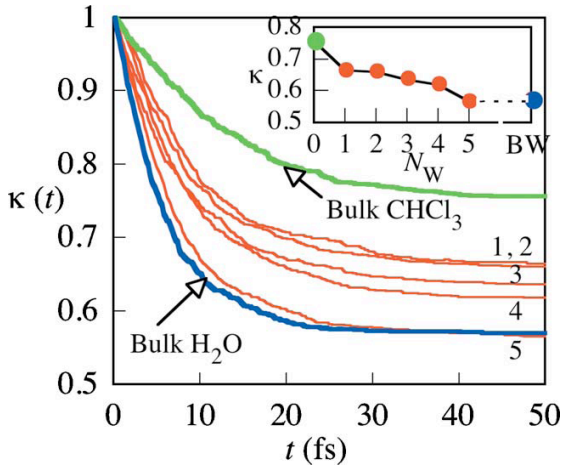

Figure 1.8: Reactive flux correlation functions for the $Cl^- + CH_3Cl \longrightarrow CH_3Cl + Cl^-$ reaction for the different systems. Blue and green lines are the result in bulk water and chloroform, respectively. Red lines are the results in bulk chloroform with the indicated number of water molecules. The inset shows the transmission coefficient as a function of the number of water molecules.

the inverse of the barrier frequency (about 10 fs). On this time scale, the solvent molecules are essentially frozen, and thus their orientation (which is optimized to stabilize the transition state) gives rise to an effective barrier to motion away from the transition state.[51] The time scale for the reorganization of the solvent molecules determines the time scale of the solvent to accommodate the evolving charge distribution and the time scale for the flux correlation function to reach the plateau value.

The inset of Fig 1.8 shows the value of the transmission coefficient as a function of the number of water molecules. As the number of water molecules is increased, the solvent barrier (mentioned in the previous section) increases. As a result, recrossings of the barrier increase and κ decreases toward the value in bulk water.

In general, however, deviation from transition state theory values are not large, and κ falls in between the values in bulk water ($\kappa = 0.57$) and bulk chloroform ($\kappa = 0.76$).

1.4 Summary and Conclusions

The free energy profile of the benchmark symmetric $Cl^- + CH_3Cl$ S_N2 reaction in liquid chloroform is highly sensitive to the addition of a few water molecules. The activation-free energy increases and the free energy of the nucleophile–dipole complex decreases due to the stabilization of the products relative to the transition state. The empirical valence bond model with the fully molecular solvents description provides structural and energetic insight into how the gradual addition of one-to-five water molecules changes the electronic structure along the reaction coordinate. Dynamic calculations show that deviations from transition state theory due to barrier recrossings are not large and fall between the behavior calculated in bulk water and bulk chloroform.

The sensitivity of the reaction free-energy profile of an S_N2 reaction to the presence of a few water molecules in the bulk organic solvent has important consequences for the rate of interfacial S_N2 reactions. This phenomenon, in the context of phase transfer catalysis as well as the extension of the present study to other S_N2 reactions and in other solvents, will be described in future publications.

Acknowledgments

This work has been supported by a grant from the National Science Foundation (Grant No. CHE-0809164).

Chapter 2

A Molecular Dynamics-Empirical Valence Bond Study of an S_N2 Reaction at the Water–Chloroform Interface

2.1 Introduction

It is well known that the strong reactivity of anionic nucleophiles in gas-phase nucleophilic substitution reactions (S_N2) is markedly diminished when the reaction is taking place in a protic polar solvent such as water.[6,38,58,60,62,64,70,83,107,110,133,141]

To enhance the reactivity in solution, one typically picks a low-polarity aprotic solvent, which can significantly lower the barrier compared with that in bulk water. A difficulty with this approach is the low solubility of small nucleophiles such as F^- and Cl^- in low-polarity solvents. One method for dealing with this difficulty is the utilization of a phase transfer catalyst to assist with the transfer of the nucleophile from the aqueous to the organic phase.

However, several fundamental questions about phase transfer catalysis (PTC) have not received much attention.[47,80,119,123,135] It is well known that the transfer of small hydrophilic anions from water to an organic solvent is accompanied by a few water molecules.[135] Theoretical studies of S_N2 reactions in gas-phase clusters[31,109,147] and in bulk liquids,[56,107] and experimental studies in bulk nonpolar solvents suggest that the hydration state of the anion strongly influences its nucleophilicity.[4,76,79] In reactions that are carried out under PTC conditions with vigorous mixing, is it likely that hydrated or partially hydrated nucleophilic ions participate in the reaction and thus influence its kinetics? Another open issue is whether the reactions carried out under PTC conditions are truly interfacial reactions. This is important since it has been recently demonstrated using second harmonic generation spectroscopy that the polarity of the interface region could be significantly different from that of the bulk phases.[136,138,139,144] Computer simulations of spectral line shapes[18,20,87] as well as experiments[136,145] also suggest the strong dependence of solvent polarity on the surface location and orientation.

In this chapter, we utilize a recently developed[21] empirical valence bond (EVB) model to examine in detail the simple benchmark symmetric S_N2 reaction $Cl^- + CH_3Cl \longrightarrow CH_3Cl + Cl^-$ at eight different locations of the water–chloroform ($CHCl_3$) interface. In each location, we calculate the reaction free-energy profile and several structural and dynamical characteristics of the reaction. In recent years, experimental and theoretical studies have clarified the influence of surface roughness on several interfacial processes.[23] By repeating all of our calculations under conditions where the interface remains molecularly sharp, we are also able to examine the effect of surface roughness on the reactivity of the above reaction.

The rest of the chapter is organized as follows: In Section 2.2, we briefly review the main features of the EVB model and the methodology used to compute the free energy and the dynamical corrections to the transition state theory rate constant. In Section 2.3, the results of the reaction free-energy profile, as well as the structural and time-dependent calculations, are described and discussed. A summary and conclusions are given in Section 2.4.

2.2 Systems and Methods

2.2.1 The empirical valence bond (EVB) model.

Theoretical modeling of S_N2 reactions has a long history and is still an active area of research.[2,10,25,27,29,38,42,49,50,59,64,70,91,106,108,109,116] The model we use is similar to the EVB model first developed by Warshel and coworkers.[60,141] It was discussed in an earlier publication[21] in detail, and here we briefly summarize the main components.

The two-state EVB approach is the simplest way to describe the main feature of the system, namely the changing electronic structure along the reaction coordinate. We assume[21,83] that only two orthonormal valence states, $\psi_1 = \mathrm{Cl{-}CH_3\ Cl}:^-$ and $\psi_2 = \mathrm{Cl}:^-\mathrm{CH_3{-}Cl}$, contribute to the total wave function:

$$\Psi = c_1\psi_1 + c_2\psi_2 \qquad \langle\psi_1 \,|\, \psi_2\rangle = \delta_{ij} \tag{2.1}$$

The total Hamiltonian is written as

$$\hat{H} = \begin{pmatrix} H_{11}(\vec{r}_i, \vec{r}_d, \vec{r}_s) & H_{12}(r_1, r_2, \theta) \\ H_{12}(r_1, r_2, \theta) & H_{22}(\vec{r}_i, \vec{r}_d, \vec{r}_s) \end{pmatrix}, \tag{2.2}$$

$$H_{11} = E_k + H^0_{11}(r_1, r_2, \theta) + U_{ss}(\vec{r}_s) + U_{si}(\vec{r}_s, \vec{r}_i) + U_{sd}(\vec{r}_s, \vec{r}_d), \tag{2.3}$$

where H_{11} is the diabatic Hamiltonian, which includes E_k, the kinetic energy of all atoms; $H^0_{11}(r_1, r_2, \theta)$, the gas-phase interaction between the Cl^- ion and the CH_3Cl molecule; $U_{ss}(r)$, the solvent potential energy; $U_{si}(\vec{r}_s, \vec{r}_i)$, the solvent–ion potential

energy; and $U_{sd}(\vec{r}_s, \vec{r}_d)$, the solvent–$CH_3Cl$ potential energy. In Eqs. 2.2 and 2.3, $\vec{r}_i$ is the vector position of the Cl^- ion, $\vec{r}_d$ are the vector positions of the CH_3Cl atoms, and $\vec{r}_s$ stands for the positions of all the solvent atoms. r_1 is the distance between the Cl^- ion and the carbon atom, r_2 is the C−Cl bond distance in CH_3Cl, and θ is the $Cl^-\cdots$C−Cl angle. Due to the symmetry of the reaction, H_{22} has the same functional form, but with the two chlorine atom labels interchanged.

The detailed functional forms and parameter values of all the potential energy terms in Eq. 2.3 are given in Ref. 21. Here we note that the gas-phase potential energy, $H^0_{11}(r_1, r_2, \theta)$, is a generalization to noncollinear geometries of the form suggested by Mathis et al.[83] It includes a Morse potential for the CH_3Cl bond, an exponential repulsive term for the interaction between the Cl^- ion and the CH_3 radical, and an ion–dipole term for combined short-range repulsion and long-range attractive interactions between the Cl^- ion and the CH_3Cl bond. These terms are obtained from a fit to the *ab initio* calculations of Tucker and Truhlar[131] and to experimental data.[83] The generalization to nonlinear geometry is accomplished by making some of the parameters θ-dependent and adding a bending energy term with parameters determined by a best fit to the gas-phase *ab initio* values of the energy, location of the transition state, and the ion–dipole well depth as a function of θ. Additional details about the different terms appearing in H^0_{11} can be found in Ref. 83.

$U_{ss}(\vec{r}_s), U_{si}(\vec{r}_s, \vec{r}_i)$, and $U_{sd}(\vec{r}_s, \vec{r}_d)$ are all given by the sum of Lennard-Jones

plus Coulomb interactions between every two sites on different molecules:

$$u_{ij} = 4\epsilon_{ij}\left[\left(\frac{\sigma_{ij}}{r_{ij}}\right)^{12} - \left(\frac{\sigma_{ij}}{r_{ij}}\right)^{6}\right] + \frac{q_i q_j}{4\pi\epsilon_0 r_{ij}}, \tag{2.4}$$

where i and j are two sites on two different (solvent or solute) molecules, r_{ij} is the distance between the sites, and ϵ_0 is the vacuum permittivity constant. The Lennard-Jones parameters σ_{ij} and ϵ_{ij} are determined from the parameters of the different sites by the usual combination rules:[54] $\sigma_{ij} = (\sigma_{ii}+\sigma_{jj})/2,\ \epsilon_{ij} = (\epsilon_{ii}\epsilon_{jj})^{1/2}$. The partial charges on the CH_3Cl are selected to reproduce its experimental dipole moment of 1.94 D.[85] These parameters, together with the Lennard-Jones parameters for the Cl^- ion and the CH_3Cl molecule, are given in Ref. 21. The Lennard-Jones parameters and the charges for the different sites on the chloroform molecule were selected to reproduce a number of solvent bulk properties and structures. In addition, the chloroform potential energy function includes intramolecular stretching and bending terms. The solvents' Lennard-Jones parameters, the intramolecular potential terms, and the corresponding intramolecular parameters can be found elsewhere.[13] The water model was selected to be the model previously used to study the bulk and interfacial properties of water. The water and chloroform potentials used here give rise to to a stable liquid/liquid interface with a surface tension of 25 ± 3 dyn/cm. For other force-field models for chloroform, see Refs. 39, 40, 57.

The off-diagonal electronic coupling term H_{12} in Eq. 2.2 is the one suggested

by Hynes and coworkers:[83,130]

$$H_{12} = -QS(r_1)S(r_2) \tag{2.5}$$

where $S(r)$ is the overlap integral for the σ orbital formed from the carbon 2p and chlorine 3p atomic orbitals. $S(r)$ is determined using Slater-type orbitals and the approximation of Mulliken et al.[93] These expressions can also be found in Ref. 21. $Q = 678.0$ kcal/mol is a parameter which is fitted to obtain the correct gas-phase activation energy.

The diagonalization of Eq. 2.2 yields the electronic ground state adiabatic Hamiltonian as a function of all nuclear coordinates:

$$H_{ad} = \tfrac{1}{2}(H_{11} + H_{22}) - \tfrac{1}{2}[(H_{11} - H_{22})^2 + 4H_{12}^2]^{1/2}. \tag{2.6}$$

This Hamiltonian is used for the classical propagation of the system. The gas-phase adiabatic ground-state potential energy is given by

$$U_{ad}^0 = \tfrac{1}{2}(H_{11}^0 + H_{22}^0) - \tfrac{1}{2}[(\Delta H^0)^2 + 4H_{12}^2]^{1/2}, \tag{2.7}$$

where $\Delta H^0 = H_{11}^0 - H_{22}^0$.

The reaction coordinate is defined by

$$\xi = r_2 - r_1, \tag{2.8}$$

so the reactants and products correspond to $\xi \ll 0$ and $\xi \gg 0$, respectively. The minimum energy path along ξ for the collinear geometry will be shown below.

The transition state is located at $r_1 = r_2 = 2.19$ Å and has an energy of 2.74 kcal/mol above the energy of the separate reactants and an activation energy of 13.72 kcal/mol above the ion–dipole minimum energy.

The total wave function is given by the solution for c_1 and c_2:

$$c_1^2 = \frac{1}{2 + \chi^2/2 + \chi(1 + \chi^2/4)^{1/2}}, \qquad c_2^2 = 1 - c_1^2, \tag{2.9}$$

where $\chi = \Delta H^0/H_{12}$ in the gas phase and $\chi = (H_{11} - H_{22})/H_{12}$ in solution. The effective charge on the nucleophile is given by $-c_1^2$. Because of the reaction's symmetry, at the transition state $r_1 = r_2$, so $\chi = 0$ in a vacuum (and on average it is also zero in solution). Thus, at the transition state $c_1^2 = c_2^2 = 1/2$. Since the coupling H_{12} falls off rapidly to zero as $|\xi|$ increases, we get $\chi \to \pm\infty$, and $c_1^2(\chi \to \infty) = 0$, $c_1^2(\chi \to -\infty) = 1$. Thus, as ξ varies from $-\infty$ to $+\infty$, the ground state varies from $\psi_2(c_1 = 0, c_2 = 1)$ to $\psi_1(c_1 = 1, c_2 = 0)$. In practice, the limiting values of 0 and 1 for c_1 and c_2 are reached for $|\xi|$ near 1 Å.

2.2.2 Reaction free-energy profile

The reaction free-energy profile as a function of the reaction coordinate $\xi = r_2 - r_1$, is calculated using umbrella sampling with overlapping windows and a biasing

potential[36] according to

$$W(\xi) = -\beta^{-1} \ln P(\xi) - U_b(\xi)$$
$$P(\xi) = \frac{\int \delta(r_1 - r_2 - \xi) exp[-\beta(H_{ad} + U_b(\xi)] d\Gamma}{\int exp[-\beta(H_{ad} + U_b(\xi))] d\Gamma} \tag{2.10}$$

where $\beta = 1/kT$ with k being the Boltzmann constant, T is the temperature, and $U_b(\xi)$ is a biasing potential. This is an arbitrary analytic function of ξ chosen to be as close as possible to $-W(\xi)$ in order to accelerate the convergence of the ensemble average in Eq. 2.10. We chose for the biasing potential an approximate Gaussian fit of the transition-state region of the free-energy profile in bulk chloroform[21] :

$$U_b(\xi) = 20.6928 e^{-2.63322\xi^2} \quad \text{kcal/mol.} \tag{2.11}$$

Other details about the exact umbrella sampling procedure are given below and in Ref. 21.

2.2.3 Reactive flux calculations

The activation free energy E_a obtained from the reaction free-energy profile $W(\xi)$ can be used to compute the transition state theory (TST) approximation of the rate constant $k_{\text{TST}} = Ae^{-\beta E_a}$, where A is the pre-exponential factor. The actual rate is reduced by the value of the transmission coefficient $\kappa < 1$, due to the fact that not every trajectory that reaches the transition state and heads toward the products ends as products. κ can be calculated using the reactive flux correlation

function formalism.[28,52,142] Starting from the solute molecules constrained to the transition state ($\xi = 0$), random velocities are assigned from a flux-weighted Maxwell-Boltzmann distribution, and the constraint is released. The value of the reaction coordinate is followed for a long enough time for the solvent-induced recrossings of the transition state to cease and for the system to reach the stable reactant state. The normalized flux correlation function can be calculated using[52]

$$\kappa(t) = N_+^{-1} \sum_{i=1}^{N_+} \theta[\xi_i^+(t)] - N_-^{-1} \sum_{i=1}^{N_-} \theta[\xi_i^-(t)], \tag{2.12}$$

where $\xi_i^{\pm}$ is the value of the reaction coordinate for the ith trajectory at time t, given that at $t = 0$, $d\xi/dt$ is positive (negative), $N_+(N_-)$ is the corresponding number of trajectories, and θ is the unit step function.

The reactive flux calculations are done by equilibrating the system at a constant temperature (298 K) with the constraint $\xi = 0$ (the system at the transition-state configuration $[Cl^{\delta-}-CH_3-Cl^{\delta-}]$, $\delta \approx 0.5$), for 1 ns, saving 100 independent configurations. These 100 equilibrated independent transition-state configurations are used to run 1000 constant energy trajectories using 10 different selections of flux-weighted initial velocities per configuration. Each trajectory is 0.2 ps long, which is long enough for $\kappa(t)$ to reach its plateau value.

2.2.4 Other simulation details

The system includes 500 water molecules, 213 $CHCl_3$ molecules, and the reactive system in a box of cross section 100 Å × 25 Å × 25 Å. This geometry gives rise to a single liquid/liquid interface, with each bulk phase at equilibrium with its own vapor phase.[11] We study eight different systems in which the reactants' center of mass is located in different positions along the interface normal Z, as indicated in Figure 2.1, which also depicts the water and chloroform density profiles of the neat interface. Z = 0 is taken to be the Gibbs dividing surface with respect to the water, which is approximately where the water density is half of its bulk value. In each system, the reactants' center of mass is restricted to moving inside a window of width $\delta Z = 3$ Å in order to increase the sampling statistics in each location. This is accomplished with the help of a Z-dependent potential acting on the center of mass of the reactants relative to the center of mass of the full simulation system. Since in each system the reactants can move freely within a window, their actual average location could be quite sensitive to the value of the reaction coordinate (as will be shown below). The × symbols in Figure 2.1 give the average location of the reactive system's center of mass when it is at the transition state. In what follows, we will refer to this location simply as the "reactants location." These locations are labeled a, b, c, ... from low to high Z values.

The reaction free-energy calculations in the interval $|\xi| < 4$ Å are done by

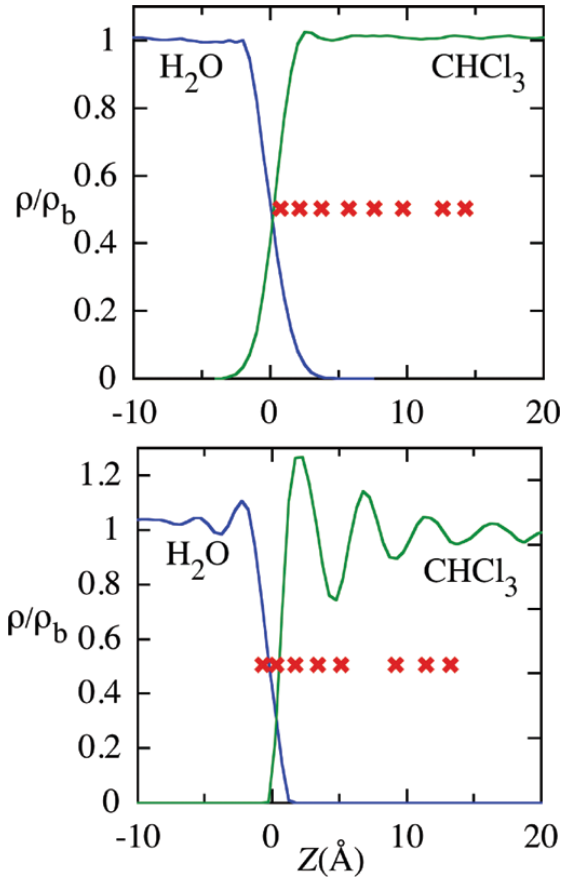

Figure 2.1: Density profiles of water and chloroform (normalized by their respective bulk densities) at the liquid/liquid interface. The red ×s denote the reactants' location (the average location of the reactants' center of mass when the system is at the transition state). Top panel: Normal interface; bottom panel: The interface is constrained to remain flat.

dividing the interval into "windows" that are each 0.5 Å wide and have a 0.2 Å overlap with the two neighboring windows. (4 Å is where the free energy profile reaches a plateau.) Calculations are done for both the $\xi > 0$ and $\xi < 0$ regions, despite the symmetry of the reaction, as an additional check for convergence. In each window, a total simulation time of 1 ns allows for an accurate calculation of the probability $P(\xi)$, from which the free energy profile is determined using Eq. 2.10, with a statistical error that is less than 0.3 kcal/mol.

From the simulations in each ξ-window, the ensemble averages of a number of system properties are determined as a function of ξ. This includes the solvent–solute radial distribution functions, the interaction energy of the two solvents with the reactants and products, and the value of c_1^2. To get a more refined expression in the region where these quantities vary the most, additional 1 ns simulations are done at 10 different fixed ξ values separated by 0.1 Å, starting from $\xi = 0$.

In order to examine the importance of liquid/liquid interface roughness on the reaction system, all of the above calculations are repeated for the solute molecules placed at eight different locations of a specially constrained liquid/liquid interface. In these calculations, the interface is forced to remain approximately flat by adding a continuous cubic constraining potential, ($U = 200\, Z^3$ kcal/mol), which prevents the molecules of each solvent from crossing the plane $Z = 0$. The water and chloroform density profiles and the solute locations of these systems are shown in the bottom panel of Figure 2.1.

The integration time step is 0.5 fs for all systems, using the velocity version of the Verlet algorithm.[5] The constant temperature calculations utilize a combination of the Andersen stochastic method and the Nosé-Hoover thermostat.[104]

2.3 Results and Discussion

2.3.1 Reaction free-energy profiles.

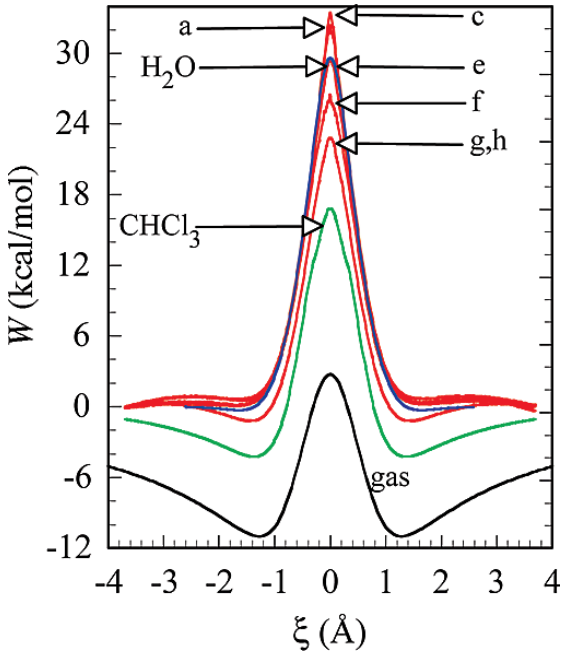

Figure 2.2: The free energy along the reaction coordinate for the $Cl^- + CH_3Cl$ reaction at the water–chloroform interface (red lines). The lines are labeled a, b, c, ... consecutively according to the reactants' location along the interface normal (see Figure 2.1), with line a corresponding to the smallest Z value, etc. Lines a, b, d and g, h fall on top of each other, and for clarity only of of each case is shown. Also shown are the reaction free energy in bulk water (blue) and bulk chloroform (green) and the minimum energy path for the collinear geometry in the gas phase (black). The temperature is $T = 298$ K in all cases.

The results of the umbrella sampling calculations of the free energy profile $W(\xi)$ for the $Cl^- + CH_3Cl \longrightarrow CH_3Cl + Cl^-$ reaction at the different locations of the water–chloroform interface are shown in Figure 2.2. As a comparison, the gas phase potential energy along the minimum energy path for the collinear reaction geometry and the free energy profiles in bulk chloroform and in bulk water are also shown. Since the separate reactants (or products) with the localized charge distribution on the chloride ion are much more favorably solvated than the delocalized charges on the transition state, as the polarity of the medium increases, the reactants and products experience a much greater lowering of their free energy than does the transition state. This gives rise to a marked increase in the activation free energy when one goes from the gas phase to bulk chloroform and to bulk water. The calculated activation free energy as a function of the average location along the interface normal is shown as red circles in Figure 2.3. Since the average location of the reactive system center of mass depends somewhat (but not strongly) on the reaction coordinate, the average location refers to that of the transition state.

Since the polarity of the interface region is expected to be somewhere between that of the two bulk phases,[18,139] one would expect the activation free energy ΔA^* of the reaction at the different interface locations to fall in between the values in bulk water and in bulk chloroform. Figure 2.3 (red circles) shows several unexpected results:

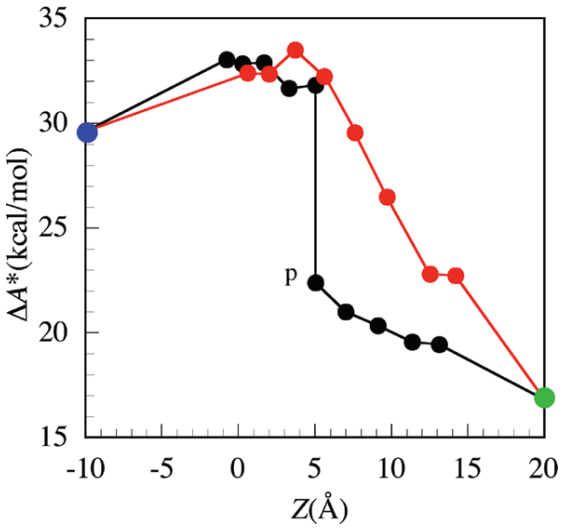

Figure 2.3: The activation free energy of the reaction $Cl^- + CH_3Cl \longrightarrow CH_3Cl + Cl^-$ as a function of the reactants' location at the water–chloroform interface. Also shown are the results in bulk water (blue circle) and bulk chloroform (green circle). Red circles: normal interface; black circles: The interface is constrained to be flat. The point labeled p corresponds to the reactants constrained to lie parallel to the interface.

(1) When the system's center of mass is in the region 0 Å $< Z <$ 5 Å, which is the region where the water density falls from 0.5 of the bulk density (at $Z = 0$) to 0.02 of the bulk density (which is slightly more than the width of the neat interface region), the activation free energy is *greater* than in bulk water. This result is statistically significant, given the estimated error in the free energy calculations mentioned above.

(2) In the region $Z >$ 5 Å, the activation free energy is lower than in bulk water, but still higher than in bulk chloroform, even in the window with the largest Z studied (approximately 13 Å).

Both of these results can be summarized by the important conclusion that *for*

the system to exhibit marked rate enhancement relative to bulk water, the reaction must be carried out significantly away from the interface region (in the organic phase).

The fundamental reason for the relatively high barrier at or near the interface is the significant interaction of the nucleophile with interfacial water molecules. An examination of simulation snapshots, like the one shown in Figure 2.4, demonstrates that the nucleophile is able to retain some number of water molecules when it is in the vicinity of the interface, and as a result the neat interface is deformed and gives rise to higher local polarity and thus reduced reactivity. This deformation is coupled to the reaction coordinate, since the charge distribution and the corresponding interaction with water depend on the reaction coordinate.

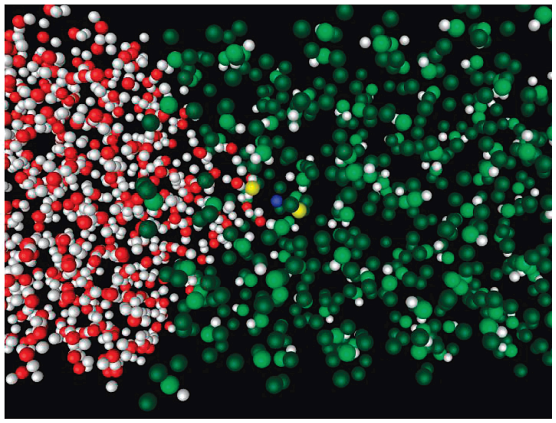

Figure 2.4: A snapshot from a molecular dynamics simulation of the $Cl^- + CH_3Cl$ reactants ($\xi = 1$ Å) on the organic side ($Z = 5$ Å) of the water–chloroform interface.

The importance of local surface fluctuations (the nanometer-scale capillaries)

on the reaction free energy can be quantitatively demonstrated by computing the reaction free-energy profile while the interface is forced to remain flat. The corresponding activation free energies as a function of the reactants' location are shown as the black circles in Figure 2.3. When the reactants are near the Gibbs surface, there is little difference between the activation free energy at the normal and at the constrained interface. However for $Z > 5$ Å, while at the normal interface ΔA^* decreases gradually, at the flat interface there is a sharp drop in ΔA^*. It is interesting to note that the values of ΔA^* at the normal interface correspond approximately to ΔA^* of the reaction when a cluster of one-to-five water molecules, $[Cl^- + CH_3{-}Cl](H_2O)_{N_w}$, is interacting with the reactants in bulk chloroform.[97] For example, at $Z = 15$ Å, $\Delta A^* = 22$ kcal/mol, which is similar to $\Delta A^* = 21$ kcal/mol calculated in bulk chloroform with $N_w = 1$. In contrast, the value of ΔA^* when the reactants are at $Z = 12$ Å of the *flat interface* is consistent with no water molecules in direct contact with the reactants.

At this point it is worth noting that the free energy profiles shown in Figure 2.2, with the corresponding ΔA^* shown in Figure 2.3, are obtained with no constraints imposed on the orientation of the $Cl{-}CH_3{-}Cl$ vector. The system is allowed to equilibrate to the preferred orientation in each of the windows in which the reaction coordinate is sampled. An examination of the orientational distribution of this vector at different values of the reaction coordinate and at different locations of the reactants relative to the interface shows that, in the region $Z < 5$ Å, there

is a strong dependence of the solute orientation on the reaction coordinate: When the system is at or near the transition state ($\xi = 0$), the $Cl^{0.5-}-CH_3-Cl^{0.5-}$ vector tends to lie parallel to the interface, and when the charge on the nucleophile is more or less fully developed (at $\xi \geq 0.3$ Å, see the next section), the vector $Cl^{-}\cdots CH_3-Cl$ tends to lie perpendicular to the interface, with the Cl^- pointing toward the water phase. Thus, the transition state experiences an environment that is significantly less polar than the reactants, explaining the high barrier in the $Z < 5$ Å region. This can be demonstrated by computing the free energy profile with the system constrained to be parallel to the interface. The corresponding activation free energy is shown in Figure 2.3 as the point labeled with p for the reactants at $Z = 5$ Å of the flat interface. The significant drop in the value of the activation free energy relative to the case when no restrictions are placed on the orientation of the reactants is clear. For $Z > 5$ Å, the vector $Cl-CH_3-Cl$ is, in general, randomly oriented at both the normal and flat interfaces.

The deformation of the neat interfacial water structure can be made quantitative by computing the surface excess of water in the presence of the solute. Consider the following relation used to define the Gibbs dividing surface,[114] Z_G:

$$\int_{Z_b}^{Z_G} (\rho_0(z) - \rho_b)dz + \int_{Z_G}^{\infty} \rho_0(z)dz = 0 \tag{2.13}$$

where $\rho_0(z)$ is the density profile of water at the neat water–$CHCl_3$ interface, Z_b is a location in the bulk water where the density is ρ_b, and $CHCl_3$ is assumed to

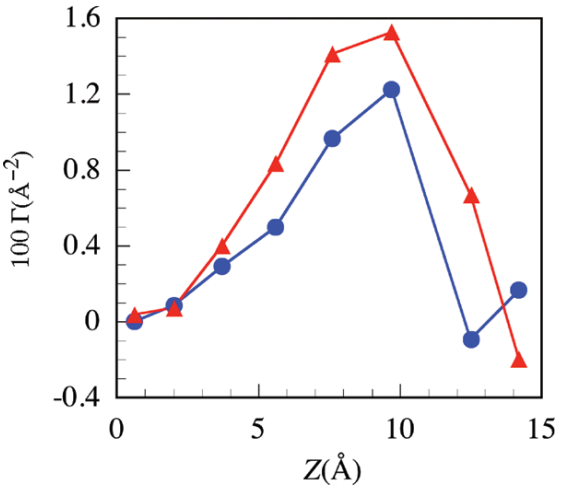

Figure 2.5: Water surface excess as a function of the location of the reactants for the case where the reactants are at the transition state (blue circles) and the reaction coordinate is at $\xi = 1$ Å (red triangles).

occupy the positive region of z [so $\rho_0(z) \to 0$ as $z \to \infty$]. In the presence of a solute, the density profile $\rho(z)$ will be different from $\rho_0(z)$, and Eq. 2.13 suggests that the surface excess may be defined as

$$\Gamma = \int_{Z_G}^{\infty} (\rho(z) - \rho_0(z)) dz \tag{2.14}$$

Figure 2.5 demonstrates the fact that as the solute moves deeper into the organic phase, there is a significant increase in the water surface excess. This is especially so when the nucleophile is fully charged (red triangles), but also when the system is at the transition state. However, the reactants at the transition-state configuration no longer induce much perturbation when they are located at 12 Å, due to their relatively lower ability to bind water molecules that far from the water phase. We estimate the error in the value of Γ at each Z location to be

about 0.002 Å^{-2} (using block averages of 10 sets), so the slight negative values near $Z = 14$ Å are within the statistical margin of no water excess.

As a further demonstration of the unique influence of the interface on the reaction free-energy profile, we consider its negative curvature (2nd derivative) at the transition state, which can be expressed using an effective mass μ and the equilibrium barrier frequency ω_b by

$$\mu\omega_b^2 = -\left(\frac{\partial^2 W(\xi)}{\partial \xi^2}\right)_{\xi=0} \tag{2.15}$$

This quantity determines the "sharpness" of the barrier and thus the thermally-average acceleration experienced by the reaction coordinate at the transition state. This quantity is depicted in Figure 2.6 as a function of the interface location for the normal as well as for the "flat" interface.

The barrier's curvature in bulk water ($Z = -10$ Å, blue circle) is larger than that in bulk chloroform ($Z = 20$ Å, green circle). This is due to the more rapid change in the solute charge distribution (and the corresponding solvation) in water than in the low-polarity organic solvent, as the system moves from the transition state.[21,83] Interestingly, when the reactive system's center of mass is near the Gibbs surface (Z = 0), the barrier curvature is greater than that of either of the bulk liquids, for both the normal (red circles) and the "flat" (black circles) interface. We will see below that this is reflected in the more rapid change in the charge distribution when the reaction takes place near the Gibbs surface. Note that the

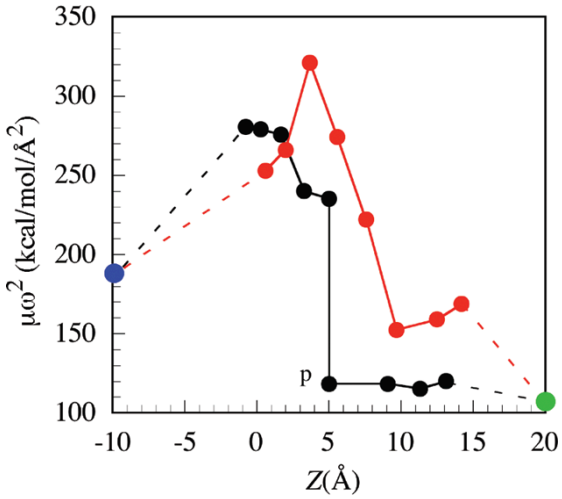

Figure 2.6: The barrier curvature (Eq. 2.15) of the $Cl^- + CH_3Cl \longrightarrow CH_3Cl + Cl^-$ reaction free-energy profile as a function of the reactants' location for the normal (red circles) and flat (black circles) interfaces. The blue and green circles represent the curvatures in bulk water and in bulk chloroform, respectively. The point labeled p corresponds to the reactants constrained to lie parallel to the interface.

barrier's curvature when the reaction is taking place deeper into the organic phase ($Z > 8$ Å), at the normal interface, is similar to that when a single water molecule is interacting with the reactants in bulk chloroform.[97] In contrast, and as expected, when the reaction is taking place deeper into the organic phase ($Z > 8$ Å) at the "flat" interface, the barrier's curvature is the same as in bulk chloroform, since in this case, when the system is at the transition state, there is almost no interaction with water molecules.

2.3.2 Electronic state variation

In this section, we demonstrate the sensitivity of the solute charge distribution as determined by the solute electronic state (the values of c_1 or c_2) to the value of the reaction coordinate. Since at each value of the reaction coordinate ξ the interaction of the polar solvent molecules is significantly dependent on the solute charge distribution, this interaction also significantly depends on ξ. One can approximately characterize any solvent configuration using a scalar "solvent coordinate" s by the solvent contribution to the energy gap $\Delta H = H_{11} - H_{22}$:

$$H_{11} - H_{22} = \Delta H^0 + s \tag{2.16}$$

This definition is analogous to the one used in simulations of electron transfer reactions in polar solvents.[71]

The electronic state of the system may be characterized by the quantum weight of one of the diabatic states, e.g., c_1^2. Combining Eqs. 2.9 and 2.16 and the relation $\chi = (H_{11} - H_{22})/H_{12}$ gives in solution

$$c_1^2 = \frac{1}{2 + \chi^2/2 + \chi(1 + \chi^2/4)^{1/2}} \qquad \chi = \frac{\Delta H^0 + s}{H_{12}} \tag{2.17}$$

The top panel of Figure 2.7 shows a sample of $c_1^2(\xi)$ vs. ξ plots for some of the systems considered in this chapter, as well as in bulk chloroform and in bulk water. As the reactants are converted to products, c_1^2 varies from 0 to 1, and the charge distribution on the solute atoms varies accordingly. At the transition state ($\xi = 0$),

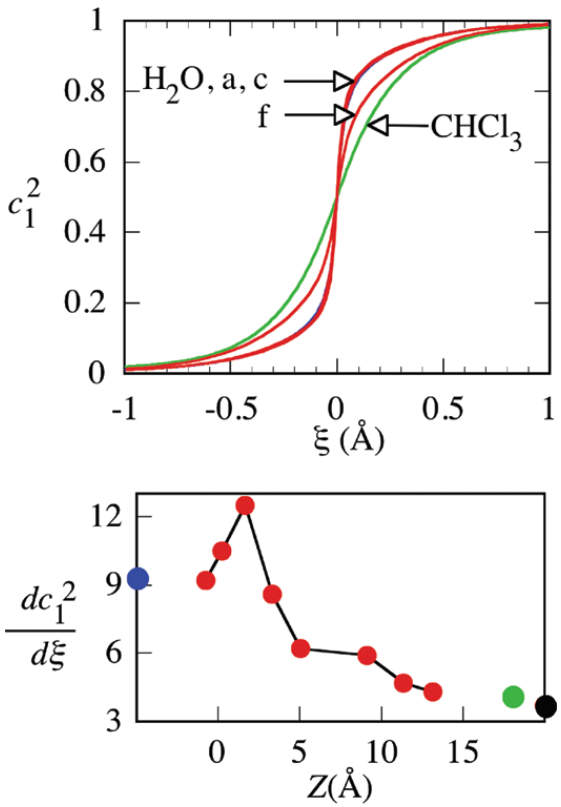

Figure 2.7: (Top panel) Equilibrium average quantum population of one of the diabatic states as a function of the reaction coordinate. The red lines are for the reaction in several surface locations as labeled. The blue and green lines are in bulk water and in bulk chloroform, respectively. (Bottom panel) The rate of change of the quantum population at the transition state as a function of the location along the interface normal. The blue, green, and black circles correspond to the rate in bulk water, bulk chloroform, and the gas phase, respectively.

the gas phase energy difference $\Delta H^0 = 0$. In addition, because of symmetry, if $\xi = 0$, we must have $\langle s \rangle = s_{eq}(\xi = 0) = 0$, where $s_{eq}(\xi)$ is the equilibrium value of s when the reaction coordinate is equal to ξ. Thus, at the transition state we have $\chi = 0$, and so $\langle c_1^2 \rangle \approx 1/2$ for all of the systems.

Since H_{12} decays exponentially as $|\xi|$ increases from zero, c_1^2 varies rapidly near the transition state. The rate of this variation depends on the medium. The higher the polarity, the larger the stabilization energy of the nonsymmetric charge distribution that is developed as soon as $|\xi|$ increases from zero, and the more rapid the change in c_1^2. This is reflected in the difference observed between bulk chloroform (green line) and bulk water (blue line near the edge of the red lines labeled a and c). The behavior of the interfacial systems is in general mostly between these limits, but nonmonotonic. This is easier to see by considering the "electronic state switching rate,"[9,27,38,42,59,109] $d\langle\, c_1^2(\xi)\,\rangle/d\xi$ at $\xi = 0$, shown in the bottom panel of Figure 2.7.

The rate of change of $\langle\, c_1^2(\xi)\,\rangle$ for the reaction taking place at the Gibbs surface (system a) is the same as that in bulk water (blue circle) around 9 Å^{-1}. It first increases as the system is moved toward the organic phase, reaching the maximum value of 12.5 Å^{-1} for system c. A further push toward the organic phase reduces the rate, reaching a value quite similar to that in bulk chloroform (4.1 Å^{-1}, green circle). Also shown as the black circle is the value in the gas phase (3.7 Å^{-1}). This variation provides the rationale for the mirror variations we observed in

the activation free energy and the barrier frequency discussed above. It is also interesting to note that the rate of change of $\langle\, c_1^2(\xi)\,\rangle$ at the interface locations deep in the organic phase is similar to that calculated when one or two water molecules interacts with the reactants in bulk chloroform.[97] The results of $\langle\, c_1^2(\xi)\,\rangle$ and its rate of change, when the reaction is taking place at the flat interface (not shown), are consistent with the discussion of the last section as well. In particular, the rate of change of $\langle\, c_1^2(\xi)\,\rangle$ when the systems are at the locations $Z < 5$ Å, are similar to that at the normal interface, while for $Z > 5$Å, they are all very similar to the value in bulk chloroform.

2.3.3 Hydration structure

The discussion in the previous two sections suggests that the barrier height and frequency of the reaction and the electronic state of the reactants are strongly influenced by the strength of the interaction of the solute with the water molecules. This was demonstrated crudely in Section 2.3.1 by examination of the water excess in the organic phase, as the system is moved across the interface. Another, more sensitive, way to quantify the gradual development of the hydration structure as a function of the reaction coordinate and solute location is by examining the oxygen(water)–chlorine(nucleophile) radial distribution function $g_{O-Cl}(r)$. Figure 2.8 depicts the peak value of $g_{O-Cl}(r)$ vs. ξ for the reaction taking place in different

locations of the water–chloroform interface, in bulk water and in one location of the flat liquid/liquid interface.

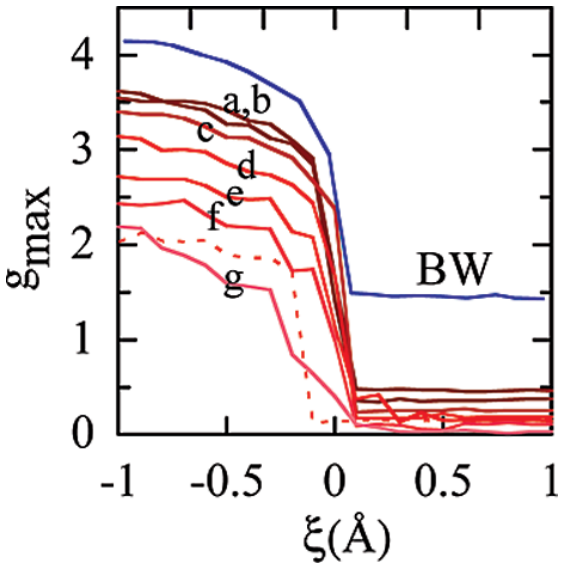

Figure 2.8: The peak value of the oxygen(water)-Cl(nucleophile) radial distribution function as a function of the reaction coordinate at different locations of the water–chloroform interface (solid lines with different shades of red), in bulk water (blue line labeled BW) and at $Z = 5$ Å of the flat interface (dashed red line). The interface locations are labeled $a, b, c, ...$, corresponding to an increasing value of Z, which can be inferred from Figure 2.1.

In bulk water, the peak value of $g_{O-Cl}(r)$ attains its largest value at large negative values of ξ, reflecting the complete hydration shell of the free nucleophile Cl^-. As the charge on the nucleophile diminishes near the transition state, the peak value decreases markedly and becomes the fixed value appropriate to the bulk hydration of the Cl atom in the CH_3Cl molecule for $\xi > 0$. Lines a - g in Figure 2.8 show that, in general, the hydration of the Cl^- is decreased as the reaction location is moved toward the organic phase. This decrease is relatively

mild at large negative values of ξ, but becomes more marked near the transition state. This demonstrates the ability of the fully charged nucleophile to retain part of the hydration shell as it crosses the interface, an ability that is rapidly lost as one approaches the transition state $Cl^{0.5-}-CH_3-Cl^{0.5-}$, leading to the behavior of the activation free energy discussed in Section 2.3.1, and it clearly correlates with the changes in the electronic structure described earlier. For positive ξ, the small peak value for all the interfacial systems reflects the weak interfacial hydration of the Cl atom in the CH_3Cl product.

The calculations at the flat interface show that for the systems with $Z < 5$ Å, there is very little difference in the behavior of the normal and flat interface, as at these distances the reactants can reorient themselves to provide a similar degree of nucleophile hydration. Marked differences appear at $Z = 5$ Å, which at the flat interface is shown as the dashed line in Figure 2.8, which should be compared with line *d* of the normal interface. At this distance, the removal of surface roughness significantly decreases the hydration of Cl^-, especially at the transition state. For all systems with $Z > 5$ Å, there is no well-defined peak in the radial distribution function, since they have no water in the Cl^- first hydration shell.

2.3.4 Solvent coordinate and solvent free energy

The discussion above, especially in Section 2.3.1, clearly demonstrates that the free energy surface for the S_N2 reaction at the liquid/liquid interface is a four-dimensional object, since the free energy profile along the reaction coordinate is sensitive to the location of the reactants' center of mass and the orientation of the nucleophilic attack with respect to the Gibbs surface. While one approach for describing this object, presented above, involves computing the free energy profile for specific locations and orientations, a more convenient (and reduced) description utilizes the concept of solvent coordinate, s, defined earlier in Eq. 2.16. Although this solvent coordinate itself is a function fo the reactants' location and orientation, its simplicity, being a scalar quantity, is very useful. As the reactive system moves along the reaction coordinate, the interaction of the two diabatic states with the water and chloroform molecules depends on the reactants' location and instantaneous surface structural fluctuations. The solvent coordinate quantifies this difference by simply taking the solvent contribution to the energy difference between the two diabatic states at a given nuclear configuration. This is analogous to the definition used in simulations of electron transfer reactions.[71]

Figure 2.9 shows the equilibrium average $s_{eq}(\xi) = \langle s(\xi) \rangle$ as a function of the reaction coordinate ξ, as well as the separate contributions of the water and the

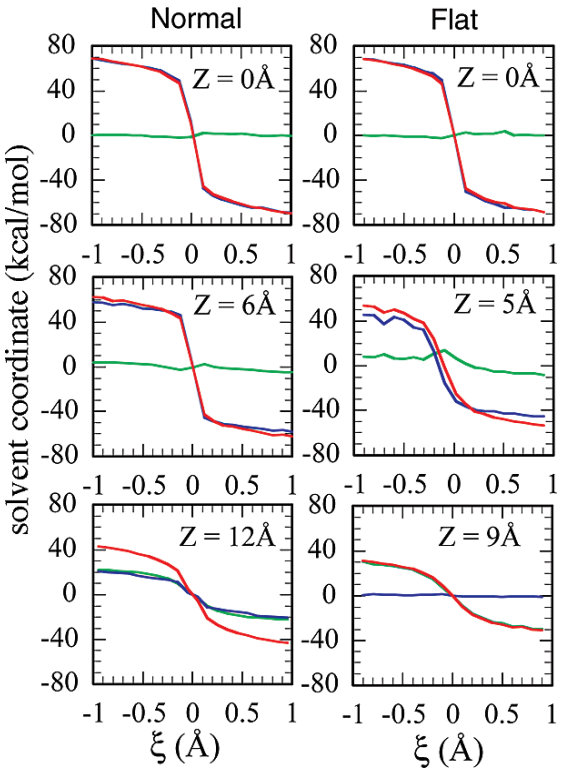

Figure 2.9: The equilibrium value of the solvent coordinate s as a function of the reaction coordinate ξ. Different panels correspond to different locations of the reactants' center of mass, as indicated. In each panel, the blue and green lines correspond to the water and chloroform contribution to the solvent coordinate, respectively, while the red line shows the total. The left panels are for the normal interface and the right panels for the interface constrained to remain flat.

chloroform molecules:

$$s_{eq}(\xi) = s^{w}_{eq}(\xi) + s^{c}_{eq}(\xi). \tag{2.18}$$

As previously discussed, because of the symmetrical nature of the transition state, $s_{eq}(\xi = 0) = 0$. As soon as an asymmetric charge distribution is developed, there is a significant shift toward more favorable interactions with the localized charge of Cl^- than with the dipolar CH_3Cl molecule, reflected by the large increase

in $|s_{eq}|$ as ξ varies from zero. When the reactants are located near the Gibbs surface or anywhere up to 5 Å into the organic phase at both the normal and the flat interface (top and middle panels), the contribution to s is almost entirely due to the water molecules, $s^w_{eq}(\xi) \gg s^c_{eq}(\xi)$, consistent with the discussion of the previous section. This contribution is almost identical to that in bulk water.[21] At the normal interface, as the reactants are moved deeper into the organic phase, the water contribution decreases, but it is still significant. For example, even at $Z = 12$ Å (bottom left panel) the water and chloroform contributions are similar, reflecting the fact that solute interaction with one or two water molecules is equivalent energetically to the interaction with the rest of the chloroform molecules. In contrast, when surface roughness is removed, the water contribution to s is essentially zero at $Z = 9$ Å (bottom right panel). Note also that the rate at which s_{eq} varies with ξ (e.g., the slope of the line at $\xi = 0$) also varies with the degree to which the water molecules contribute to s. This is due to the fact that this slope reflects the strength of the interaction of the solvent molecules with the localized charge distribution of the products (or reactants) relative to the weaker interaction with the delocalized charge distribution of the transition state.

The $s_{eq}(\xi)$ discussed above represents the equilibrium value of the solvent coordinate when the reaction coordinate is fixed at ξ. However, solvent orientational and translational fluctuations (and surface dynamic roughness at the normal interface) will cause fluctuations in the value of s. The probability of observing a

given value of s, denoted by $P(s;\xi)$, is, to a good approximation, a Gaussian centered at s_{eq}, which means that the free energy associated with a given solvent fluctuation, $\delta s = s - s_{eq}$, is quadratic in δs

$$G(s;\xi) = -kT \ln P(s;\xi) \approx \tfrac{1}{2} k_s(\xi)[s - s_{eq}(\xi)]^2 \tag{2.19}$$

where $k_s(\xi)$ is referred to as the solvent force constant.[51] It expresses the "resistance" of the solvent to a change in its orientational and translational polarization, and it is expected to increase as the solute charge distribution gets more localized. $k_s(\xi)$ can be easily determined by binning the value of δs from an equilibrium simulation at a fixed ξ, to get the probability distribution $P(s;\xi)$ and fitting $G(s;\xi) = -kT \ln P(s;\xi)$ to a parabola. A 1 ns simulation at each value of ξ gives an accurate fit to a parabola in the interval $|\delta s| < 2$ kcal/mol.

The top panel of Figure 2.10 shows as an example the variation of $k_s(\xi)$ with ξ at three different locations of the normal interface. As explained above, $k_s(\xi)$ increases with the reaction coordinate ξ and, as in the case of other properties discussed above, the variation is most rapid near the transition state ($|\xi| < 0.2$ Å). The middle panel of Figure 2.10 shows how the ratio $k_s(\infty)/k_s(0)$ varies with the location of the reactants at the interface. The rapid increase in this ratio at the surface location relative to bulk water mainly represents the very small solvent force constant when the system is at the transition state. At these locations, small fluctuations in translational and orientational motion of interfacial water

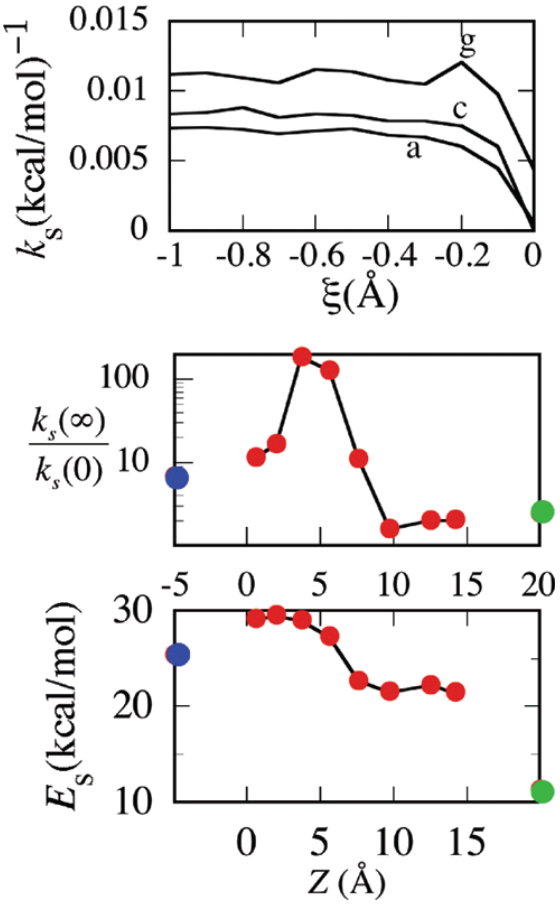

Figure 2.10: (Top panel) The solvent force constant vs. the reaction coordinate for three different surface locations. The a, c, and g labels correspond to the locations $Z = 0$, 4, and 12 Å, respectively. (Middle panel) The solvent force constant on the product (or reactant) side relative to the force constant at the transition state, as a function of the center of mass location of the transition state along the interface normal. (Bottom panel) Approximate solvent activation free energy, $E_s \approx \frac{1}{2}k_s(\infty)[s_{eq}(\infty)]^2$ as a function of surface location. The blue and green circles in the middle and bottom panels correspond to the values in bulk water and chloroform, respectively.

molecules are quite common, but they produce quite a large shift in the energy difference of the two diabatic states.

The solvent free energy parameters discussed above can be useful for an independent quantitative account of the contribution of the solvent to the activation free energy. While the exact value can be deduced from comparing the gas-phase and the condensed-phase free energy profiles discussed in Figure 2.3, an approximate measure of the work required to change the solvent configuration from that of the products to that of the transition state can be found by analogy to electron transfer, by substituting the values $s = 0$ and $\xi = 0$ into Eq. 2.19, leading to $E_s \approx 1/2 k_s(\infty)[s_{eq}(\infty)]^2$. This quantity is shown in the bottom panel of Figure 2.10. As expected, it follows the general behavior depicted in Figure 2.3.

Figure 2.11 shows that when the interface is forced to remain flat by removing the surface fluctuations normal to the interface, the solvent force constant at the transition state increases relative to the normal interface, as expected. This results in reducing the ratio $k_s(\infty)/k_s(0)$ compared with the normal interface. The other observed changes reflect the sudden removal of interactions with the water molecules when $Z > 5$ Å, as mentioned above.

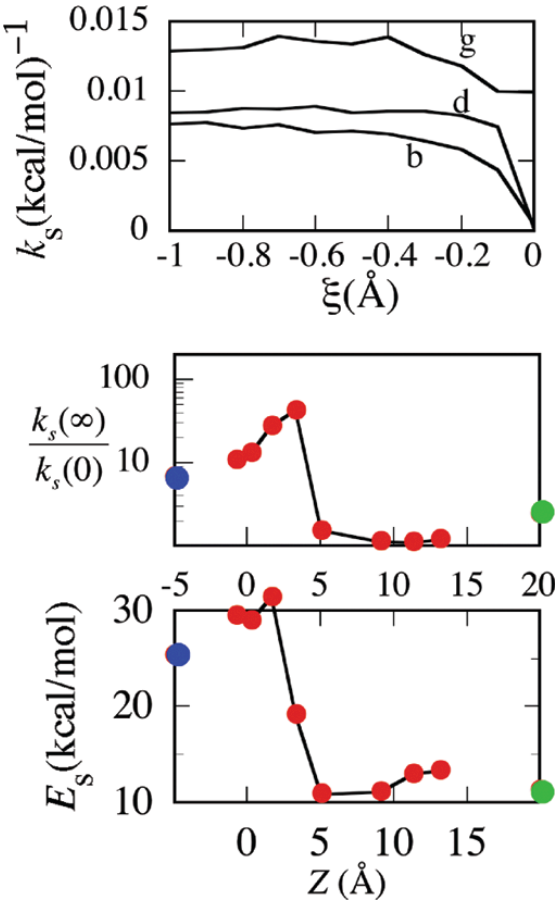

Figure 2.11: Same as in Figure 2.10 for the interface constrained to remain flat. In the top panel, the b, d, and g labels correspond to the locations $Z = 0, 3,$ and 11 Å, respectively.

2.3.5 Reaction dynamics

We conclude by briefly discussing the dynamical correction to k_{TST}, the transition state theory rate constant, which can be calculated from the activation free energy and by assuming that every trajectory that reaches the transition state continues directly to form the products. This assumption may fail due to interaction of the solute with the solvent molecules, causing the trajectory to recross the top of

the barrier.[28,61] In particular, as is clear from the discussion in the previous section (and as has been discussed extensively for this reaction in bulk water[27]), the solvent nuclear polarization, which is equilibrated to the transition state charge distribution, is not the proper polarization necessary to solvate the product charge distribution. Indeed, $\langle s(\xi = 0)\rangle \ll |\langle s(|\xi| > 0)\rangle|$. This may give rise to an additional temporary (polarization) barrier that prevents the system from directly proceeding to the product side.[51] As a result, the actual rate constant is reduced by the transmission coefficient factor κ. This factor can be obtained from the plateau value of the reactive flux correlation function $\kappa(t)$, defined in Eq. 2.12.

The top panel of Figure 2.12 shows the flux correlation functions $\kappa(t)$ for the reaction at different interface locations, as well as in bulk water and chloroform. The correlation functions rapidly decay with a time constant that varies from 3 fs at the interface location c to 6 fs in bulk water and to 14 fs in bulk chloroform, and they reach their plateau values in less than 50 fs. $\kappa(t)$ is determined by the dynamics near the transition state, and these dynamics are controlled by the barrier frequency ω_b and by solvent motion. The barrier frequency gives rise to a crossing time on the order of $1/\omega_b$ (a few femtoseconds). On this time scale the solvent molecules are essentially frozen and their orientation, which is optimized to stabilize the transition state, gives rise to an effective barrier to motion away from the transition state.[51] The time scale for the reorganization of the solvent molecule determines the time scale of the solvent to accommodate the evolving

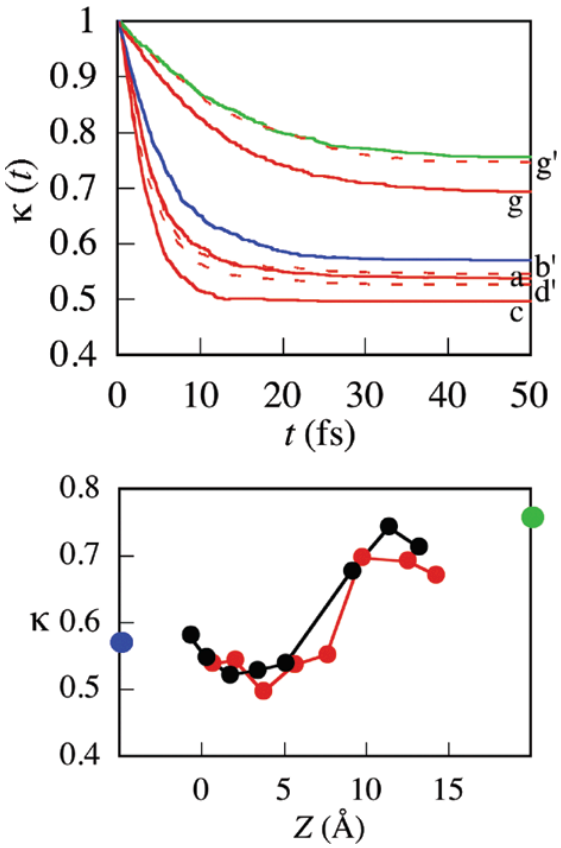

Figure 2.12: (Top panel) Reactive flux correlation function for the $Cl^- + CH_3Cl$ reaction at the normal and flat water–chloroform interfaces. Blue and green lines are the results in bulk water and bulk chloroform, respectively. Solid red lines are the results in several normal interface locations labeled a, c, and g, corresponding to the locations $Z = 0, 4,$ and 12 Å. Dashed red lines are the results in several flat interface locations labeled b′, d′, and g′, corresponding to the locations $Z = 0, 3,$ and 11 Å. (Bottom panel) The transmission coefficient as a function of the surface location for all systems at the normal (red circles) and flat (black circles) interfaces. The blue and green circles are the results in bulk water and bulk chloroform, respectively.

charge distribution and the time scale for the flux correlation function to reach the plateau value. The higher barrier frequency and the faster solvent motion in water and at the interface compared to those in bulk chloroform explain the different shape of the correlation functions.

The bottom panel of Figure 2.12 shows the value of the transmission coefficient as a function of reactants' locations at the normal and flat interfaces. As the solvent barrier (discussed in the previous section) increases, recrossings of the barrier height increase and κ decreases. In general, however, deviation from transition state theory values are not large, and κ falls in between the values that are slightly below those in bulk water ($\kappa = 0.57$) and bulk chloroform ($\kappa = 0.76$).

2.4 Summary and Conclusions

The detailed study of the benchmark $Cl^- + CH_3Cl$ S_N2 reaction at the water–chloroform interface demonstrates that the free energy profile of this reaction is sensitive to the reactants' location and orientation with respect to the interface. The activation free energy as a function of the distance from the interface is non-monotonic. The barrier when the reactants are located a few angstroms into the organic phase is slightly higher than when the reactants are at the Gibbs surface and in bulk water, and it begins to decrease toward the value of bulk chloroform only when the distance from the interface is larger than 1 nm. By studying the

reaction at an interface that is forced to remain flat (by removing surface fluctuations perpendicular to the interface), we confirm the important role played by interfacial water molecules in inhibiting the reactivity of this reaction. The decrease in the stabilization of the products relative to the transition state, which is responsible for the rate enhancement in chloroform relative to water, is disrupted by the ability of a few water molecules at the interface to reverse this trend. The empirical valence bond model with the fully molecular solvent description provides quantitative insight into how interfacial water molecules change the electronic structure and other structural and energetic properties along the reaction coordinate. Dynamic calculations show that deviations from transition state theory due to barrier recrossings are not large, and while some interfacial locations show the largest deviation, these deviations mostly fall between those in bulk water and bulk chloroform.

This study has important consequences for the rate of interfacial S_N2 reactions, since it demonstrates that for true rate enhancement the reaction must be carried out mostly away from the interface region. The present work has established the base interfacial reactivity of a benchmark S_N2 reaction without the presence of a catalyst. While the role of the catalyst (typically a large ammonium cation) is simply to transfer the nucleophile to the organic phase, it could alter the reaction barrier. In subsequent publications, we will examine this reaction at the water–$CHCl_3$ interface, in the presence of several different sized tetraalkylammonium

catalysts.

Acknowledgments

This work has been supported by a grant from the National Science Foundation (CHE-0809164).

Chapter 3

A Molecular Dynamics/EVB Study of an S_N2 Reaction in Water Clusters

3.1 Introduction

The study of chemical reaction dynamics in small gas-phase clusters has a very long history, and it is still of extensive interest.[33,46,53,86,112] This study has been motivated by the fundamental questions of the nature of the transition from gas-phase to bulk behavior (e.g., what size cluster is necessary for achieving bulk properties) and by the fact that many environmentally important reactive processes take place in small water or ice clusters in the atmosphere. The references above

provide reviews of several reactions including photodissociation, proton transfer, acid dissociation, and more.

An interesting case that has been studied experimentally and theoretically, due to its large dependence on the medium, is that of the nucleophilic substitution reaction (S_N2). It is well known that the rate of some S_N2 reactions is lower by up to 20 orders of magnitude when the reaction is taking place in water compared with the gas phase.[6,38,58,60,62,64,70,83,107,110,133,141] Studies in clusters have demonstrated that the addition of only a few water molecules can have a significant effect on the barrier height.[31,53,109,147]

With the exception of one study by Re and Laria,[109] the theoretical attempts to investigate this reaction in water clusters have been limited to small clusters, so the nature of the transition to bulk behavior could not be elucidated. In this chapter, we go beyond the classical potential energy function used in Reference 109 and utilize a recently developed[21] empirical valence bond (EVB) model to examine the stepwise hydration of the simple benchmark symmetric S_N2 reaction $Cl^- + CH_3Cl \longrightarrow CH_3Cl + Cl^-$ in different-sized water clusters from 3 to 40 water molecules. For each cluster, we calculate the reaction free-energy profile and several structural and dynamical characteristics of the reaction, taking into account the influence of the water molecules on the evolving electronic state of the solute as a function of the reaction coordinate.

The rest of the chapter is organized as follows: In Section 3.2 we briefly re-

view the main features of the EVB model and the methodology used to compute the free energy and the dynamical corrections to the transition state theory rate constant. In Section 3.3, the results of the reaction free-energy profile, as well as the structural and time-dependent calculations are described and discussed. A summary and conclusions are given in Section 3.4.

3.2 Systems and Methods

3.2.1 The empirical valence bond (EVB) model

A simple and straightforward way to describe the changing electronic structure along the reaction coordinate, including a realistic description of the solvent, is based on the empirical valence bond model first developed by Warshel and coworkers.[60,141] The method we used is similar, and it was discussed in an earlier publication[21] in detail. Here we briefly summarize the main ideas. For other theoretical approaches, the reader should consult Reference 53 and more recent references.[70,91,106,108,116]

To describe the reactive solute molecules in the water cluster, we assume that only two orthonormal valence states, $\psi_1 = \mathrm{Cl{-}CH_3\ Cl:^-}$ and $\psi_2 = \mathrm{Cl:^-\ CH_3{-}Cl}$, contribute to the total wave function of the solute:[21,83]

$$\Psi = c_1\psi_1 + c_2\psi_2, \qquad \langle \psi_1 \,|\, \psi_2 \rangle = \delta_{ij} \tag{3.1}$$

The total Hamiltonian in this representation is written as:

$$\hat{H} = \begin{pmatrix} H_{11}(\vec{r}_i, \vec{r}_d, \vec{r}_s) & H_{12}(r_1, r_2, \theta) \\ H_{12}(r_1, r_2, \theta) & H_{22}(\vec{r}_i, \vec{r}_d, \vec{r}_s) \end{pmatrix}, \tag{3.2}$$

where H_{11} and H_{22} are the diagonal diabatic Hamiltonians, which include the kinetic energy of all atoms, the gas phase interaction between the Cl^- ion and the CH_3Cl molecule and the water, the water–ion and the water–CH_3Cl potential energies. Due to the symmetry of the reaction H_{11} and H_{22} have the same functional form, but with the two chlorine atom labels interchanged. The kinetic energy terms in H_{11} and H_{22} are identical and since they appear only in the diagonal terms, they could be pulled out of the Hamiltonian matrix, leaving H_{11} and H_{22} to be just the classical potential energies described above. The off-diagonal electronic coupling term H_{12} in Eq. 3.2 is the one suggested by Hynes and coworkers:[83,130]

$$H_{12} = -QS(r_1)S(r_2) \tag{3.3}$$

where r_1 and r_2 are the distances between the two chlorine atoms and the carbon atom and $S(r)$ is the overlap integral for the sigma orbital formed from the carbon 2p and chlorine 3p atomic orbitals. $S(r)$ is determined using Slater-type orbitals and the approximation of Mulliken et al.[93] $Q = 678.0$ kcal/mol is a parameter which is fitted to obtain the correct gas-phase activation energy.

The details of all the potential energy terms mentioned above are given in Ref. 21. Here we briefly describe some of their most important characteristics. The

(global) gas-phase potential energy for $Cl^- + CH_3Cl$ is a generalization to non-collinear geometries of the form suggested by Mathis et al.[83] It includes a Morse potential for the CH_3Cl bond, an exponential repulsive term for the interaction between the Cl^- ion and the CH_3 radical, an ion–dipole term for combined short-range repulsion and long-range attractive interactions between the Cl^- ion and the CH_3Cl molecule, and a bending energy term. These terms are obtained from a fit to the *ab initio* calculations of Tucker and Truhlar[131] and to experimental data.[83] The intermolecular potential energy terms for water and for the water–solute interactions are all given by the sum of Lennard-Jones plus Coulomb interactions between every pair of sites on different molecules. The partial charges on the CH_3Cl are selected to reproduce its experimental dipole moment of 1.94 Debye.[85] The water model is a flexible SPC model extensively used.[94]

The diagonalization of Eq. 3.2 yields the electronic ground-state adiabatic Hamiltonian as a function of all nuclear coordinates:

$$H_{ad} = \tfrac{1}{2}(H_{11} + H_{22}) - \tfrac{1}{2}[(H_{11} - H_{22})^2 + 4H_{12}^2]^{1/2}. \tag{3.4}$$

This Hamiltonian is used for the classical dynamics of the system. The gas-phase adiabatic ground-state potential energy is given by the same expression, except that the diabatic terms (denoted here with the 0 superscript) include the gas-phase potentials only:

$$U_{ad}^0 = \tfrac{1}{2}(H_{11}^0 + H_{22}^0) - \tfrac{1}{2}[(\Delta H^0)^2 + 4H_{12}^2]^{1/2}, \tag{3.5}$$

where $\Delta H^0 = H^0_{11} - H^0_{22}$. Thus U^0_{ad} is a function of r_1, r_2, and the Cl−C−Cl bending angle θ. If one defines the reaction coordinate as follows:

$$\xi = r_2 - r_1, \tag{3.6}$$

(so the reactants and products correspond to $\xi \ll 0$ and $\xi \gg 0$, respectively), then the minimum energy path along ξ for the collinear geometry ($\theta = 180°$) has the well-known characteristic of a double well. The transition state is located at $r_1 = r_2 = 2.19$ Å and has an energy of only 2.74 kcal/mol above the energy of the separate reactants, but an activation energy of 13.72 kcal/mol above the ion–dipole minimum (see Fig. 3.1).

3.2.2 Reaction free-energy profile

The reaction free-energy profile as a function of the reaction coordinate, $\xi = r_2 - r_1$, is calculated using umbrella sampling with overlapping windows and a biasing potential,[36] according to:

$$\begin{aligned} W(\xi) &= -\beta^{-1} \ln P(\xi) - U_b(\xi) \\ P(\xi) &= \frac{\int \delta(r_1 - r_2 - \xi) exp[-\beta(H_{ad} + U_b(\xi)] d\Gamma}{\int exp(-\beta H_{ad}) d\Gamma} \end{aligned} \tag{3.7}$$

where $\beta = 1/k_B T$ (k_B being the Boltzmann constant and T the temperature) and $U_b(\xi)$ is an arbitrary analytic function of ξ. This function is chosen to be a reasonable estimate of $-W(\xi)$ in order to "flatten" the distribution $P(\xi)$ so as to

accelerate the convergence of the ensemble average in Eq. 3.7. We chose for the biasing potential an approximate Gaussian-plus-exponential fit of the transition-state region of the free-energy profile in bulk water.[21]

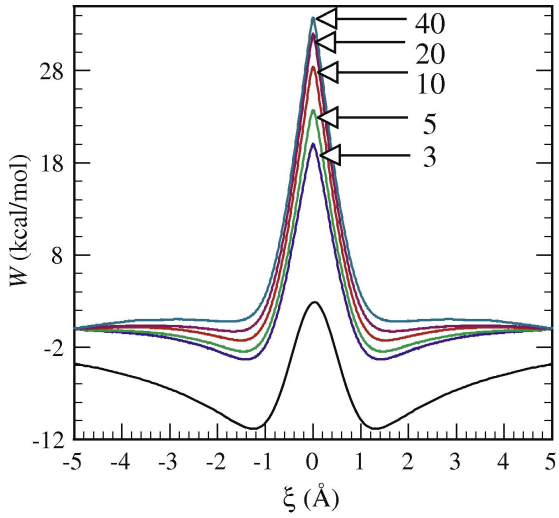

Figure 3.1: The free energy along the reaction coordinate for the $Cl^- + CH_3Cl$ reaction taking place in several water clusters (colored lines). The lines are labeled by the number of water molecules in the cluster, N_w. Also shown is the minimum energy path for the collinear geometry in the gas phase (black). The temperature is T = 175 K for all the clusters.

The reaction free-energy-calculations in the interval $|\xi| < 5.3$ Å, (which is where the free energy profile reaches a plateau) are done by dividing the interval into "windows" that are mostly 0.5 Å wide (narrower near the transition state to increase accuracy) and have a 0.2 Å overlap with the two neighboring windows. Calculations are done for both the $\xi > 0$ and $\xi < 0$ regions despite the symmetry of the reaction, as an additional check for convergence. In each window, a total simulation time of 4 ns allows for an accurate calculation of the probability $P(\xi)$,

from which the free-energy profile is determined using Eq. 3.7, with a statistical error that is less than 0.1 kcal/mol. Other details about the exact umbrella sampling procedure are given in Ref. 21.

The equilibrium free-energy calculations are done at a constant temperature of T = 175 K using a combination of the Andersen stochastic method and the Nosé-Hoover thermostat.[104] The integration time step is 0.1 fs for all systems, using the velocity version of the Verlet algorithm.[5]

3.2.3 Reaction rate

The reaction rate is given by $k = \kappa A e^{-\beta \Delta A^{\ddagger}}$, where $\Delta A^{\ddagger}$ is the activation free-energy obtained from the reaction free-energy profile $W(\xi)$, A is the pre-exponential factor, and $\kappa < 1$ is the transmission coefficient, which accounts for the fraction of trajectories that end as products given that they reach the transition state and head towards the products state. κ can be calculated using the reactive flux correlation function formalism,[28,52,61,142] by following the dynamics of a flux-weighted Maxwell-Boltzmann distribution of solute molecules initially constrained to the transition state configuration [$Cl^{\delta-}-CH_3-Cl^{\delta-}$], $\delta \approx 0.5$). The normalized flux correlation function can be calculated using[52]

$$\kappa(t) = N_+^{-1} \sum_{i=1}^{N_+} \theta[\xi_i^+(t)] - N_-^{-1} \sum_{i=1}^{N_-} \theta[\xi_i^-(t)], \tag{3.8}$$

where $\xi_i^{\pm}$ is the value of the reaction coordinate for the ith trajectory at time t, given that at $t = 0$ $d\xi/dt$ is positive (negative), $N_+(N_-)$ is the corresponding number of trajectories, and θ is the unit step function. Once recrossings of the transition state no longer occur, $\kappa(t)$ reaches the fixed value of κ.

$\kappa(t)$ is determined by first equilibrating the system at a constant temperature (175 K) with the constraint $\xi = 0$ for 1 ns, saving 100 independent configurations. These 100 equilibrated independent transition-state configurations are used to run 4000 constant-energy trajectories using 40 different selections of flux-weighted initial velocities per configuration. Each trajectory is integrated for 0.2 ps, which is long enough for $\kappa(t)$ to reach its plateau value κ. This procedure is repeated for every cluster size.

3.3 Results and Discussion

3.3.1 Reaction free-energy profiles

The results of the umbrella-sampling calculations of the free-energy profile $W(\xi)$ for the $[Cl^- + CH_3Cl \longrightarrow CH_3Cl + Cl^-](H_2O)_{N_w}$ reaction for a selection of water cluster sizes N_w is shown in Fig. 3.1. The gas-phase potential energy along the minimum energy path for the collinear reaction geometry is also shown. As the number of water molecules (N_w) increases, the preferential hydration of the chloride ion

over that of the transition state's more delocalized charges $Cl^{0.5-}-CH_3-Cl^{0.5-}$ results in a lowering of the free energy of the reactants and products relative to the transition state. This well-known[62,110] effect gives rise to a marked increase in the activation free-energy $\Delta A^{\ddagger}$ and to a gradual disappearance of the double-well minimum as N_w increases. The calculated activation free-energy as a function of N_w for all the clusters studied is shown as black circles in Fig 3.2

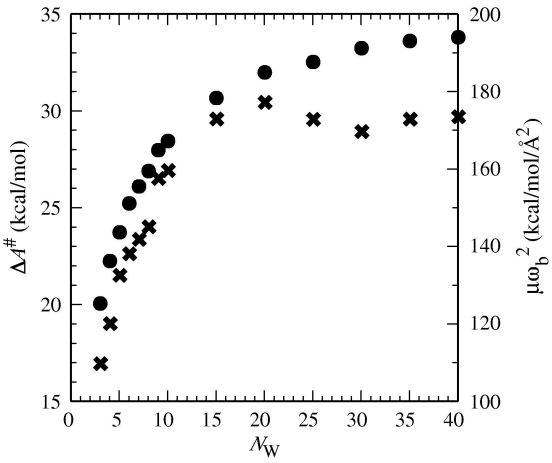

Figure 3.2: The activation free energy (•) and the barrier curvature (×) of the reaction $Cl^- + CH_3Cl \longrightarrow CH_3Cl + Cl^-$ as a function of the number of water molecules in the cluster.

The increase in $\Delta A^{\ddagger}$ with N_w is monotonic, rising very rapidly with N_w for small clusters, but leveling off at around 33 kcal/mol as N_w approaches the largest cluster studied. This correlates quite clearly with the increase of the (negative) chloride ion–water hydration energy with N_w (not shown). The value in bulk water calculated with the same model potentials at 298 K is 29.5 ± 0.3 kcal/mol.[21] The larger value in the biggest clusters studied here compared with bulk water is

consistent with negative entropy of activation (and the lower temperature of the clusters). These results are also consistent with the calculation of the reaction profile in large (> 32) water clusters[109] using the LEPS classical potential with the charge switching function.

Another important characterization of the reaction free-energy profile is its negative curvature (2nd derivative) at the transition state, which is typically expressed using an effective mass μ and the (equilibrium) barrier frequency ω_b by:

$$\mu\omega_b^2 = -\left(\frac{\partial^2 W(\xi)}{\partial \xi^2}\right)_{\xi=0}. \tag{3.9}$$

This quantity determines the thermally average acceleration experienced by the reaction coordinate at the transition state. It is shown in Fig. 3.2 as a function of cluster size (depicted on the right axis). Starting from a value of 59 kcal $\text{mol}^{-1}\text{Å}^{-2}$ in a vacuum, there is a very rapid increase that is nearly monotonic, and which levels off when the cluster size approaches 25 water molecules at values that are close to that of the reaction in bulk water[21] (180 kcal $\text{mol}^{-1}\text{Å}^{-2}$). As the system is moved away from the transition state, the average force on the reaction coordinate varies due to the intrinsic gas-phase potential energy function and two distinct medium contributions. One of them reflects the rapid change in the solute charge distribution and the corresponding change in the solvation energy. The other represents a negative contribution to the barrier frequency corresponding to the fact that the solvent configuration at the transition state is a

local minimum in the solvent free energy. These two effects are of course coupled, as will be discussed below. Central to a quantitative discussion of the effect of the water molecules on the reaction free energy (and other properties) is the concept of solvent coordinate, which we discuss next.

3.3.2 Solvent coordinate and solvent configuration

In the discussion below we freely use the word "solvent" to refer to the water molecules in the cluster. The configuration of water molecules around the reactants, transition state, and products, which is fundamental to understanding the medium effects on the reaction, can be expressed in varying degrees of detail. A very simple one-dimensional scalar quantity that is quite helpful is the so-called "solvent coordinate"', denoted by s, which we define by looking at the energy gap between the two diabatic states at some fixed solute and water configuration: $\Delta H = H_{11} - H_{22}$. This difference is comprised of the vacuum energy difference, ΔH^0, and the *solvent contribution*, which we use as the definition of s:

$$H_{11} - H_{22} = \Delta H^0 + s. \tag{3.10}$$

This definition is similar to the one used in simulations of electron transfer reactions in polar solvents.[71]

As the system moves along the reaction coordinate, the interaction of the two diabatic states with the water molecules depends on the configuration of the

water molecules. The solvent coordinate replaces this detailed information by a single number, s. At each fixed value ξ of the reaction coordinate, s depends on the solvent configuration and fluctuates as the positions and orientations of these water molecules fluctuate. A useful characterization of the solvent configuration is the equilibrium ensemble average of s at fixed ξ, $s_{eq}(\xi) = \langle s(\xi) \rangle$.

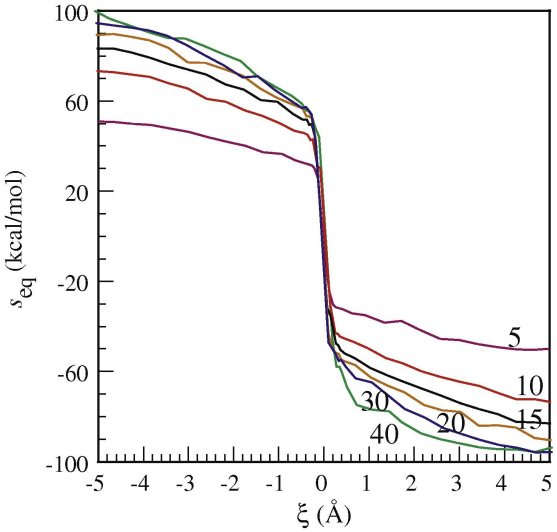

Figure 3.3: The equilibrium value of the solvent coordinate s as a function of the reaction coordinate ξ for selected cluster sizes, as indicated.

Fig. 3.3 shows the equilibrium average $s_{eq}(\xi)$ as a function of the reaction coordinate ξ for the selected cluster sizes. Because of the symmetry of the transition state, we must have $s_{eq}(\xi = 0) = 0$. As the system moves away from the transition state, an asymmetric charge distribution is developed. There is a significantly more favorable interaction of the water molecules with the localized charge of Cl^- than with the dipolar CH_3Cl molecule, making the corresponding diabatic state

much lower in energy, which is reflected by the large increase in $|s_{eq}|$ as ξ varies from zero. The rate at which s_{eq} varies with ξ (the slope of the line at $\xi = 0$) increases with the cluster size due to the increased strength of the interaction between the water molecules and the localized charge distribution that develops on the nucleophile. This very rapid increase becomes much more gradual when $|\xi|$ increases past 0.2 Å and slowly reaches an asymptotic value that depends on the cluster size. This value converges to near 90 kcal/mol as the cluster size reaches about 30 water molecules. The asymptotic value in bulk water at T = 298 K, $s_{eq}(|\xi| \to \infty) = 85$ kcal/mol,[21] is slightly smaller than the above values of the largest clusters due to higher temperature.

As a more detailed way to quantify the hydration structure as a function of the reaction coordinate and cluster size, we have examined the spatial distribution of the water molecules around the solute. It is not surprising that for small cluster size, the symmetric water arrangement around the solute when the system is at the transition state becomes highly asymmetric as soon as the reaction coordinate reaches a value as low as 0.5 Å. It is interesting that this is also the case for the larger cluster, as shown in Fig. 3.4. This behavior is consistent with the rapid change in the solvent coordinate as the system moves away from the transition state.

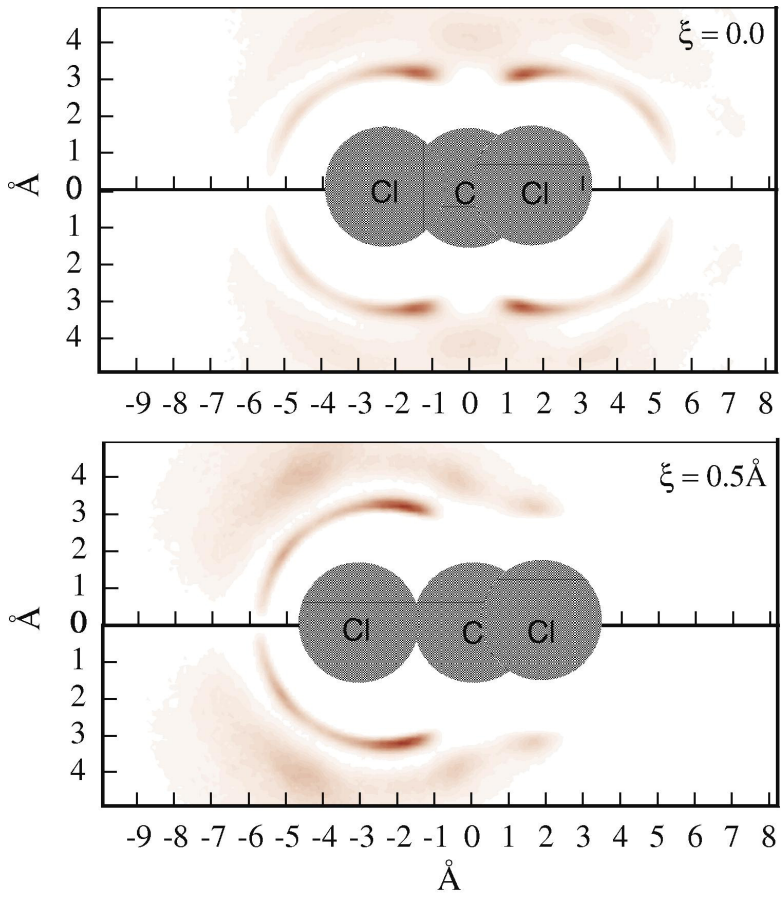

Figure 3.4: The probability distribution of finding an oxygen water atom around the reactive system atoms in a 30 water molecule cluster. The reactants' configuration corresponds to a fixed value of the reaction coordinate ξ. Top panel: $\xi = 0$, bottom panel: $\xi = 0.5$ Å.

3.3.3 Solute charge variation

The empirical valence bond model allows for a very simple representation of the fact that as the reaction proceeds, the contribution of the two diabatic states varies and is solvent-dependent. The total wavefunction is given by the solution

for c_1 and c_2:

$$c_1^2 = \frac{1}{2 + \chi^2/2 + \chi(1 + \chi^2/4)^{1/2}} \qquad c_2^2 = 1 - c_1^2 \tag{3.11}$$

where

$$\chi = \chi_0 = \Delta H^0/H_{12} \quad \text{in the gas phase,}$$

$$\chi = (H_{11} - H_{22})/H_{12} = (\Delta H^0 + s)/H_{12} = \chi_0 + s/H_{12} \quad \text{in solution.} \tag{3.12}$$

(See Eqs. 3.4, 3.5, and 3.10.) The effective charge on the leaving group is given by $-c_1^2$. Because of the reaction's symmetry, at the transition state $r_1 = r_2$, so $\chi_0 = 0$ in a vacuum. In the cluster, χ is a function of the water molecules' configuration, but its average $\langle\chi\rangle = \chi_0 + s_{eq}/H_{12}$ is zero because of the symmetry of the solvent configuration, $s_{eq}(\xi = 0) = 0$. Thus, at the transition state ($\xi = 0$): $c_1^2 = c_2^2 = 1/2$. Since the coupling H_{12} exponentially decreases to zero as $|\xi|$ increases, one gets $\chi \to \pm\infty$, and thus $c_1^2(\chi \to \infty) = 0$, $c_1^2(\chi \to -\infty) = 1$. Thus, as ξ varies from $-\infty \to +\infty$, the ground state varies from $\psi_2(c_1 = 0, c_2 = 1)$ to $\psi_1(c_1 = 1, c_2 = 0)$. In practice, the limiting values of 0 and 1 for c_1 (and c_2) are reached for $|\xi|$ near 1 Å.

As noted above, the reaction free energy and the water structure variation with the reaction coordinate are intimately related to the variation in the solute molecules' charge distribution. Fig 3.5 demonstrates the sensitivity of the solute charge distribution to the value of the reaction coordinate for some selected clus-

ters and shows as comparison the behavior in a vacuum and in bulk water (at 298 K).

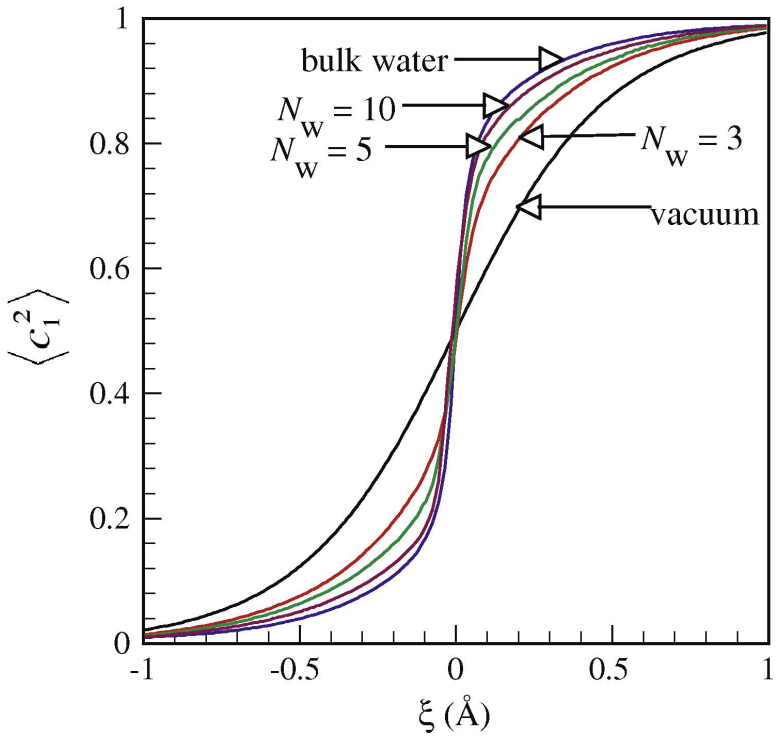

Figure 3.5: Equilibrium average quantum population of one of the diabatic states as a function of the reaction coordinate. The different lines are for the reaction in several cluster sizes, in a vacuum, and in bulk water (at 298 K), as labeled.

As the reaction coordinate varies from $-\infty$ to $+\infty$, c_1^2 varies from 0 to 1, and the charge distribution on the solute atoms varies accordingly. At the transition state ($\xi = 0$), as explained above, $\langle c_1^2 \rangle \approx 1/2$ for all of the systems. Since H_{12} decays exponentially as the system moves away from the transition state and $|\xi|$ increases from zero, c_1^2 varies rapidly. The rate of this variation depends on the medium. The larger the number of water molecules, the larger the stabilization

energy of the non-symmetric charge distribution that is developed as soon as $|\xi|$ increases from zero, and the more rapid the change in c_1^2. This rate is closely related to the 'electronic state switching rate', which was assumed to be fixed in a previous treatment of this system.[109]

The trend observed for $\langle c_1^2(\xi)\rangle$ with N_w is consistent with the variations observed in other properties discussed above. However, it is interesting to note that the rate of change of $\langle c_1^2(\xi)\rangle$ already reaches the value similar to that in bulk water for clusters as small as 10 water molecules. This suggests that most of the influence on $\langle c_1^2(\xi)\rangle$ is due to the nearest water molecules, unlike the case of the activation free energy (Fig. 3.2) or the asymptotic value of the solvent coordinate (Fig. 3.3).

3.3.4 Reaction dynamics

The dynamical correction to the transition state theory rate constant κ, calculated as discussed in Section 3.2.3 from the plateau value of the reactive flux correlation function $\kappa(t)$ is summarized in Fig 3.6. The figure depicts the value of κ as a function of cluster size and shows as an insert the normalized flux correlation function for two extreme-sized clusters.

Dynamical studies of this reaction in bulk water[21,27] suggest that recrossing of the transition state in trajectories which are temporarily trapped in that region is

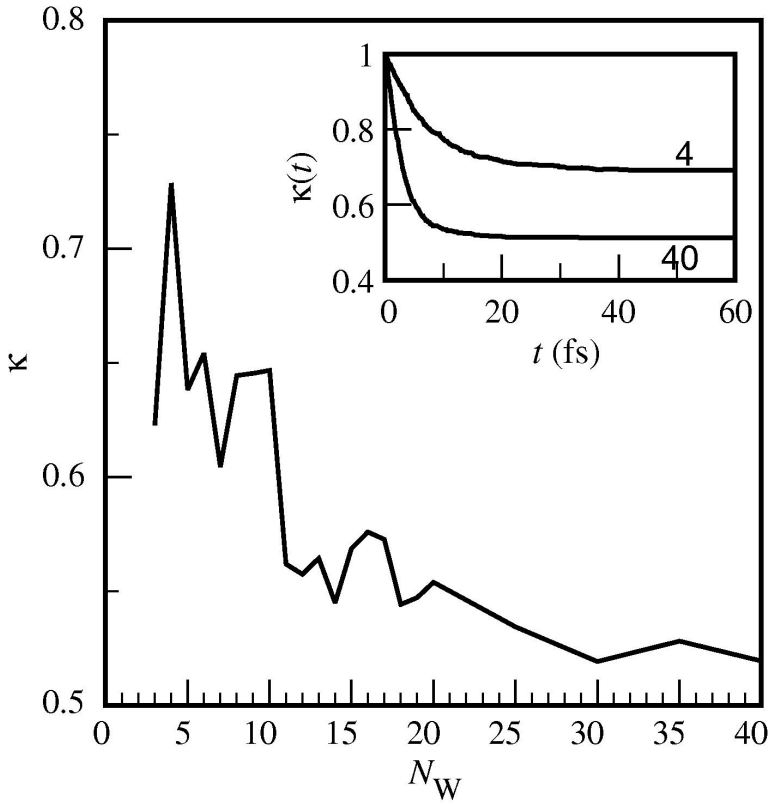

Figure 3.6: The transmission coefficient for the $Cl^- + CH_3Cl \longrightarrow CH_3Cl + Cl^-$ reaction in water clusters as a function of cluster size. The insert shows the reactive flux correlation function for two cluster sizes, as indicated.

responsible for the fact that κ is less than unity. This trapping is due to the fact that the water molecules, which are equilibrated to the transition-state charge distribution, are not properly oriented to solvate the product charge distribution. This may give rise to an additional temporary (polarization) barrier that prevents the system from directly proceeding to the product side.[51]

Since this situation prevails also in the cluster $\langle s(\xi = 0)\rangle \ll |\langle s(|\xi| > 0)\rangle|$, we expect similar behavior and an increase in the fraction of trajectories that recrosses

the transition state as the cluster becomes larger. While generally speaking κ indeed falls off with the cluster size, approaching the value in bulk water ($\kappa = 0.57$), the behavior is quite erratic for the smallest clusters. It is interesting that an examination of the thousands of trajectories used to compute the reactive flux shows that while the rapid decay in $\kappa(t)$ is mostly due to trajectories that recrossed the transition state within the first 10 fs after leaving the transition state, these trajectories remained near the transition state. Trajectories that reach the ion–dipole complex minimum-energy region are not able to climb back and recross the transition state even in the smallest clusters. This suggests that there is an efficient energy flow from the reactive atoms to the water molecules. This energy appears as an increase in the temperature of the water molecules. It is not transmitted back to the reaction coordinate on the simulation time scale, and thus the reactants are unable to return to the transition state.

3.4 Summary and Conclusions

The detailed study of the benchmark $Cl^- + CH_3Cl$ S_N2 reaction in water clusters of different sizes, using the empirical valence bond model with the fully molecular solvent description, provides quantitative insight into how a few water molecules change the electronic structure and other structural and energetic properties along the reaction coordinate. The study demonstrates that the con-

vergence to bulk behavior occurs with different rates, depending on the quantity studied. Thus, while the activation free energy and dynamical correction to the rate constant reach about 90% of the values in bulk water for clusters made up of 12-15 water molecules, the rate of change of the solute charge distribution at the transition state converges more rapidly. This reflects the important contribution of the nearby water molecules. Dynamic calculations show that the deviations from the transition state theory due to barrier recrossings are not large, and are mostly smaller than those in bulk water.

Acknowledgements

This work has been supported by a grant from the National Science Foundation (CHE-0809164).

Chapter 4

Effect of a Phase Transfer Catalyst on the Dynamics of an S_N2 Reaction. A Molecular Dynamics Study

4.1 Introduction

Phase transfer catalysis (PTC) is an environmentally friendly and economically feasible approach to organic synthesis involving reactants that are not miscible in the same phase. The phase transfer agent (acting in catalytic amounts) fa-

cilitates the transport of one reactant into the phase where the second reactant exists. A common example is the transport of a water-soluble nucleophilic anion (Y^-) by a quaternary ammonium cation (Q^+) to the organic phase where a water-insoluble electrophilic reagent RX resides. The catalytic action is based on (among several things) the condition that the catalyst–nucleophile ion pair (Q^+Y^-) is favorably partitioned into the organic phase, that the nucleophilic substitution (S_N2) reaction $Q^+Y^- + RX \rightarrow RY + Q^+X^-$ in the organic phase is fast and that the Q^+X^- ion pair is favorably partitioned into the aqueous phase. There is extensive chemical and engineering literature on the subject, which has been reviewed.[3,47,80,95,119,123,135]

Most of our fundamental understanding of the PTC process is based on kinetic studies and mathematical modeling involving chemical kinetics and mass transport.[95] However, several important issues affecting the PTC process require a molecular-level understanding of the multiple steps involved:

1. In many cases, and this is typically the situation for the S_N2 reaction mentioned above, the reaction barrier is highly sensitive to the polarity of the solvent.[6,38,58,60,62,64,70,83,107,110,133,141] Second harmonic generation spectroscopy experiments[136,138,139,144,145] and molecular dynamics simulations[18,20,87] have demonstrated that the polarity of the interfacial region could be significantly different from that of the two bulk phases and strongly dependent on surface location and orientation. Determining the sensitivity

of the catalyzed reaction to the reactants' surface location and orientation is thus critical for correct PTC modeling.

2. Experimental studies have demonstrated that the hydration state of the anion strongly influences its organic phase nucleophilicity.[4,76,79] It is also well known that ions and ion pairs transported across organic/aqueous interfaces may be accompanied by water molecules.[22,30,113,135] Taking into account the hydration state of the nucleophile during the PTC process is thus important.
3. PTC kinetic modeling and theoretical analysis assume that the role of the catalyst is limited to bringing the nucleophile across the interface. While bulk studies have shown that the ion-paired anion is usually less reactive than the naked anion,[110] the possibility that the catalyst may affect the reaction thermodynamics at the interface has not been studied theoretically. In addition, it is not clear whether the anion–catalyst ion pair remains in contact during the reaction or how hydration by a small number of water molecules influences its stability.

We have recently developed a fully molecular empirical valence bond (EVB) model for the simple benchmark symmetric S_N2 reaction $Cl^- + CH_3Cl \longrightarrow CH_3Cl + Cl^-$ and used it to examine in detail issues 1 and 2 above.[21,97,98] We found that the activation free energy is sensitive to the reagents' location relative to the interfacial region and to the orientation of the nucleophilic attack. The barrier height at the

interface is *equal to or slightly larger than* the barrier in bulk water and approaches the value in bulk chloroform only when the solute is a few nanometers deep into the organic phase. We showed that this is due to the ability of the nucleophile to keep part of its hydration shell when it is transferred from the aqueous to the organic solution. This suggests that, for appreciable acceleration of the reaction rate relative to that in bulk water, the reaction should take place away from the interface region. The "polluting" effect of few water molecules on the rate is consistent with experiments.[4,75,76,79]

In this chapter we consider in detail the issues listed under 3 above. By calculating the reaction free energy profile with the catalyst present at different interface locations, we can determine the structure of the activated complex and whether the catalyst affects the thermodynamics and the dynamics of the reaction. By repeating these calculations in bulk chloroform with the catalyst–nucleophile complex hydrated by a small number of water molecules $(Q^+Y^-)(H_2O)_n$, n = 0 - 5, we can also determine how hydration by a small number of water molecules influences the stability and the structure of the complex and the thermodynamics and dynamics of the reaction.

The rest of the chapter is organized as follows: In Section 4.2 we briefly review the main features of the EVB model and the methodology used to compute the free energy and the dynamical corrections to the transition state theory rate. In Section 4.3, the results of the reaction free-energy profile, as well as the structural

and time-dependent calculations, are described and discussed. A summary and conclusions are given in Section 4.4.

4.2 Systems and Methods

4.2.1 The empirical valence bond (EVB) model.

Several theoretical approaches are available for the modeling of S_N2 reactions in solution.[53,70,91,106,108,116] We chose the EVB model, first developed by Warshel and coworkers,[60,141] as a simple and straightforward way to take into account the solvent response and its influence on the changing solute electronic structure along the reaction coordinate. The details of our particular implementation of the EVB method are described in an earlier publication.[21] Here we briefly summarize the main features.

To describe the reactive solute molecules in the condensed phase, we assume that only two orthonormal valence states, ψ_1 = Cl$-$$CH_3$ Cl:$^-$ and ψ_2 = Cl:$^-$ CH_3-Cl, contribute to the total wave function:[21,83]

$$\Psi = c_1\psi_1 + c_2\psi_2 \qquad \langle\psi_1 \,|\, \psi_2\rangle = \delta_{ij} \tag{4.1}$$

The total Hamiltonian in this representation is written as:

$$\hat{H} = \begin{pmatrix} H_{11} & H_{12} \\ H_{12} & H_{22} \end{pmatrix}, \tag{4.2}$$

where H_{11} and H_{22} are the diagonal diabatic Hamiltonians, which, due to the symmetry of the reaction, have the same functional form but with the two chlorine atom labels interchanged. Each of them has the form:

$$H_{11} = E_k + U_{11}^0 + U_W + U_C + U_T + \sum_{\mu \neq \nu} U_{\mu\nu} \tag{4.3}$$

where E_k is the kinetic energy of all atoms and $U_{11}^0(r_1, r_2, \theta)$ is the global gas-phase potential energy for the $Cl^- + CH_3Cl$ reactive system, in which r_1 is the C−Cl bond distance in CH_3Cl, r_2 is the distance between the Cl^- ion and the carbon atom, and θ is the $Cl^- - CH_3 - Cl$ angle. U_W and U_C are the pure water and chloroform solvents' potential energies, respectively. U_T is the tetramethylammonium cation (TMA^+) intramolecular potential energy. The last term is a sum over the nine intermolecular interaction potentials between the different chemical species in the system (water–chloroform, water–TMA^+, water–Cl^-, water–CH_3Cl, chloroform–TMA^+, chloroform–Cl^-, chloroform–CH_3Cl, TMA^+–Cl^-, and TMA^+–CH_3Cl).

The detailed mathematical expression of the gas-phase potential energy, U_{11}^0 (and U_{22}^0), is given in Ref. 21. Briefly, it is a generalization to noncollinear geometries of the form used by Mathis et al.[83] It includes a Morse potential for the $CH_3 - Cl$ bond, an exponential repulsive term for the interaction between the Cl^- ion and the CH_3 radical, and an ion–dipole term for combined short-range repulsion and long-range attractive interactions between the Cl^- ion and the CH_3Cl bond. These terms are obtained from a fit to the *ab initio* calculations of Tucker

and Truhlar[131] and to experimental data.[83] The generalization to nonlinear geometry is done by making some of the potential energy parameters dependent on the $Cl^-{-}CH_3{-}Cl$ angle θ and by adding a bending energy term with parameters determined by a best fit to the gas-phase *ab initio* values of the energy, location of the transition state, and the ion–dipole well depth as a function of θ.

The intermolecular terms appearing in the solvent potentials (U_W, U_C, and U_T) and in the sum $\sum_{\mu\neq\nu} U_{\mu\nu}$ appearing in Eq. 4.3 are all given by the sum of Lennard-Jones plus Coulomb interactions between every pair of sites on different molecules:

$$u_{ij} = 4\epsilon_{ij}\left[\left(\frac{\sigma_{ij}}{r_{ij}}\right)^{12} - \left(\frac{\sigma_{ij}}{r_{ij}}\right)^{6}\right] + \frac{q_i q_j}{4\pi\epsilon_0 r_{ij}} \tag{4.4}$$

where i and j are two sites on two different molecules, r_{ij} is the distance between the sites, and ϵ_0 is the vacuum permittivity constant. The Lennard-Jones parameters σ_{ij} and ϵ_{ij} are determined from the parameters of the different sites by the usual combination rules:[54] $\sigma_{ij} = (\sigma_{ii} + \sigma_{jj})/2,\ \epsilon_{ij} = (\epsilon_{ii}\epsilon_{jj})^{1/2}$. The partial charges on the CH_3Cl are selected to reproduce its experimental dipole moment of 1.94 D.[85] These parameters, together with the Lennard-Jones parameters for the Cl^- ion and the CH_3Cl molecule, are given in Ref. 21. The Lennard-Jones parameters and the charges for the different sites on the chloroform molecule were selected to reproduce a number of solvent bulk properties and structures. In addition, the chloroform potential energy function includes intramolecular stretching and bend-

ing terms. The solvents' Lennard-Jones parameters, the intramolecular potential terms, and the corresponding intramolecular parameters can be found elsewhere.[13] For other force-field models for chloroform see Refs. 39, 40, 57. The water model was selected to be the model previously used to study the bulk and interfacial properties of water. The water and chloroform potentials used here give rise to a stable liquid–liquid interface with a surface tension of 25 ± 3 dyn/cm. For TMA^+, we use the Lennard-Jones, Coulomb, and intramolecular force field parameters of Ref. 117.

The off-diagonal electronic coupling term H_{12} in Eq. 4.2 is assumed to be:[83,130]

$$H_{12} = -QS(r_1)S(r_2) \tag{4.5}$$

where S(r) is the overlap integral for the σ orbital formed from the carbon 2p and chlorine 3p atomic orbitals, calculated using Slater-type orbitals and the approximation of Mulliken et al.[93] $Q = 678.0$ kcal/mol is a parameter which is fitted to obtain the correct gas-phase activation energy.

The diagonalization of Eq. 4.2 yields the electronic ground state adiabatic Hamiltonian as a function of all nuclear coordinates:

$$H_{ad} = \tfrac{1}{2}(H_{11} + H_{22}) - \tfrac{1}{2}[(H_{11} - H_{22})^2 + 4H_{12}^2]^{1/2}. \tag{4.6}$$

This Hamiltonian is used for the classical dynamics of the system. The gas-phase adiabatic ground-state potential energy is given by the same expression, except

that the diabatic terms include the gas-phase reaction potential only:

$$U^0_{ad} = \tfrac{1}{2}(U^0_{11} + U^0_{22}) - \tfrac{1}{2}[(\Delta U^0)^2 + 4H^2_{12}]^{1/2}, \tag{4.7}$$

where $\Delta U^0 = U^0_{11} - U^0_{22}$. U^0_{ad} is a function of r_1, r_2, and the Cl−C−Cl bending angle θ. Choosing the reaction coordinate to be:

$$\xi = r_2 - r_1 \tag{4.8}$$

(so the reactants and products correspond to $\xi \ll 0$ and $\xi \gg 0$, respectively) one finds that the minimum energy path along ξ for the collinear geometry ($\theta = 180°$) has the well-known characteristic of a double well. The transition state is located at $r_1 = r_2 = 2.19$ Å and has an energy of only 2.74 kcal/mol above the energy of the separate reactants, but an activation energy of 13.72 kcal/mol above the ion–dipole double minimum.

4.2.2 Reaction free-energy profile.

To obtain the activation free energy (among other important properties), the reaction free-energy profile as a function of the reaction coordinate, $\xi = r_2 - r_1$, is calculated using umbrella sampling with overlapping windows and a biasing potential,[36] according to:

$$\begin{aligned} W(\xi) &= -\beta^{-1} \ln P(\xi) - U_b(\xi) \\ P(\xi) &= \frac{\int \delta(r_1 - r_2 - \xi) \exp[-\beta(H_{ad} + U_b(\xi)] d\Gamma}{\int \exp[-\beta(H_{ad})] d\Gamma} \end{aligned} \tag{4.9}$$

where $\beta = 1/k_BT$ (k_B being the Boltzmann constant and T the temperature) and $U_b(\xi)$ is the biasing potential—an arbitrary analytic function of ξ, chosen to be a reasonable estimate of $-W(\xi)$ to accelerate the convergence of the ensemble average in Eq. 4.9. For the biasing potential we chose $U_b(\xi) = 20.6928e^{-2.63322\xi^2}$ kcal/mol, which is an approximate Gaussian fit of the free energy profile of the reaction (without the catalyst) in bulk chloroform.[21]

The reaction free-energy calculations in the interval $|\xi| < 3.7$ Å, (which is where the free energy profile reaches a plateau) are done by dividing the interval into windows that are 0.5 Å wide and have a 0.2 Å overlap with the two neighboring windows. To increase accuracy near the transition state, the interval $|\xi| < 0.5$ Å is divided into windows that are 0.2 Å wide. Calculations are done for both the $\xi > 0$ and the $\xi < 0$ regions, despite the symmetry of the reaction, to improve convergence. In each window a total simulation time of 1 ns allows for an accurate calculation of the probability $P(\xi)$, from which the free energy profile is determined using Eq. 4.9, with a statistical error that is less than 0.1 kcal/mol. Other details about the exact umbrella-sampling procedure are given in Ref. 21. The simulations in each window are also used to compute ensemble averages of a number of system properties as a function of ξ. This includes the interaction energy of the two solvents with the reactants and products, the system wave function (c_1^2), and the location distribution of the catalyst.

4.2.3 Reactive flux calculations

The reaction free-energy profile $W(\xi)$ determined above can be used to compute the activation free energy E_a and from that an estimate of the transition state theory (TST) value of the rate constant $k_{\mathrm{TST}} = Ae^{-\beta E_a}$, where A is the pre-exponential factor.

TST assumes that every trajectory that reaches the transition state and heads toward the products ends as products. This assumption is checked by computing the transmission coefficient κ, which is the fraction of "successful" trajectories. This is done using the reactive flux correlation function method.[28,52,142] Starting from the system equilibrated at the transition state configuration ($[\mathrm{Cl}^{\delta-}-\mathrm{CH}_3-\mathrm{Cl}^{\delta-}]$, $\delta \approx 0.5$), at a constant temperature (298 K), random velocities are assigned from a flux-weighted Maxwell–Boltzmann distribution, and the value of the reaction coordinate is followed. The normalized flux correlation function is calculated using[52]

$$\kappa(t) = N_+^{-1} \sum_{i=1}^{N_+} \theta[\xi_i^+(t)] - N_-^{-1} \sum_{i=1}^{N_-} \theta[\xi_i^-(t)], \tag{4.10}$$

where $\xi_i^{\pm}$ is the value of the reaction coordinate for the ith trajectory at time t, given that at $t = 0, d\xi/dt$ is positive (negative), $N_+(N_-)$ is the corresponding number of trajectories, and θ is the unit step function. $\kappa(t)$ is calculated for a long enough time (0.2 ps) for the solvent-induced recrossings of the transition state to cease and for the system to reach the stable product state. The transmission

coefficient κ is the plateau value of $\kappa(t)$.

4.2.4 Other simulation details

Two sets of simulations are carried out. In the first set the reaction is carried out at the water–chloroform interface. The system includes 500 water molecules, 213 $CHCl_3$ molecules, a single tetramethylammonium cation, and the reactive system in a box of cross section 100 Å $\times$ 25 Å $\times$ 25 Å. This geometry gives rise to a single liquid–liquid interface, with each bulk phase at equilibrium with its own vapor.

$Z = 0$ is taken to be the Gibbs dividing surface with respect to the water, which is approximately where the water density is half of its bulk value. On average, the water occupies the $Z < 0$ region and the chloroform the $Z > 0$ region of the simulation box. In each system the reactants' center of mass is restricted to be inside a window of width $\delta Z = 3$ Å, utilizing a Z-dependent potential acting on the center of mass of the reactants relative to the center of mass of the full simulation system. This is done to increase the sampling statistics in each location. In each location the reactants and products can move freely within the window. Two locations are examined, one centered at $Z = 0$ which we will refer to as the "G" location and the other centered at $Z = 10$ Å which will be referred to as the "G+" location.

In the second set of simulations, the reaction is studied in bulk chloroform. The

system includes the reactants hydrated by N_w = 0, 1, 2, ..., 5 water molecules, one tetramethylammonium (TMA^+) cation and 214 chloroform molecules in a truncated octahedron box enclosed in a cube of size 38.68 $Å^3$. The initial configurations for these simulations are selected by inserting into a cavity of a proper size, the configurations $[Cl^{\delta-}-CH_3-Cl^{\delta-}](H_2O)_{N_w}$ ($\delta \approx 0.5$), selected from equilibrated transition-state configurations in bulk water, including a single TMA^+ ion. The system was first equilibrated at a constant temperature (298 K) and pressure (1 atm), with the water, the solute molecules, and the TMA^+ frozen. Next, all constraints, except for $\xi = 0$ (the system remains at the transition state), were removed and the system was equilibrated for 1 ns. The rest of the calculations are done as in the interfacial system.

The equilibrium free-energy calculations are done at a constant temperature of T = 298 K using a combination of the Andersen stochastic method and the Nosé-Hoover thermostat.[104] The integration time step is 0.5 fs for all systems, using the velocity version of the Verlet algorithm.[5]

4.3 Results and Discussion

4.3.1 Reaction free-energy profiles

Our main results for the potential of mean force of the $Cl^- + CH_3Cl$ reaction taking place at the two interface locations "G" and "G+", with and without the presence of the catalyst are shown in Figure 4.1. Two important conclusions are apparent:

i. To have a significant reduction in the activation free energy relative to that in bulk water (which is[21] 29.5 ± 0.3 kcal/mol), the reaction must be carried out deep into the organic side of the interface (the G+ location). If the reaction is taking place at the Gibbs surface, the barrier height is approximately the same as in bulk water. Note that the activation energy of this reaction in bulk chloroform is[21] 16.8 ± 0.2 kcal/mol.

ii. The presence of the catalyst does not appreciably affect the barrier height at the G location, but it significantly increases the barrier height when the reaction is taking place deeper into the organic phase. It is generally believed that the role of the phase transfer catalyst is limited to the transfer of the nucleophile from the aqueous to the organic phase. Our calculations show that, at least at the G+ location, the presence of the catalyst increases the barrier height. Experimental data showing that an increase in catalyst concentration does not increase the rate of a phase transfer reaction was interpreted as a result of mass transfer inhibition,[132] but our calculations

suggest the possibility that the reactivity of the catalyst–nucleophile complex is less than that of the "naked" nucleophile, so that an increase in the catalyst concentration can increase the concentration of this complex and reduce the reaction rate. We discuss below a possible explanation for this observation.

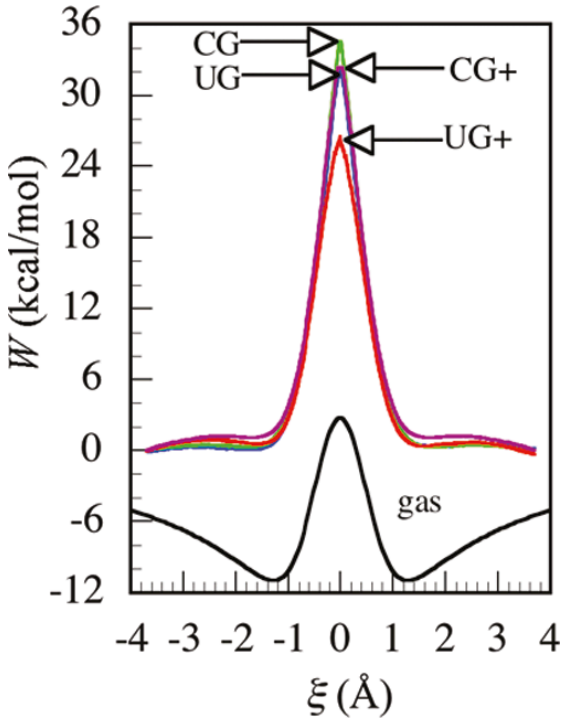

Figure 4.1: Potential of mean force (298 K) for the $Cl^- + CH_3Cl$ reaction taking place at the two different interface locations (G and G+, see text for definition) with and without the presence of the phase transfer catalyst tetramethylammonium (labeled C and U, respectively). The black line depicts the minimum energy path for the linear reaction configuration in the gas phase.

Our previous studies have demonstrated that at the interface, the hydration of the nucleophile by interfacial water molecules markedly increases the barrier

height relative to that in the bulk organic medium.[97,98] To better understand the interplay between the water and the catalyst influences on the potential of mean force, we show in Figure 4.2 the activation free energy of the reaction when the nucleophile is hydrated by 0, 1, 2, ..., 5 water molecules in bulk chloroform, with and without the catalyst. As the number of water molecules (N_w) increases, the improved hydration of the localized charge on the chloride ion relative to that of the transition state's more delocalized charges, $Cl^{0.5-}-CH_3-Cl^{0.5-}$, results in a lowering of the free energy of the reactants and products relative to the transition state,[62,110] and gives rise to a monotonic increase in the activation free energy with N_w. The presence of the catalyst provides additional ion-pair stabilization of the nucleophile and thus further increases the barrier height. This effect is more pronounced when N_w is small, presumably because when the Cl^- nucleophile is nearly fully hydrated, its ability to form the ion pair with the catalyst is reduced. This will be analyzed in the next section when we discuss the solvent coordinate.

4.3.2 Solvent coordinate and catalyst location.

To understand the medium's effect on the reaction free-energy profile, we must consider the spatial arrangement and interaction of the water, the chloroform and the tetramethylammonium (TMA^+) cation with the reactants, transition state, and products. A very simple, scalar quantity that is quite helpful in this regard

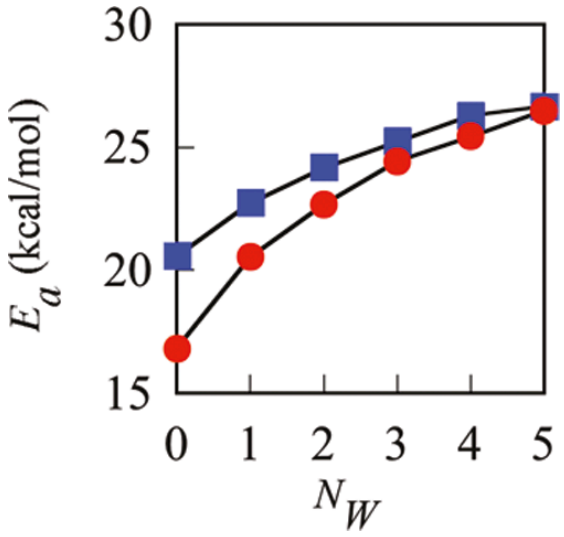

Figure 4.2: Activation free energy for the S_N2 reaction $Cl^-(H_2O)_{N_w}+CH_3Cl$ taking place in bulk chloroform as a function of the number of water molecules N_w. Blue squares: in the presence of the phase transfer catalyst; red circles: without the catalyst.

is the so-called "solvent coordinate", denoted by s, which we define as follows. Consider the energy gap between the two diabatic states at some fixed nuclear configuration: $\Delta H = H_{11} - H_{22}$. This difference is comprised of the vacuum energy difference, ΔH^0 and the *solvent contribution*, which we use as the definition of s:

$$H_{11} - H_{22} = \Delta H^0 + s \tag{4.11}$$

This expression (without the vacuum contribution) is just the one used in the definition of solvent coordinate employed in simulations of electron transfer reactions and solvation dynamics in polar solvents.[32,71]

As the reactants move along the reaction coordinate, the interaction of the two diabatic states with the solvent molecules and the TMA^+ depends on their con-

figurations. The solvent coordinate replaces this detailed information by a single number, s. At each fixed value ξ of the reaction coordinate, s depends on all other nuclear positions and fluctuates as the water, chloroform, and TMA^+ molecules translate and reorient. A useful characterization of the solvent configuration is the equilibrium ensemble average of s at fixed ξ, $s_{eq}(\xi) = \langle s(\xi) \rangle$. It follows from the symmetric charge distribution at the transition state that $s_{eq}(\xi = 0) = 0$. Fluctuations in ξ give rise to to instantaneous development of an asymmetric charge distribution, which interacts favorably with any charged solvent molecule and further drives the system away from the transition state towards the products. The significant favorable interaction of the solvent molecules with the localized charge of Cl^-, rather than with the dipolar CH_3Cl molecule, makes the corresponding diabatic state much lower in energy. This is reflected by the large increase in $|s_{eq}|$ as ξ varies from zero.

Because of the pairwise-additive nature of the intermolecular potential energy function (see Eq. 4.3), the equilibrium value of $s_{eq}(\xi)$ can be written as a sum of contributions from the interaction of the reacting system with the water, the chloroform, and the TMA^+.

Figure 4.3 shows the equilibrium average $s_{eq}(\xi)$ as a function of the reaction coordinate ξ for the two interface locations. Shown are the individual contributions due to the water, chloroform, and TMA^+ as well as their sum. Also shown is the total $s_{eq}(\xi)$ when the catalyst is absent. Figure 4.4 depicts the same type

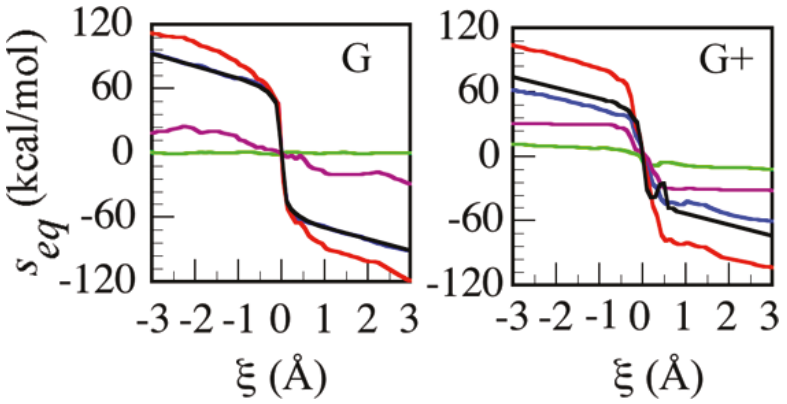

Figure 4.3: Equilibrium value of the solvent coordinate s as a function of the reaction coordinate ξ at two interface locations G and G+. In each panel, the blue, green, and purple lines correspond to the water, the chloroform, and the TMA^+ contributions to the solvent coordinate, respectively, while the red line is the total. The black line corresponds to the total solvent coordinate without the TMA^+.

of information for the reaction in bulk chloroform with the indicated number of water molecules.

Figures 4.3 and 4.4 provide a picture consistent with the activation free energy discussed above. The rate at which s_{eq} varies with ξ at the transition state (the slope of the line at $\xi = 0$) increases with the increase in the number of water molecules interacting with the nucleophile and reaches a larger asymptotic value as $|\xi| \to \infty$. Most relevant to understanding the catalyst effect on the activation free energy mentioned above is the fact that the TMA^+ makes a contribution that is larger than that of the chloroform molecules (even in bulk chloroform) and larger than that of one or two water molecules.

The significant contribution that the TMA^+ molecule makes to the solvent

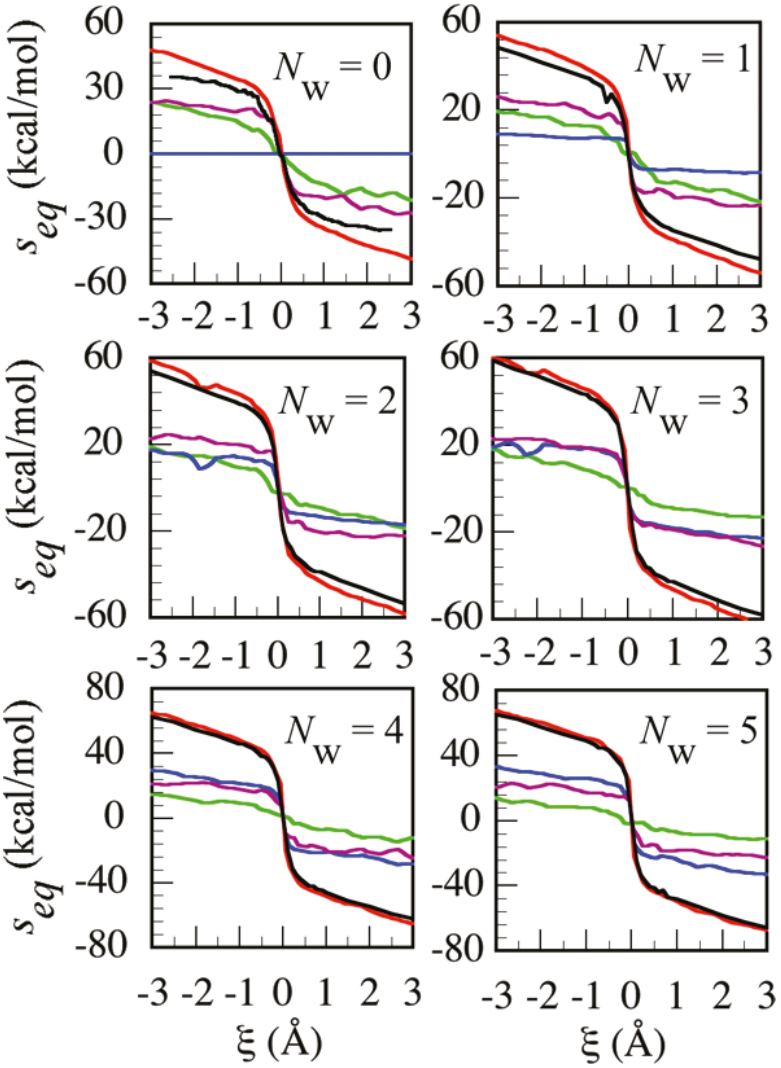

Figure 4.4: Equilibrium value of the solvent coordinate s as a function of the reaction coordinate ξ in bulk chloroform in the presence of N_w water molecules as indicated. In each panel the blue, green, and purple lines correspond to the water, chloroform, and TMA^+ contributions to the solvent coordinate, respectively, while the red line is the total. The black line corresponds to the total solvent coordinate without the TMA^+.

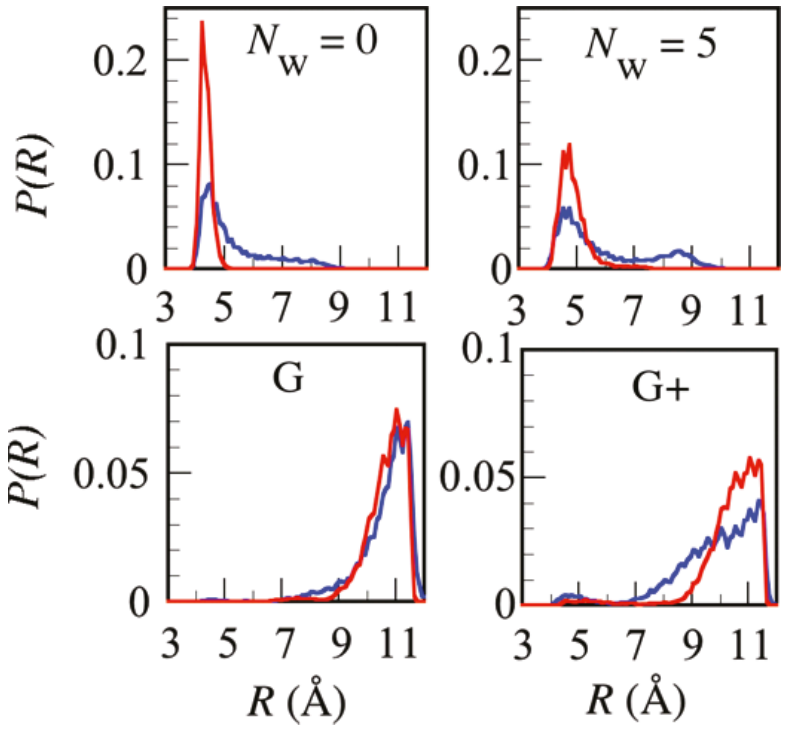

Figure 4.5: Normalized probability distributions for the distance R between the TMA^+ catalyst and the Cl^- ion. Top panels: in bulk chloroform with no water and with five water molecules present, as indicated. Bottom panels: at the G and G+ interface locations. In each panel, the red line corresponds to the reactants (or products) state ($\xi = 3$ Å) and the blue line is the system at the transition state.

coordinate suggests that this molecule has a significant interaction with the nucleophile, creating additional stabilization of the localized charge distribution of the reactants and products relative to the transition state. Figure 4.5 demonstrates this by showing the probability distribution of the distance R between the center of the TMA^+ and the Cl^- at the transition state and at the products (or reactants) state.

When the full charge is localized on the nucleophile (which is fully established

for $|\xi|$ as low as 1 Å), the catalyst forms an ion pair TMA^+Cl^- in bulk chloroform with the presence of any number of water molecules from $N_w = 0$ to $N_w = 5$. When the charge is fully delocalized at the transition state, the probability distribution $P(R)$ is much broader. The TMA^+ is near the transition state complex, weakly interacting with both Cl atoms. As the number of water molecules increases, the TMA^+Cl^- ion pair is less tight, since the water molecules can provide partial screening. At the interfacial location, where significantly more water molecules are involved in the interaction, the TMA^+ is located further away from the reacting system.

4.3.3 Electronic state variation

In the previous section it was pointed out that fluctuations in the reaction coordinate at the transition state break the symmetry of the charge distribution, which drives the system away from the transition state by stabilizing one of the diabatic states. In this section we show this quantitatively by considering the equilibrium average of the quantum weight of the diabatic state.

The diagonalization of the EVB Hamiltonian (Eqs. 4.2 and 4.6) leads to the following expression for the quantum weight:

$$c_1^2 = \frac{1}{2 + \chi^2/2 + \chi(1 + \chi^2/4)^{1/2}} \qquad c_2^2 = 1 - c_1^2 \tag{4.12}$$

where in the gas phase $\chi = \chi_0 = \Delta H^0/H_{12}$ and in solution:

$$\chi = (H_{11} - H_{22})/H_{12} = (\Delta H^0 + s)/H_{12}$$
$$= \chi_0 + s/H_{12} \tag{4.13}$$

The effective charge on the leaving group is given by $-c_1^2$. The symmetric transition state ($r_1^* = r_2^*$ and thus $\Delta H^0 = 0$) gives $\chi_0 = 0$ in the gas phase. In solution, χ is a function of the solvent coordinate s, but its equilibrium average, $\langle\chi\rangle = \chi_0 + s_{eq}/H_{12}$ is zero because of the symmetry of the solvent configuration, $s_{eq}(\xi = 0) = 0$ (as noted in the previous section). Thus, at the transition state ($\xi = 0$): $c_1^2 = c_2^2 = 1/2$. As $|\xi|$ increases, the coupling H_{12} exponentially decreases to zero, and so one gets

$\chi \to \pm\infty$, and thus $c_1^2(\chi \to \infty) = 0,\ c_1^2(\chi \to -\infty) = 1$. Thus, as ξ varies from $-\infty$ to $+\infty$, the ground state wave function varies from $\psi_2(c_1 = 0, c_2 = 1)$ to $\psi_1(c_1 = 1, c_2 = 0)$.

In practice, the asymptotic values of 0 and 1 for c_1 (1 and 0 for c_2) are reached for $|\xi|$ near 1 Å.

Figure 4.6 demonstrates the sensitivity of the solute charge distribution to the value of the reaction coordinate for the two interface locations with and without the TMA^+. The gas-phase behavior is also shown for comparison. Because H_{12} decays exponentially as the system moves away from the transition state, $\langle c_1^2(\xi)\rangle$ varies very rapidly with a rate that depends on the medium. The larger the number of water molecules, the larger the stabilization energy of the nonsymmetric charge

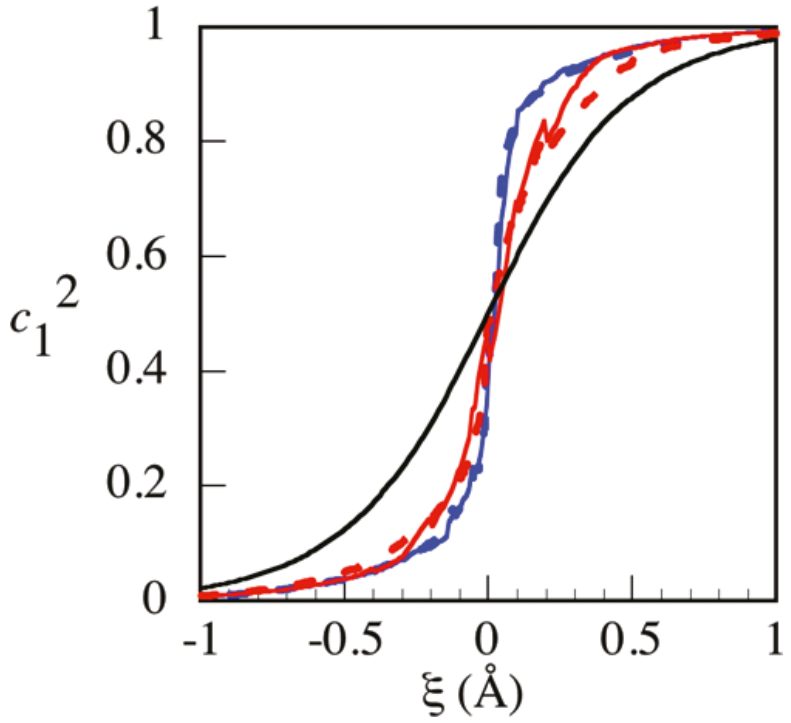

Figure 4.6: Equilibrium average quantum population of one of the diabatic states as a function of the reaction coordinate. Blue and red lines are for the interface locations G and G+, respectively. Solid and dashed lines are with and without the presence of TMA^+, respectively. The solid black line is Eq. 4.12 for the linear geometry in the gas phase.

distribution that is developed as soon as $|\xi|$ increases from zero and the more rapid the change in $\langle c_1^2(\xi)\rangle$. This explains the more rapid change in $\langle c_1^2(\xi)\rangle$ when the reaction is taking place at the G location compared with the G+ location. However, the catalyst has almost no observable effect on the charge switching rate. This is likely due to the fact that most of the influence on $\langle c_1^2(\xi)\rangle$ is due to the nearest water molecules, unlike the case of the activation free energy or the asymptotic value of the solvent coordinate.

4.3.4 Reaction dynamics

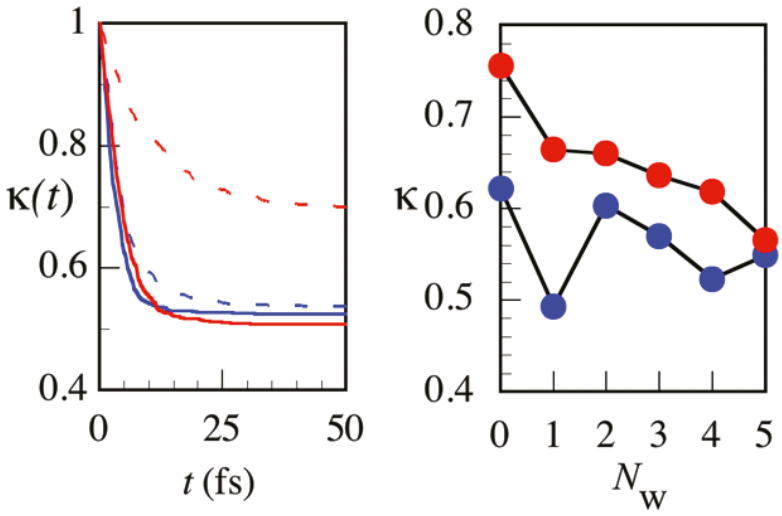

Figure 4.7: Left panel: Reactive flux correlation function for the reaction taking place at the interface location G (blue lines) and G+ (red lines) with TMA^+ (solid lines) and without TMA^+ (dashed lines) Right panel: The transmission coefficient κ as a function of the number of water molecules present when the phase transfer catalyst TMA^+ is associated with the nucleophile (blue) and without the TMA^+ (red).

Reactive flux calculations are carried out in bulk chloroform as a function of the number of water molecules as well as in the two interface locations with and without the presence of the catalyst. The methodology underlying these calculations was discussed in Section 4.2.3. The main outcome of these calculations is the dynamical correction to the transition state theory rate constant κ, determined from the plateau value of the reactive flux correlation function $\kappa(t)$. Figure 4.7 (left) shows $\kappa(t)$ at the two interface locations with and without TMA^+, and figure 4.7 (right) shows the plateau value in bulk chloroform as a function of the

number of associated water molecules, with and without TMA^+.

As suggested by studies of this reaction in bulk water,[21,27] κ is less than unity due to the fact that a trajectory initiated at the transition state is temporarily trapped and this leads to a recrossing of the transition state and thus deviation from transition state theory $\kappa = 1$. The trapping is due to the fact that the solvent (and TMA^+) molecules, which are equilibrated to the transition-state charge distribution, are not properly oriented to solvate the product charge distribution. This gives rise to an additional temporary (polarization) barrier that prevents the system from directly proceeding to the product side.[51]

In all cases (including the calculations in bulk chloroform), $\kappa(t)$ reaches its plateau value in less than 50 fs. Within this time period, every trajectory overcame the temporary trapping near the transition state and proceeded to the products state with no more recrossing of the barrier peak. We note the decrease in κ as the number of water molecules increases in bulk chloroform (approaching the value in bulk water $\kappa = 0.57$), or in the interface location G compared with the G+ location. The addition of the catalyst gives rise to an additional reduction in the value of κ, especially when few water molecules are involved. These results are consistent with the idea that the polarization trapping is enhanced when more water molecules are hydrating the nucleophile and when the TMA^+ is paired with it.

4.4 Summary and Conclusions

We have extended our previous studies of the benchmark $Cl^- + CH_2Cl$ S_N2 reaction at the water–chloroform interface to include the effect of a phase transfer catalyst, tetramethylammonium cation (TMA^+), on the reaction free-energy profile and dynamics. TMA^+ moderately *increases* the barrier height of this reaction when it is associated with the Cl^- nucleophile. The effect is most noticeable when the number of nearby water molecules is low, as in bulk chloroform when the nucleophile is hydrated by few water molecules or at water–chloroform interface locations that are deep into the organic side of the interface. The contributions of the different species to this effect were elucidated by examining the contribution of TMA^+, the water molecules, and the chloroform to the solvent coordinate. The presence of TMA^+ also slightly increases the deviation from transition state theory by increasing the rate of trajectories recrossing the barrier height.

Since both water molecules and TMA^+ association with the nucleophile increase the barrier height, the most effective role of the phase transfer catalyst is to bring the nucleophile deep into the organic phase, with a minimal number of associated water molecules. In addition, our calculations suggest that inhibiting the degree of nucleophile–catalyst ion pairing in the organic phase will further enhance the reaction rate. This can be achieved by keeping the catalyst concentration down and by choosing a catalyst for which the nucleophile–catalyst ion

pair dissociation is more favored in the bulk organic phase.

Acknowledgment

This work has been supported by a grant from the National Science Foundation (CHE-0809164).

Chapter 5

A Model S_N2 Reaction "On Water" Does Not Show Rate Enhancement

5.1 Introduction

In recent years there has been growing interest in the study of chemical reactions carried out "on water".[35,43,44,65,66,72,96] This refers to reactants with low solubility in water which thus remain adsorbed at the air–water interface. A significant increase in the *rate constant* is often observed in reactions carried out "on water" over those in organic solvents.

While only a few studies of S_N2 reactions "on water" have been reported[44]

(and no kinetic studies comparing the rate to that in organic solvents), it is a class of reactions whose reactivity on water surfaces is important to establish. It is well known that a significant rate enhancement of many orders of magnitude is observed for some S_N2 reactions carried out in the gas phase and in bulk non-protic organic solvents relative to bulk water.[6,38,58,60,62,64,70,83,107,110,133,141] One would expect that when these reactions are carried out on the water surface a significant rate enhancement relative to bulk water (and perhaps relative to an organic solvent) will be observed.

In this chapter, we utilize the recently developed[21] empirical valence bond (EVB) model to study the simple benchmark symmetric S_N2 reaction $Cl^- + CH_3Cl \longrightarrow CH_3Cl + Cl^-$ at different locations normal to the free water surface. At each location, we calculate the reaction free-energy profile, the activation free energy and several structural properties of the system. These calculations are compared with previously published bulk water calculations.[21]

The rest of the chapter is organized as follows: In Section 5.2, we briefly review the main features of the EVB model and the methodology used to compute the free energy. In Section 5.3, the results of the reaction free-energy profile, as well as some structural properties, are described and discussed. A summary and conclusions are given in Section 5.4.

5.2 Systems and Methods

5.2.1 The empirical valence bond model

We model the benchmark symmetric $Cl^- + CH_3Cl \longrightarrow CH_3Cl + Cl^-$ S_N2 reaction on the water surface using the empirical valence bond (EVB) model, first applied by Warshel and coworkers to reactions in solutions.[60,141] Since our implementation was extensively discussed in an earlier publication,[21] here we briefly summarize the main points.

The total valence bond wave function is written as a linear combination of the two orthonormal valence states,[21,83] $\psi_1 = Cl{-}CH_3\ Cl:^-$ and $\psi_2 = Cl:^-\ CH_3{-}Cl$

$$\Psi = c_1\psi_1 + c_2\psi_2, \qquad \langle \psi_1 \,|\, \psi_2 \rangle = \delta_{ij} \tag{5.1}$$

The total Hamiltonian in this representation is written as:

$$\hat{H} = \begin{pmatrix} E_k + U_{11} & U_{12} \\ U_{12} & E_k + U_{22} \end{pmatrix}. \tag{5.2}$$

In Eq. 5.2, E_k is the kinetic energy of all atoms, U_{11} includes the (global) gas phase interaction between the Cl^- ion and the CH_3Cl molecule and the water–water, water–ion, and water–CH_3Cl potential energies. Details about the functional forms and parameter values of the gas phase potential, which were selected to fit *ab initio* gas phase calculations, can be found elsewhere.[21] Due to the symmetry of the reaction, U_{22} has the same functional form as U_{11}, but with the two

chlorine atom labels interchanged. The off-diagonal electronic coupling term U_{12} in Eq. 5.2 is the one suggested by Hynes and coworkers.[83,130]

$$U_{12} = -QS(r_1)S(r_2) \tag{5.3}$$

where r_1 and r_2 are the distances between the two chlorine atoms and the carbon atom, and $S(r)$ is the overlap integral for the sigma orbital formed from the carbon 2p and chlorine 3p atomic orbitals. $S(r)$ is determined using Slater-type orbitals and the approximation of Mulliken et al.[93] $Q = 678.0$ kcal/mol is a parameter which is fitted to obtain the experimental gas-phase activation energy.

The diagonalization of Eq. 5.2 yields the electronic ground-state adiabatic Hamiltonian as a function of all nuclear coordinates:

$$H_{ad} = E_k + \tfrac{1}{2}(U_{11} + U_{22}) - \tfrac{1}{2}[(U_{11} - U_{22})^2 + 4U_{12}^2]^{1/2} \tag{5.4}$$

This Hamiltonian is used for the classical dynamics of the system.

It is convenient to define a reaction coordinate as follows:

$$\xi = r_2 - r_1 \tag{5.5}$$

so the reactants and products correspond to $\xi \ll 0$ and $\xi \gg 0$, respectively. In practice the wave function attains more than 95% reactants (or products) state character already when $\xi = 1$ Å. In the gas phase, Eq. 5.4 can be written as:

$$H_{ad}^{gas} = E_k + U_{ad}^{gas}(r_1, r_2, \theta), \tag{5.6}$$

where θ is the Cl−C−Cl angle. Note that since the CH_3 is treated as a united atom, only three coordinates are needed to specify the reactants' intramolecular potential energy function. The minimum potential energy path along ξ for the collinear geometry ($\theta = 180°$) has the well-known characteristic of a double well (see Figure 5.1). The transition state is located at $r_1 = r_2 = 2.19$ Å and has an energy of 13.72 kcal/mol above the ion–dipole double minimum, but an activation energy of only 2.74 kcal/mol above the energy of the separate reactants.

5.2.2 Reaction free-energy profile

The reaction free-energy profile as a function of the reaction coordinate, $\xi = r_2 - r_1$, is calculated using umbrella sampling with overlapping windows and a biasing potential,[36] according to:

$$\begin{aligned} W(\xi) &= -\beta^{-1} \ln P(\xi) - U_b(\xi) \\ P(\xi) &= \frac{\int \delta(r_2 - r_1 - \xi) \exp[-\beta(H_{ad} + U_b(\xi)] d\Gamma}{\int exp(-\beta H_{ad}) d\Gamma}, \end{aligned} \tag{5.7}$$

where $\beta = 1/k_B T$, k_B being the Boltzmann constant and T the temperature. $U_b(\xi)$ is an arbitrary analytic function of ξ, which is chosen to be a reasonable estimate of $-W(\xi)$. A good choice for the biasing potential is an approximate Gaussian-plus-exponential fit of the transition state region of the free-energy profile in bulk water.[21] This choice accelerates the convergence of the ensemble average in Eq. 5.7.

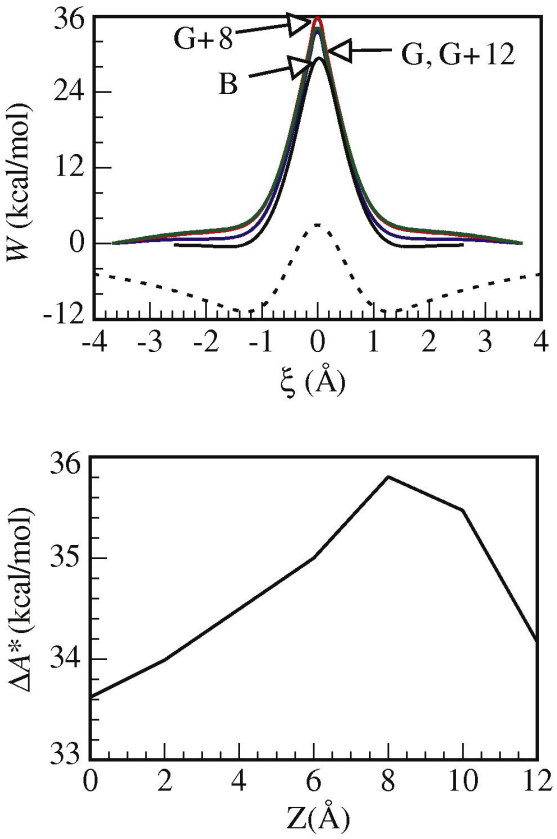

Figure 5.1: Top: The free-energy profile of the $Cl^- + CH_3Cl \longrightarrow CH_3Cl + Cl^-$ reaction at three different locations, G, G + 8, and G + 12 relative to the Gibbs surface of the water liquid–vapor interface at 298 K. The solid black line labeled B is the result in bulk water. The dashed black line is the vacuum minimum potential energy path along the reaction coordinate for the collinear geometry. Bottom: The activation free energy versus location relative to the Gibbs surface for all the systems studied.

The umbrella sampling procedure involves dividing the range of reaction coordinate values $|\xi| < 3.8$ Å into overlapping sets of "windows" that are mostly 0.5 Å wide (narrower near the transition state to increase accuracy). In each window, a total simulation time of 2 ns allows for an accurate calculation of the probability $P(\xi)$, from which the free-energy profile is determined using Eq. 5.7, with a statistical error that is less than 0.1 kcal/mol. Other details about the exact umbrella sampling procedure are given in reference 21.

5.2.3 Other simulation details

The system includes 1000 water molecules in a box of cross section $100 \times 20 \times 25$ Å. This geometry gives rise to two liquid–vapor interfaces, one of which is used to study the reactive system. We study six different systems, in which the reactants' center of mass is located in different positions along the interface normal, starting with the Gibbs dividing surface (labeled G), which is approximately where the water density is half of its bulk value,[114] and continuing with systems in which the center of mass is further moved towards the vapor phase. In each system, the reactants' center of mass is restricted to moving inside a window of width $\delta Z = 3$ Å in order to increase the sampling statistics in each location. This is accomplished with the help of a Z-dependent potential acting on the reactants' center of mass relative to the center of mass of the full simulation system. The

different systems are labeled G + n, n = 0, 2, 6, 8, 10, and 12 where n is the location in angstroms of the center of the window (relative to the Gibbs surface) in which the reactants' center of mass is restricted to move. We point out that the free-energy profile of the reactants along the interface normal has been determined by several groups,[17,45,55] which show that the CH_3Cl is weakly surface active. In order to better understand the factors that influence the reaction barrier, our choice of the different surface locations includes a range of locations and not only the location where the reactants are most likely to be found.

The calculations are done at a constant temperature of T = 298 K, using a combination of the Andersen stochastic method and the Nosé–Hoover thermostat.[104] The integration time step is 0.5 fs for all systems, using the velocity version of the Verlet algorithm.[5]

5.3 Results and Discussion

5.3.1 Reaction free-energy profiles

It is well known from theoretical and experimental studies,[62,110] that as the hydration of the Cl^- nucleophile is enhanced, the activation free energy for $Cl^- + CH_3Cl \longrightarrow CH_3Cl + Cl^-$ is increased due to the preferential stabilization of the chloride ion-localized charge distribution relative to the more extended charge dis-

tribution $Cl^{0.5-}-CH_3-Cl^{0.5-}$ of the transition state. One would therefore expect that if the reaction is carried out at the liquid–vapor interface and is moved farther out towards the vapor phase, the activation free energy will be reduced relative to that in bulk water. Our results contradict this expectation.

Figure 5.1 shows the free-energy profiles $W(\xi)$ for the reaction at three different locations of the water liquid–vapor interface compared with bulk water. The gas-phase potential energy along the minimum energy path for the collinear reaction geometry is also shown. The curves for the reaction taking place at the interface locations fall very close to each other, so for clarity we show the results for only three of the six systems studied. The corresponding activation free energies are shown in the bottom panel for all the systems studied. Despite the much lower average local density of water molecules at the Gibbs surface and above, it is surprising how little the free-energy profile changes, especially when compared with the gas-phase profile. Contrary to expectation, the activation free energy of all the interfacial systems is *higher* than that of bulk water (29.5 kcal/mol), continues to *increase* as the reaction takes place further away from the surface, and begins to decrease only as $Z > 10$ Å.

Our results are especially surprising given the fact that studies of this reaction in water clusters are clearly consistent with the above expectation: As the number of water molecules in the cluster increases, the activation free energy rises monotonically.[31,53,109,147] Clearly the water surface introduces an important

factor. A clue to the nature of the surface effect is provided by considering the water molecules' organization around the reactants and the reactants' position with respect to the interface.

5.3.2 Solvent coordinate and solute configuration

Snapshots of equilibrated reactants and transition state configurations when the solutes' center of mass is located 8 Å above the Gibbs surface are shown in Figure 5.2. The reactants' snapshot (Figure 5.2a) illustrates that due to water molecules clustering around the nucleophile, the local environment experienced by the reactants is more polar (bulk water-like) than one would expect, while the transition state (Figure 5.2b), which does not exhibit water-clustering, remains relatively weakly hydrated.

The density profiles of water and the probability distribution of the CH_3 and the two chlorine atoms (Figure 5.3) provide a corresponding statistically averaged account of the change in the surface structure accompanying the adsorption and the reaction. Figure 5.3 shows that as the reactants are moved "higher" above the Gibbs surface, a water bridge maintains a significant hydration of the Cl^- nucleophile, and more so in the reactants (or products) state (right panels) than at the transition state (left panels). The significant deformation of the water density (relative to that of neat water) raises the question of whether specifying the

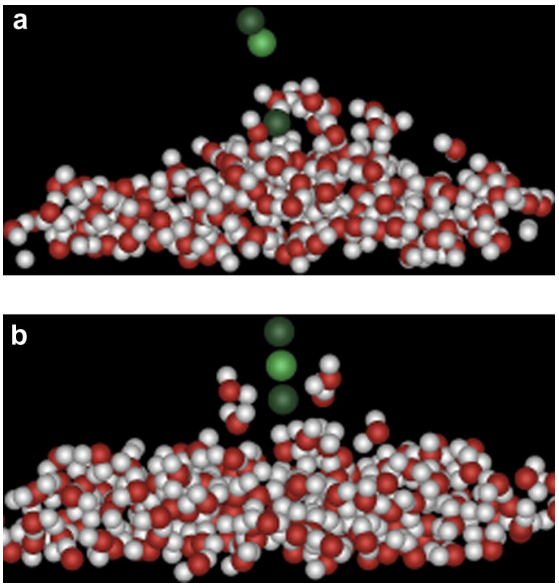

Figure 5.2: A molecular dynamics snapshot of an equilibrated configuration of the $Cl^- + CH_3Cl$ reactants (a) and of the transition state configuration (b) with the center of mass located at 8 Å above the Gibbs surface.

location of the reactants relative to the Gibbs dividing surface (which is, after all, a property of neat water) is still appropriate. One approach is to use the so-called "intrinsic profile" to specify the location of the solute relative to the nearest solvent molecules.[34,63] Another way to quantify the solvent structure in this extremely heterogeneous environment is to use the concept of a solvent coordinate, as will be discussed below.

The above discussion suggests an explanation for the increase in the activation free energy relative to bulk water, as is illustrated schematically in Figure 5.4. The free energy of the reactants at the liquid–vapor interface (R) is much lower than the free energy of the reactants in a hypothetical uniform low polarity medium

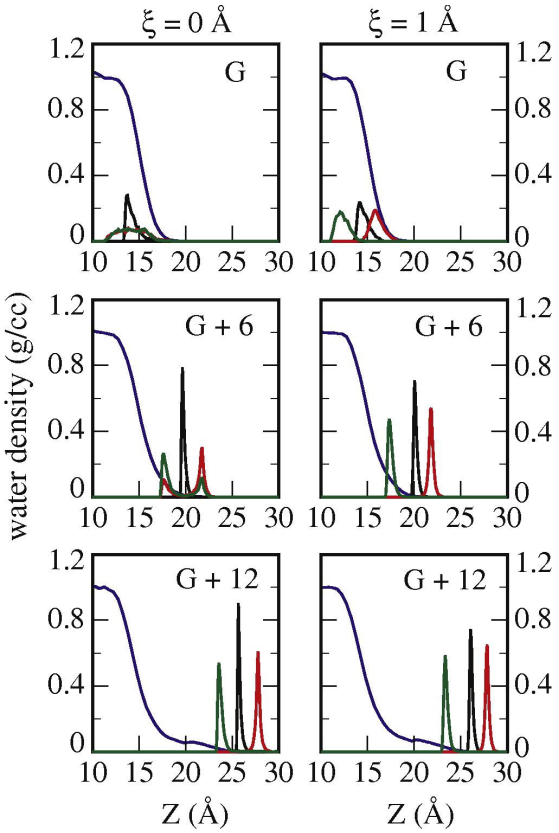

Figure 5.3: The water density profiles (blue lines) and the probability distribution of the Cl^- (green lines), the Cl atom (red lines), and the CH_3 group (black lines) for the reactant center of mass located in different locations relative to the GDS (as indicated). Left panels: The reactants at the transition state configuration. Right panels: The reaction coordinate is equal to 1 Å. The solute atoms' probability distributions are normalized to the same (arbitrary) total area.

(R′), while the transition state (TS) hydration is weaker.

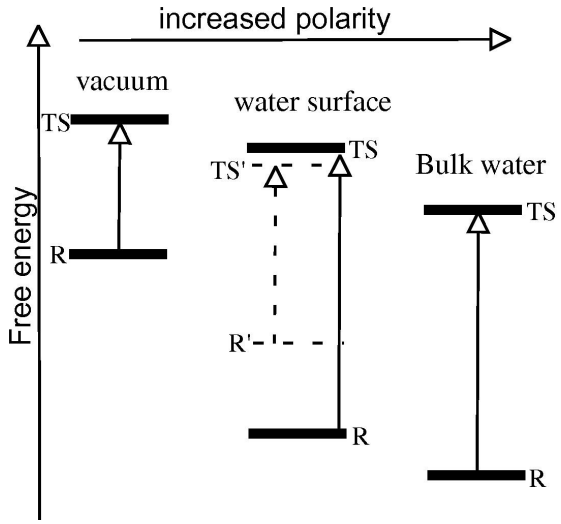

Figure 5.4: A schematic representation of the free energies of the reactants (R) and the transition state (TS) in different environments. A vertical arrow connecting the two levels represents the activation free energy. The two sets of levels shown for the interface correspond to a homogeneous low polarity region (dashed lines) and to the actual inhomogeneous clustering of water molecules around the nucleophile (solid lines).

We can quantitatively demonstrate the enhanced hydration of the reactants relative to the transition state by examining the ensemble average of the so-called solvent coordinate, which is a simple one-dimensional representation of the water configuration around the solute. This quantity, denoted by s, is defined as the solvent contribution to the energy gap between the two diabatic states at some fixed solute and water configuration:

$$s = U_{11} - U_{22} - \Delta U^0 \tag{5.8}$$

where ΔU^0 is the energy difference between the two states in a vacuum. At each

fixed value ξ of the reaction coordinate, s depends on the water molecules' orientations and distances with respect to the solute molecule.

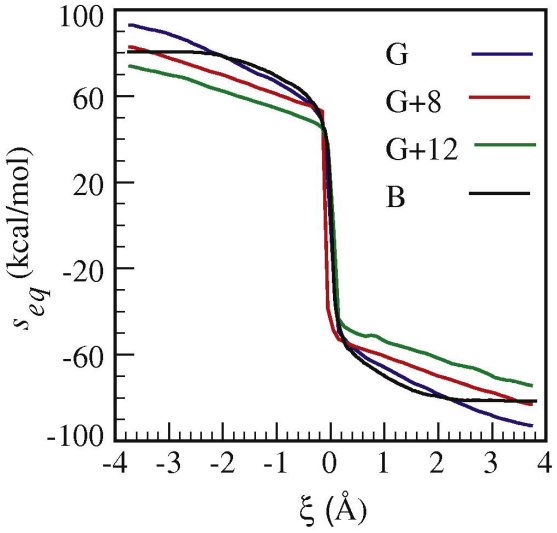

Figure 5.5: Equilibrium average of the solvent coordinate s_{eq} versus the reaction coordinate ξ when the reactants' center of mass is in different locations at the water liquid–vapor interface, as indicated by the different colored lines, and in bulk water (black line).

The equilibrium ensemble average of s at fixed ξ, $s_{eq}(\xi) = \langle s(\xi) \rangle$ is plotted in Figure 5.5 as a function of the reaction coordinate ξ for selected reactants' locations. Because of the symmetry of the transition state, the two diabatic states have on average the same energy, and thus $s_{eq}(\xi = 0) = 0$. As the system moves away from the transition state, an asymmetric charge distribution is developed, and a significant favorable interaction of the water molecules with the localized charge of Cl^- lowers the energy of the corresponding diabatic state. This results in a large increase in $|s_{eq}|$ as ξ varies from zero. The rapid increase in s_{eq} significantly

slows down when $|\xi|$ increases past 0.2 Å and slowly reaches an asymptotic value that depends on the reactants' location at the interface. We note that while in bulk water the asymptotic value $s_{eq}(|\xi| \to \infty) = 85$ kcal/mol[21] is reached around 3 Å, $|s_{eq}|$ continues to grow at the interface. This indicates that the difference in energy between the two diabatic states continues to grow as the nucleophile experiences a more bulk-like environment while the CH_3Cl molecules experiences an even lower polarity environment than that of surface water. Similar observations can be made utilizing the more familiar radial distribution function of the different solute atoms as a function of the reaction coordinate and the solute locations.

5.4 Summary

The activation free energy of the benchmark $Cl^- + CH_3Cl$ S_N2 reaction at the liquid–vapor interface of water is slightly *larger* than in bulk water, contrary to the expectation that low average polarity of the surface should lead to a significantly lower activation free energy. This is due to the fact that the reactants' state is hydrated to a much greater degree than one would expect due to both clustering of water molecules around the nucleophile and the preferred orientations of the reactants with respect to the interface normal. While we expect this result to apply to other S_N2 reactions and other classes of interfacial reactions in which an asymmetric charge distribution is generated, we caution that our results were

obtained utilizing potential energy surfaces that were fitted to gas phase and bulk data. Although it is a common practice to use the same potential energy surfaces for bulk and interfacial simulations, additional testing of this practice is worthwhile.

Acknowledgement

This work has been supported by a grant from the National Science Foundation (CHE-0809164).

Chapter 6

Electronic Absorption Line Shapes at the Water Liquid–Vapor Interface

6.1 Introduction

In recent years, significant advances in nonlinear spectroscopic techniques, especially electronically resonant second harmonic generation (SHG) and sum frequency generation (SFG), have enabled the accurate measurement of the electronic spectra of chromophore molecules adsorbed at liquid interfaces.[20,48,121,122,124–126,128,129,136–139,145] These experiments, coupled with theoretical developments,[18,20,87,88] provide valuable information about interface struc-

ture and solvent–solute interactions. In particular, the peak spectral shift relative to the spectra in the gas phase has led to the concept of surface polarity,[20,136,138,139] which attempts to characterize the strength of solute–solvent interactions at the interface in a similar fashion to the successful polarity scale of bulk solvents.[67,77,84,110,111] This polarity scale is based on the observation, supported by theory, that an increase in solvent polarity results in a larger spectral shift. Several studies have explored the limitation of this concept, and in particular the dependence of the "surface polarity" on the location of the solute[124,125,136] and its identity.[122,128,137]

Much less attention has been given to experimental studies of the spectral *width* of adsorbed solutes, which, as numerous studies in the bulk have shown,[1,8,74,78,81,82,118,120] could provide information about the orientational and translational distribution and fluctuation of the solvent molecules around the solute. This situation is in part due to the difficulty of obtaining good signal-to-noise spectra from truly interfacial molecules. While in recent years the use of broadband nonlinear optical spectroscopic techniques has resulted in much better spectra, these cannot be directly compared with bulk absorption spectra due to their quadratic power dependence and to nonresonant background contributions to the total signal.[121,124,125,129,136,145,148]

Linearized solvation models suggest that the absorption spectral width δ of a dipolar solute in a polar solvent is related to the spectral shift $|\Delta\omega|$ (relative to

the spectrum peak in vacuum) by a simple relation, $\delta^2 = CkT\Delta\omega$ (in units of $\hbar = 1$), where the constant C depends on the solute's ground- and excited-state dipoles but not on the solvent.[81] For example, $C = (\mu_g - \mu_e)/2\mu_g$ for the case of a solute modeled as a point dipole undergoing a parallel transition.[120] Since the spectral shift increases with solvent polarity, the width is also expected to increase with solvent polarity. Thus, when one utilizes the spectral line width to compare the degree of solvent orientational and translational distribution and fluctuation in two *different* media, one should account for the effect of solvent polarity on the width. Specifically, since the polarity of the water surface is smaller than that of bulk water, $|\Delta\omega_{\text{surface}}| < |\Delta\omega_{\text{bulk}}|$, and one would expect *spectral narrowing* if bulk and surface water have a similar range of solvent–solute configurations. Some experimental data suggest that this is indeed the case[129,148]

Recently, Mondal et al.,[92] using heterodyne-detected electronic sum frequency generation (HD-ESFG) spectroscopy, measured the imaginary part of the second-order nonlinear susceptibility ($\text{Im}[\chi^{(2)}]$) of several coumarin dyes at the water–air interface. By comparing the bandwidth of these spectra with the $\text{Im}[\chi^{(1)}]$ determined from the UV spectra of the same chromophore in bulk solvents of similar polarity, (thus avoiding the need to account for the effect of polarity on the width), they found that the spectra at the air/water interface were *broader* than those in bulk solvent and even broader than the spectrum in bulk water. This was attributed to the solute molecule sampling a wider distribution of solvent

configurations at the interface than in the bulk.

Using the spectral line width to determine which medium, bulk or surface, is a more heterogeneous environment is complicated by the fact that the SFG signal is generated by all the molecules in a non-centrosymmetric medium. Since it is known from simulations, continuum models, and experiments[20,124–126,136] that the peak electronic spectrum of a chromophore depends on the chromophore's location (and orientation) along the interface normal, it is likely that molecules with different spectral shifts contribute to the observed signal. Therefore, it is not clear to what degree the observed width is due to intrinsic local heterogeneity or due to the fact that the observed spectrum is a sum of shifted spectra. In this chapter we consider this question in detail with the help of a simple model of a dipolar solute adsorbed at different locations of the water liquid/vapor interface.

Previous calculations of spectral line width of adsorbed solutes at interfaces were limited to a few simulations[87,88] and a continuum model,[18] but no systematic investigation of this issue was attempted. For a very recent discussion of interfacial line width in a simple nonpolar solvent, that addresses the problem of the contribution of molecules across the interfacial region, see Ref. 24.

The rest of the chapter is organized as follows: In Section 6.2, we discuss the simple dipolar model. In Section 6.3, we give simulation details. The results are discussed in Section 6.4, and concluding remarks are in Section 6.5.

6.2 A Dipolar Solute Model

The model we use to describe the electronic transition $|i\rangle \rightarrow |f\rangle$ includes the dipolar solute constrained to be at different locations of the water liquid/vapor interface or in bulk water and in bulk methanol. The solute is described by two identical atoms rigidly held at a bond distance of $R_{eq} = 4$ Å, using the SHAKE algorithm.[115] The two atoms carry partial charges $+Q_i$ and $-Q_i$ in the initial electronic state and $+Q_f$ and $-Q_f$, respectively, in the final state. We study 64 different dipole parallel transitions by selecting the partial charges Q_i and Q_f to be all possible combinations of the values 0, 0.1, 0.2, ..., 0.7 in atomic units. These choices give rise to dipole moment values in the range of commonly studied chromophores. The solute atoms interact with water via Lennard-Jones parameters plus Coulomb terms. For simplicity, the Lennard-Jones parameters of the two atoms are taken to be the same and equal to $\sigma_i = 3$ Å and $\epsilon_i = 0.2$ kcal/mol. In addition we assume that these values are identical in the initial and final electronic states for all the transitions considered. However, some calculations were done where the polarizability of the final state was larger by selecting $\epsilon_f = 2\epsilon_i$. This increase in the effective solute polarizability is consistent with typical experimental systems, such as the $\pi \rightarrow \pi^*$ transition in aromatic compounds.[111]

Thus, the potential energy surfaces of the initial and final states are

$$H_i = U_w + U_i^{\mathrm{LJ}} + U_i^{\mathrm{Coul}}$$

$$H_f = \Delta E_0 + U_w + U_f^{\mathrm{LJ}} + U_f^{\mathrm{Coul}} \tag{6.1}$$

In Eq. 6.1, ΔE_0 is the vacuum energy difference between the final and initial states. U_w is the total water intermolecular and intramolecular potential energy surfaces, described using the flexible SPC model,[26] which has been shown to give reasonable bulk and interfacial properties.[16,89] U_ν^{LJ} and U_ν^{Coul} are the solute–water Lennard-Jones and Coulomb interaction energies, respectively, in the state ν ($\nu = i$ or f). These are explicitly given by

$$\begin{aligned} U_\nu^{\mathrm{LJ}} &= 4\sqrt{\epsilon_\nu \epsilon_O} \sum_{n=1}^{N} \left[\left(\frac{\sigma}{r_{1n}} \right)^{12} - \left(\frac{\sigma}{r_{1n}} \right)^{6} + \left(\frac{\sigma}{r_{2n}} \right)^{12} - \left(\frac{\sigma}{r_{2n}} \right)^{6} \right] \\ &= \sqrt{\epsilon_\nu}\Omega(\vec{r}) \\ U_\nu^{Coul} &= Q_\nu \sum_{n=1}^{3N} q_n [r_{1n}^{-1} - r_{2n}^{-1}] = Q_\nu \Gamma(\vec{r}) \end{aligned} \tag{6.2}$$

where r_{jn} is the distance between a solute atom j ($j = 1$ or 2) and a water site n (an oxygen atom in the case of the Lennard-Jones term, and an oxygen or a hydrogen atom in the case of the Coulomb term), $\sigma = (\sigma_O + \sigma_j)/2$ with the water SPC parameters $\sigma_O = 3.165$ Å and $\epsilon_O = 0.155$ kcal/mol, and q_n is the charge in atomic units on the nth water site. In Eq. 6.2 we made use of the standard Lorentz-Berthelot mixing rules for the Lennard-Jones interaction parameters between two

different atomic sites.[54] Note that $\Omega(r)$ and $\Gamma(r)$ depend on the instantaneous nuclear configuration, but not on the electronic state.

The above calculations are also carried out in bulk methanol in order to compare the interface spectra with the spectra in a bulk medium of a similar polarity. The model used is a three-site Lennard-Jones plus Coulomb potential, with parameters given in Ref. 12, so expressions similar to those given in Eq. 6.2 can be written in this case as well.

Neglecting solvent dynamics and assuming an infinite excited-state lifetime and the Franck-Condon approximation, the normalized static line shape is given by the distribution of energy gaps between the final and initial states governed by the initial state Hamiltonian:[8,74,78,82,118,120]

$$I_{i\to f} = \langle \delta[\omega - \Delta E_0 - \Delta U(\vec{r})] \rangle_i$$
$$\Delta U(\vec{r}) = (\sqrt{\epsilon_f} - \sqrt{\epsilon_i})\Omega(\vec{r}) + (Q_f - Q_i)\Gamma(\vec{r}) \tag{6.3}$$

(in units of $\hbar = 1$), where δ is the Dirac delta function, and $\langle ... \rangle_i = (\int e^{-\beta H_i} ... dr)/(\int e^{-\beta H_i} dr)$ represents the canonical ensemble average in the initial state and $\beta = 1/kT$. By running molecular dynamics or Monte Carlo simulations with the Hamiltonian H_i and binning the instantaneous energy gap, one obtains the absorption or emission line shape in the static inhomogeneous limit.[8,19,87,88,118,120]

Note that if the delta function in Eq. 6.3 is replaced by its Fourier representa-

tion, $\langle \delta(\omega - \Delta E) \rangle = (2\pi)^{-1} \int_{-\infty}^{\infty} e^{-i\omega t} \langle e^{i\Delta E t} \rangle dt$, and $\langle e^{i\Delta E t} \rangle$ is approximated by a second-order expansion,[118,120,127] one obtains a Gaussian line shape:

$$I_{i \to f}(\omega) = \frac{1}{\sqrt{2\pi\delta^2}} e^{-(\omega - \Delta E_0 - \Delta\omega)^2 / 2\delta^2}$$

$$\Delta\omega = \langle \Delta U \rangle_i$$

$$\delta^2 = \langle (\Delta U)^2 \rangle_i - \langle \Delta U \rangle_i^2 \tag{6.4}$$

Equation 6.4 can be used as the starting point of several statistical mechanics[37,41,118,120,127] or continuum models[1,5,18,68,69,81,90] approximate theories of line shape, but here we use direct binning of the energy gap to compute the exact line shape (in the static Franck-Condon limit). Note also that because of the pair approximation of the total potential energy function, a simulation of one initial state can provide the line shape for transitions to multiple final states, as long as the probability distribution of the quantities U_i^{LJ} and U_i^{Coul} (or, equivalently, $\Gamma(r)$ and $\Omega(r)$) are known.

6.3 Simulation Details

The simulation system includes 1000 water molecules in a rectangular box of cross section 31.3 Å × 31.3 Å and a diatomic solute molecule, which is adsorbed at different locations of the water liquid/vapor interface and in bulk water. Periodic boundary conditions are used in all three dimensions, with a molecule-based

continuous force-switching function at half the box length, and a reaction field correction for the long-range electrostatic forces.[5] The simulations in bulk methanol used 215 molecules in a truncated octahedron (TO) box, whose enclosing cube has a size of 30.74 Å. (The volume of the TO box is half the volume of the defining cube.)

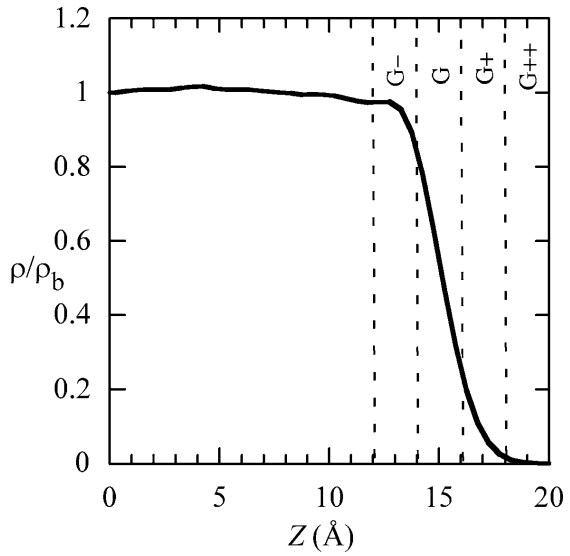

Figure 6.1: The density profile of an FSPC water–vapor interface at 298 K. Depicted are the different surface regions in which a chromophore is located.

The geometry of the system leads to two liquid/vapor interfaces with the Gibbs dividing surface located at ±15 Å. (This is the plane perpendicular to the Z-axis, where the excess water on the bulk side is equal to the decrease on the vapor side,[103,114] which is approximately where the water density is half the bulk value.) Because of the complete symmetry with respect to the box midpoint, one may use both surfaces to study the solute spectra, but we present the results using

the positive half of the system (see Figure 6.1 for the density profile). To obtain statistically accurate spectra for the solute located in different slabs parallel to the interface, we constrain the center of mass of the solute using a window potential given by

$$U_w(z) = k_w \theta(x) x^2, \qquad x = |z - Z_{cm}| - h \tag{6.5}$$

where k_w is a force constant on the order of 10^3 kcal/mol/Å (the exact value is not important), and $\theta(x)$ is the unit step function ($\theta(x) = 0$ if $x < 0$; $\theta(x) = 1$ if $x > 0$). Thus the solute is free to move inside a slab of thickness h (selected to be 2 Å) centered at Z_{cm}. We select $Z_{cm} = 0$, 13, 15, 17, and 19 Å. These locations are labeled B, G–, G, G+, and G++, respectively (see Figure 6.1).

The temperature in all the calculations is 298 K. The equations of motion are integrated using the velocity Verlet algorithm[5] with a time step of 0.5 fs.

6.4 Results and Discussion

In this section we first discuss the results for one particular "electronic" transition, then show the combined data for all the transitions investigated. For an electronic transition that involves only a change in the charge distribution $Q_i \rightarrow Q_f$, the shift in the peak position of the spectrum of the solute adsorbed at the location z relative to the peak position when the solute is in the bulk is approximately given

by combining Eqs. 6.3 and 6.4:

$$\Delta\omega(z) - \Delta\omega(0) = (Q_f - Q_i)[\langle\Gamma_z(\vec{r})\rangle_i - \langle\Gamma_0(\vec{r})\rangle_i] \tag{6.6}$$

(The relation is exact if the spectrum shape is symmetrical). Since the expression inside the square parentheses is typically positive (polar solute–water electrostatic interaction energies are less negative when the solute is at the interface than in the bulk), transitions that involve an increase in the solute electric dipole ($Q_f > Q_i$) are shifted to higher energies at the surface.

The top panel of Figure 6.2 shows, as an example, the calculated spectra for one particular "electronic" transition ($Q_i = 0.2 \rightarrow Q_f = 0.7$) of the solute adsorbed at different water surface locations and in bulk water. As expected, there is a shift to the "blue" when the solute is moved from bulk water to the interface, which is also found experimentally. However, there is a slight *narrowing* of the spectra as the solute is moved to the lower density (and lower polarity) interface regions. While this is qualitatively consistent with the linear response relation between the peak width and shift mentioned earlier ($\delta \propto (|\Delta E|)^{1/2}$), it clearly suggests that any increase in inhomogeneous broadening due to a more heterogeneous environment is smaller than the narrowing expected because of the reduced polarity.

The significant dependence of the spectrum's peak location on the solute Z-location presents a difficulty when comparing calculated and experimental spectral shift and width, since in reality, the adsorbed solute will sample all locations with a

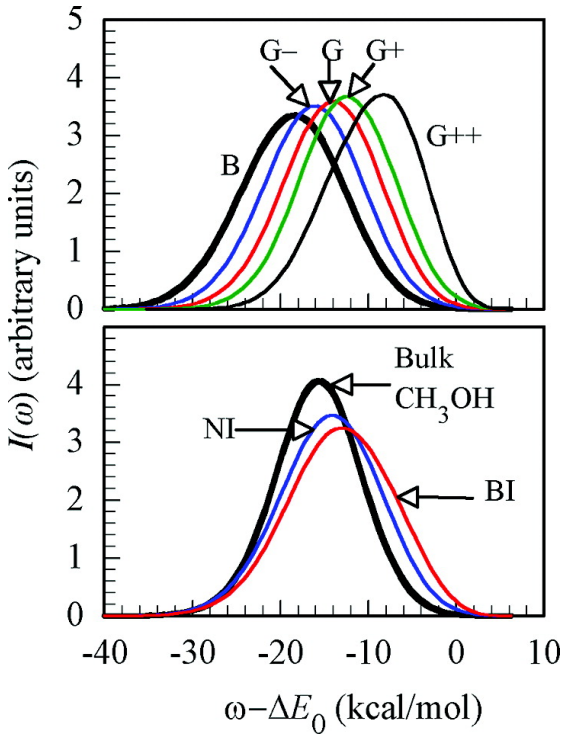

Figure 6.2: Top panel: Electronic absorption spectra (normalized to the same area) for the transition: $Q_i = 0.2 \rightarrow Q_f = 0.7$ of a chromophore at different locations of the water liquid/vapor interface and in bulk water. Bottom panel: The spectra for the same transition in bulk methanol and at two composite interface regions, as defined in the text.

probability that is reflected by its local free-energy profile. The spectrum will be a weighted average of all locations that are in the non-centrosymmetric region. Since the adsorption behavior of the simple dipolar solute in our model is not expected to follow that of the experimentally studied chromophore, we instead show in the bottom panel of Figure 6.2 two other spectra calculated by taking a wider slice of the interface than the individual slices shown in the top panel. The "narrow" interface spectrum (labeled NI) is obtained by including locations G–, G, and

G+, and the "broad" interface (labeled BI) also includes the G++ location. The peak positions of these spectra are, as expected, close to the average of the spectra from the individual slabs. Now, however, one does obtain a slightly *broader* surface spectrum when one combines the contributions from a wider interface region, as is shown in the bottom panel of Figure 6.2.

Using the spectral width to compare the heterogeneity of two different media is appropriate when their polarity is similar. This was demonstrated experimentally by measuring the absorption spectra in bulk organic solvents whose polarity is similar to that of surface water. Following this approach, the bottom panel of Figure 6.2 shows the spectrum calculated for the $Q_i = 0.2 \rightarrow Q_f = 0.7$ transition (same solute) in bulk methanol. For this case, the spectral shift suggests that bulk methanol's effective polarity is similar to that of region G– of the water liquid/vapor interface. The bulk methanol spectrum is narrower than the corresponding spectrum in the G– region, which is consistent with a lower degree of heterogeneity of the bulk compared with the surface and with the experimental observation.

Turning next to a discussion of all the transitions examined, we note from Eq. 6.6 that for a given initial state (characterized by a given value of Q_i), the spectral shift relative to the bulk, $\Delta\omega(z) - \Delta\omega(0)$, is linear in ΔQ. This is demonstrated in the top panel of Figure 6.3 for a particular choice of Q_i, for all solute surface locations. The slope $[\Delta\omega(z) - \Delta\omega(0)]/\Delta Q$ increases as the solute is moved to

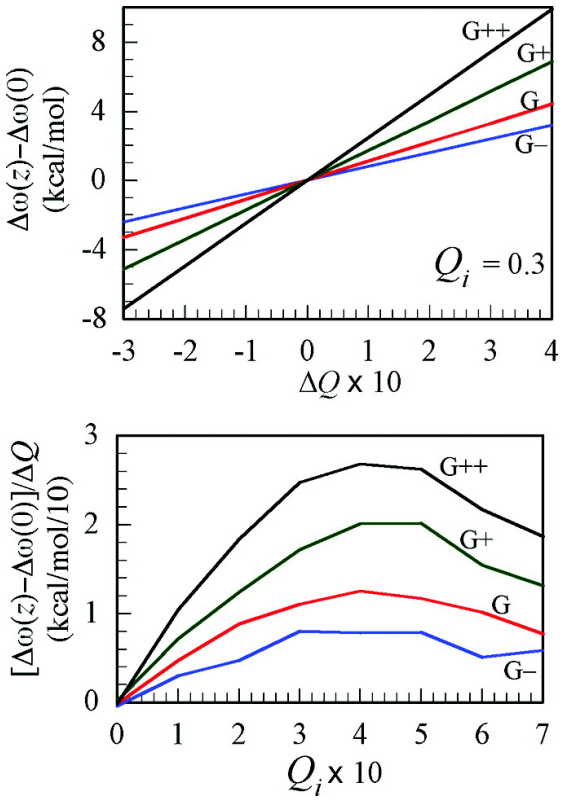

Figure 6.3: Top panel: The spectral shift relative to the bulk, $\Delta\omega(z) - \Delta\omega(0)$, versus the change in the solute charge ΔQ for one specific choice of the initial solute charge at the different solute surface locations. Bottom panel: The slope $[\Delta\omega(z)-\Delta\omega(0)]/\Delta Q$ versus the initial solute charge for all solute surface locations.

a lower polarity region simply because the dehydration increases relative to the bulk. Since the slope for a given surface location depends on Q_i alone, the bottom panel depicts the slope versus Q_i for all solute surface locations. Interestingly this plot exhibits a maximum for each solute location at $Q_i = 0.4$. This is due to the effect of two competing factors: As Q_i increases from zero, the weaker hydration relative to the bulk becomes more pronounced. However, for large enough values of Q_i, the tightening of the solute's hydration shell as it is moved to the interface

("electrostriction") reduces the difference in the total solute/water interaction energy. Each of these two effects is most pronounced in the G++ region. The diminished surface effect due to this "electrostriction" effect has consequences for many other solute properties.[23]

We next summarize the results for the spectral width of all the transitions at all locations. Assuming the spectral line shapes are Gaussians, Eqs. 6.3 and 6.4 show that the spectral line width for the $Q_i \rightarrow Q_f$ transition is given by:

$$\delta = (Q_f - Q_i)\sqrt{\langle \Gamma^2(\vec{r})\rangle_i - \langle \Gamma(\vec{r})\rangle_i^2} \tag{6.7}$$

Given δ_s and δ_b, the width of the spectrum when the solute is at some interface location and in the bulk, respectively, we are interested in the relative change in width:

$$\frac{\delta_s - \delta_b}{\delta_b} = \frac{\sqrt{\langle \Gamma_s^2(\vec{r})\rangle_i - \langle \Gamma_s(\vec{r})\rangle_i^2}}{\sqrt{\langle \Gamma_b^2(\vec{r})\rangle_i - \langle \Gamma_b(\vec{r})\rangle_i^2}} - 1 \tag{6.8}$$

where Γ_s and Γ_b are defined in Eq. 6.2 and calculated when the solute's center of mass is located at the surface and in the bulk, respectively. Note that the expression in Eq. 6.8 is independent of the final electronic state. A negative value of this quantity corresponds to spectral narrowing relative to the bulk. Figure 6.4 shows that the example discussed earlier reflects the general case: there is a significant narrowing for most transitions, especially those that correspond to an initial state with a small dipole. Initial states with large dipoles do not have much change in the spectral width (for transitions to any final state). This reflects the

relatively small change in the local environment of such a solute when it is moved from the bulk to the interface. We conclude that if there is any broadening due to an increase in the heterogeneity of the local solute environment, it is smaller than the narrowing expected from the reduced polarity (according to linear response). Experimental observations of broader surface spectra in *the same solvent* could be due to the sampling of a wider region. In this case, the superposition of spectra with significantly different peak positions could produce a broad spectrum. This is demonstrated in the bottom panel of Figure 6.4.

It is worth noting that the "heterogeneity in the local environment" mentioned above is expected to increase at the interface due to the rapid variation in the intermolecular interactions along the interface normal, as well as the dependence of these interactions on the solute orientation. While in the bulk the average intermolecular potential experienced by the solute is orientation-independent, this is not so at the interface. The dependence of the degree of heterogeneity on the solute dipole will increase the asymmetry in the effective angle-dependent potential experienced by the solute, but at the same time will likely limit the range of observed orientations around the most likely solute surface orientation.

Finally, we consider electronic transitions that involve a change in the solute polarizability. We model these transitions by increasing the value of the parameter ϵ in the Lennard-Jones potential energy function of the excited electronic state by a factor of two. The energy differences corresponding to this change are significantly

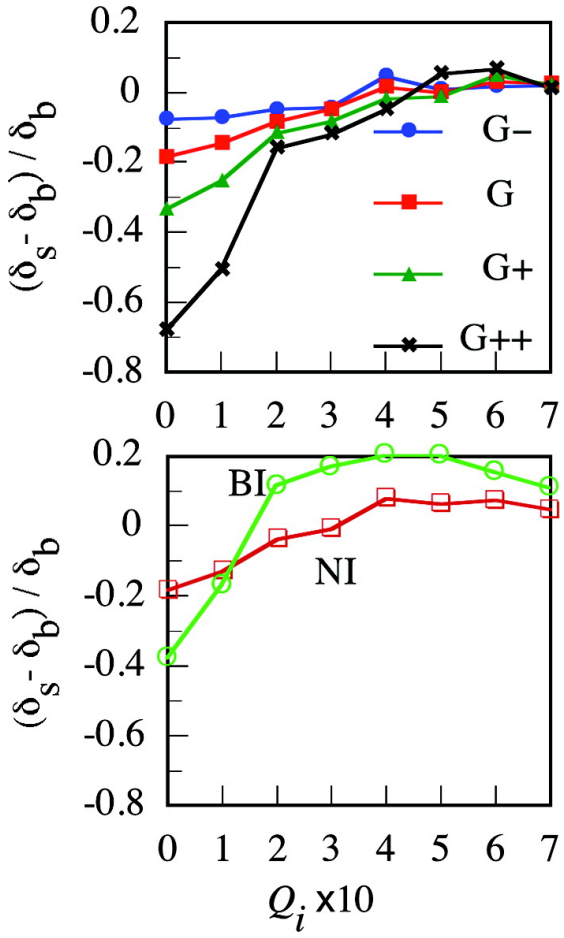

Figure 6.4: The change in the spectral width of the electronic transition at the interface relative to the bulk versus the initial solute charge. The top panel shows the results at different surface locations, and the bottom panel shows results at two composite interface regions, as defined in the text.

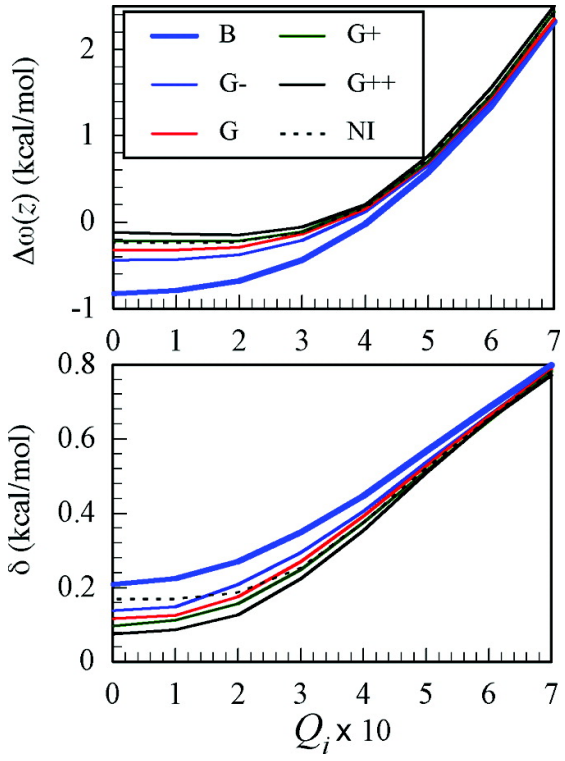

Figure 6.5: Top panel: The spectral shift $\Delta\omega(z)$ versus the (fixed) solute charge for all solute surface locations (as indicated) for a solute undergoing a change in the electronic polarizability. Bottom panel: The corresponding spectral width.

smaller than those that involve a change in the permanent dipole moment, so we limit our discussion of the effect on the spectral width to the case where there is no change in the dipole moment, $Q_i = Q_f$. From Eqs. 6.3 and 6.4 we note that for this case

$$\Delta\omega(z) = (\sqrt{\epsilon_f} - \sqrt{\epsilon_i})\,[\langle\Omega_z(\vec{r})\rangle_i] \tag{6.9}$$

where $\Omega_z(\vec{r})$ is given by the first term in Eq. 6.2, calculated when the solute center of mass is located in a slab centered at the location z along the interface normal. Note that the quantity inside the square brackets of Eq. 6.9 is proportional to

the average Lennard-Jones contribution to the total solvent–solute interaction energy in the initial state: $\langle \Omega_z(\vec{r}) \rangle_i = \langle U_i^{\mathrm{LJ}}(\vec{r}) \rangle_i / (\epsilon_i)^{1/2}$. From this expression, we see that $\langle \Omega_z(\vec{r}) \rangle$ is negative if the solute–solvent configurations are mostly near the minimum of the Lennard-Jones potential. This is the case when the Coulomb interactions in the initial state are weak (a small value of Q_i). However, for a large Q_i, the strong electrostatic attractions put the most probable solvent–solute distance on the repulsive side of the Lennard-Jones potential, and $\langle \Omega_z(\vec{r}) \rangle$ becomes positive and increases as Q_i increases.

Figure 6.5 summarizes the results. The top panel shows that for small values of the initial solute charge, the spectral shift relative to the gas phase is negative and gets smaller in value as the solute is moved from the bulk to the interface. As the initial charge Q_i increases, the shift becomes positive, consistent with the above discussion regarding the sign of the quantity $\langle \Omega_z(\vec{r}) \rangle$. As the solute is transferred from the bulk to the interface, the number of nearest neighbors is reduced due to the lower density, which makes $\langle |\Omega_z(\vec{r})| \rangle$ smaller. However, this effect is diminished as Q_i increases, since the solute's ability to keep the local solute hydration shell intact increases.

The bottom panel shows the width of the spectra versus Q_i in all the regions. The increase in width with increasing value of Q_i suggests an increase in the degree of fluctuations in the local hydration shell. This does not represent an increase in heterogeneity but rather the fact that fluctuations in the solute–water distance

around the equilibrium value result in larger energy fluctuations when the when the equilibrium distance is located on the repulsive side of the Lennard-Jones potential. For a given value of Q_i, the spectral width decreases as the solute is moved from the bulk to the surface because of the decrease in the number of water molecules in the solute hydration shell. Again, this effect diminishes when Q_i increases because of the tightening of the hydration shell.

We conclude that transitions involving a change in solute polarizability at a fixed permanent solute dipole give rise to a spectral narrowing when comparing bulk and surface spectra, although the effect is small and gets smaller when the size of the solute dipole increases. However, as in the case of transitions that involve a change in the solute dipole, some broadening is expected when the solute is allowed to explore a wider surface region. This gives rise to some broadening, but it is still narrower than the spectral width in the bulk.

6.5 Conclusions

Our model calculations suggest that three factors contribute to the difference between the bulk and interface electronic spectral line width of a chromophore undergoing a change in its permanent dipole moment: local solvation shell heterogeneity, polarity of the interface region, and the width of the surface region accessible to the solute. The local solute environment is more heterogeneous at

the interface, which leads to spectral broadening. However, the reduced polarity of the interface region leads to a spectral narrowing, which typically is more pronounced. This leads to overall narrowing when the spectrum of the solute in the bulk is compared with the spectrum taken when the solute is restricted to a narrow surface slab. The spectrum obtained when several surface slabs contribute to the electronic transition is wider. The dependence of the spectral shift and width on the initial solute charge can be understood by invoking the idea that the structure of the solute hydration shell at the interface more resembles that in the bulk as the solute charge is increased.

Acknowledgments

This work was supported by the National Science Foundation (Grant CHE-0809164).

Conclusion

We modeled the benchmark symmetric S_N2 reaction $Cl^- + CH_3Cl \longrightarrow CH_3Cl + Cl^-$ using the empirical valence bond model with a fully-molecular solvent description in bulk liquid and at liquid–liquid and liquid–vapor interfaces. In each case, the reactivity of the S_N2 system is highly sensitive to the presence of a few water molecules due to the water's stabilization of the reactants/products relative to the transition state. This water caging of the Cl^- nucleophile inhibits the reactivity of the S_N2 system. In each solvent environment examined, water molecules change the reagents' electronic structure and other structural and energetic properties along the reaction coordinate.

In bulk chloroform, the addition of one to five water molecules changes the electronic structure along the reaction coordinate. The hydration shell around the reacting system becomes highly asymmetrical as soon as the reaction moves away from the transition state, with the water molecules found around the charged nucleophile/leaving group. Corrections to the rate constant, due to recrossings

of the activation energy barrier, compared with the transition state theory rate constant (k_{TST}), fall between the behavior calculated in bulk water and bulk chloroform.

As we saw in the previous water-polluted bulk chloroform study, at the chloroform–water interface a small number of water molecules is able to stabilize the reactants relative to the transition state, thereby disrupting the rate enhancement that would otherwise be found in the bulk chloroform phase. At the chloroform–water interface the $Cl^- + CH_3Cl$ reaction is sensitive to both the reactants' location and orientation relative to the interface. The activation energy barrier is slightly higher a few angstroms into the organic phase than it is at the Gibbs surface or in bulk water. By comparing the reaction to that at an interface constrained to be flat (removing surface roughness), we confirmed that interfacial water molecules reduce the S_N2 system's reactivity, as the nucleophile is able to keep part of its hydration shell at the unconstrained interface. For true rate enhancement, as expected in chloroform, the reaction must be carried out mostly away from the interface region. As before, deviations from k_{TST} due to barrier recrossings are small and mostly fall between those in bulk water and bulk chloroform.

In water clusters made up of from 3 to 40 water molecules, different properties of the system converge to the values of bulk water at different rates. The activation free energy and dynamical correction to k_{TST} reach about 90% of the values in bulk water for clusters made up of 12 to 15 water molecules. The rate of change

of the solute charge distribution at the transition state converges more rapidly, in clusters as small as 10 water molecules. Deviations from the k_{TST} are small and mostly less than those in bulk water.

The addition of a tetramethylammonium cation TMA^+ phase transfer catalyst to the $\mathrm{Cl}^- + \mathrm{CH_3Cl} \longrightarrow \mathrm{CH_3Cl} + \mathrm{Cl}^-$ reaction at the water–chloroform interface moderately *increases* the barrier height of the reaction when the Cl^- nucleophile forms an ion pair with the TMA^+. This effect is most pronounced when the number of nearby water molecules is low, such as in bulk chloroform or far into the bulk chloroform phase away from the interface. The presence of the TMA^+ also slightly increases the deviation from k_{TST} by increasing the the rate of trajectories recrossing the activation energy barrier. In order for the TMA^+ to act as an effective catalyst, its role is best limited to bringing the nucleophile deep into the organic phase with a minimum of associated water molecules. The reaction rate may be further enhanced by choosing a phase transfer catalyst that forms a weaker ion pair with the nucleophile, allowing the nucleophile to dissociate more easily in the organic phase.

At the water liquid–vapor interface the activation free energy of the $\mathrm{Cl}^- + \mathrm{CH_3Cl}$ reaction is slightly *larger* than in bulk water. This is the opposite of the effect expected when one takes into account the lower average polarity of the water surface relative to the bulk. In the reactants' state, the Cl^- nucleophile is oriented towards the bulk water phase and water molecules cluster around it. This

results in greater than expected hydration of the reacting system. These results are expected to be generalizable to other reactions with an asymmetric charge distribution, although our results were obtained with potential energy surfaces that were fitted to gas phase and bulk data. This is a common practice, but additional testing of this method would be appropriate.

We generated electronic absorbance spectra of a series of differently-charged model dipolar chromophores adsorbed at different locations of the water–air interface and undergoing a change in their permanent dipole moments. Our results indicate that three competing factors contribute to the electronic spectral line width, resulting in a difference between spectra obtained in the bulk and at the interface. These factors are: increased heterogeneity of the local solvation shell, which broadens the spectrum; decreased polarity of the interface region, which results in spectral narrowing; and the depth of the surface region accessible to the solute—the more slabs of the interface included in the spectrum, the broader the spectrum. The spectral shift and width also depend on the initial solute charge, due to increasingly bulk-like hydration of more highly charged molecules.

Bibliography

[1] Hans Ågren and Kurt V. Mikkelsen. Theory of solvent effects on electronic spectra. *J. Mol. Struct. (THEOCHEM)*, 234:425, 1991.

[2] M. Aguilar, R. Bianco, S. Miertus, M. Persico, and J. Tomasi. Chemical reactions in solution: modelling of the delay of solvent synchronism (dielectric friction) along the reaction path of an S_N2 reaction. *Chem. Phys.*, 174:397, 1993.

[3] D. Albanese. Liquid–liquid phase transfer catalysis: Basic principles and synthetic applications. *Catal. Rev. - Sci. Eng.*, 45:369, 2003.

[4] D. Albanese, D. Landini, A. Maia, and M. Penso. Key role of water for nucleophilic substitutions in phase-transfer-catalyzed processes: A mini-review. *Ind. Eng. Chem. Res.*, 40:2396, 2001.

[5] M. P. Allen and D. J. Tildesley. *Computer Simulation of Liquids*. Clarendon, Oxford, 1987.

[6] G. I. Almerindo and J. R. Pliego. Rate acceleration of S_N2 reactions through selective solvation of the transition state. *Chem. Phys. Lett.*, 423:459, 2006.

[7] J. Aqvist and A. Warshel. Simulation of enzyme reactions using valence bond force fields and other hybrid quantum/classical approaches. *Chem. Rev.*, 93:2523, 1993.

[8] J. S. Bader and B. J. Berne. Solvation energies and electronic spectra in polar, polarizable media: Simulation tests of dielectric continuum theory. *J. Chem. Phys.*, 104:1293, 1996.

[9] P. B. Balbuena, K. P. Johnston, and P. J. Rossky. Molecular simulation of a chemical reaction in supercritical water. *J. Am. Chem. Soc.*, 116:2698, 1994.

[10] P. B. Balbuena, K. P. Johnston, and P. J. Rossky. Computer simulation study of an S_N2 reaction in supercritical water. *J. Phys. Chem.*, 99:1554, 1995.

[11] I. Benjamin. *Molecular dynamics methods for studying liquid interfacial phenomena. In Modern Methods for Multidimensional Dynamics Computations in Chemistry*, page 101. World Scientific, Singapore, 1988.

[12] I. Benjamin. Vibrational spectrum of water at the liquid/vapor interface. *Phys. Rev. Lett.*, 73:2083, 1994.

[13] I. Benjamin. Photodissociation of ICN in liquid chloroform: Molecular dynamics of ground and excited state recombination, cage escape, and hydrogen abstraction reaction. *J. Chem. Phys.*, 103:2459, 1995.

[14] I. Benjamin. Theory and computer simulations of solvation and chemical reactions at liquid interfaces. *Acc. Chem. Res.*, 28:233, 1995.

[15] I. Benjamin. Chemical reactions and solvation at liquid interfaces: A microscopic perspective. *Chem. Rev.*, 96:1449, 1996.

[16] I. Benjamin. *Molecular dynamics simulations in interfacial electrochemistry. In Modern Aspects of Electrochemistry*, volume 31, page 115. Plenum Press, New York, 1997.

[17] I. Benjamin. Molecular structure and dynamics at liquid-liquid interfaces. *Annu. Rev. Phys. Chem.*, 48:407, 1997.

[18] I. Benjamin. Solvent effects on electronic spectra at liquid interfaces. A continuum electrostatic model. *J. Phys. Chem. A*, 102:9500, 1998.

[19] I. Benjamin. Polarity of the water/octanol interface. *Chem. Phys. Lett.*, 393:453, 2004.

[20] I. Benjamin. Static and dynamic electronic spectroscopy at liquid interfaces. *Chem. Rev.*, 106:1212, 2006.

[21] I. Benjamin. Empirical valence bond model of an S_N2 reaction in polar and nonpolar solvents. *J. Chem. Phys.*, 129:74508, 2008.

[22] I. Benjamin. Structure and dynamics of hydrated ions in a water-immiscible organic solvent. *J. Phys. Chem. B*, 112:15801, 2008.

[23] I. Benjamin. Solute dynamics at aqueous interfaces. *Chem. Phys. Lett.*, 469:229, 2009.

[24] I. Benjamin. Inhomogeneous broadening of electronic spectra at liquid interfaces. *J. Chem. Phys.*, 515:45, 2011.

[25] G. E. Bennett, P. J. Rossky, and K. P. Johnston. Continuum electrostatics model for an S_N2 reaction in supercritical water. *J. Phys. Chem.*, 99:16136, 1995.

[26] H. J. C. Berendsen, J. P. M. Postma, W. F. V. Gunsteren, J. Hermans, and B. Pullman. *Intermolecular Forces*, page 331. Dordrecht, The Netherlands, 1981.

[27] J. P. Bergsma, B. J. Gertner, K. R. Wilson, and J. T. Hynes. Molecular dynamics of a model S_N2 reaction in water. *J. Chem. Phys.*, 86:1356, 1987.

[28] B. J. Berne, M. Borkovec, and J. E. Straub. Classical and modern methods in reaction rate theory. *J. Phys. Chem.*, 92:3711, 1988.

[29] R. Bianco, S. Miertus, M. Persico, and J. Tomasi. Molecular reactivity in solution. Modelling of the effects of the solvent and of its stochastic fluctuation on an S_N2 reaction. *Chem. Phys.*, 168:281, 1992.

[30] P. Bisson, H. Xiao, M. Kuo, N. Kamelamela, and M. J. Shultz. Ions and hydrogen bonding in a hydrophobic environment: CCl_4. *J. Phys. Chem. A*, 114:4051, 2010.

[31] D. K. Bohme and A. B. Raksit. Gas-phase measurements of the influence of stepwise solvation on the kinetics of S_N2 reactions of solvated F^- with CH_3Cl and CH_3Br and of solvated Cl^- with CH_3Br. *Can. J. Chem.*, 63:3007, 1985.

[32] E. A. Carter and J. T. Hynes. Solvation dynamics for an ion pair in a polar solvent: Time-dependent fluorescence and photochemical charge transfer. *J. Chem. Phys.*, 94:5961, 1991.

[33] A. W. Castleman. Recent advances in cluster science. *European Journal of Mass Spectrometry*, 13:7, 2007.

[34] E. Chacón, P. Tarazona, and J. Alejandre. The intrinsic structure of the water surface. *J. Chem. Phys.*, 125:014709, 2006.

[35] A. Chanda and V.V. Fokin. Organic synthesis "on water". *Chem. Rev.*, 109:725, 2009.

[36] D. Chandler. *Introduction to Modern Statistical Mechanics*. Oxford University Press,, Oxford, 1987.

[37] D. Chandler, K. S. Schweizer, and P. G. Wolynes. Electronic states of a topologically disordered system: Exact solution of the mean spherical model for liquids. *Phys. Rev. Lett.*, 49:1100, 1982.

[38] J. Chandrasekhar, S. F. Smith, and W. L. Jorgensen. S_N2 reaction profiles in the gas phase and aqueous solution. *J. Am. Chem. Soc.*, 106:3049, 1984.

[39] T. M. Chang and L. X. Dang. Ion solvation in polarizable chloroform: A molecular dynamics study. *J. Phys. Chem. B*, 101:10518, 1997.

[40] T. M. Chang, L. X. Dang, and K. A. Peterson. Computer simulation of chloroform with a polarizable potential model. *J. Phys. Chem. B*, 101:3413, 1997.

[41] Y. C. Chen, J. L. Lebowitz, and P. Nielaba. Line shifts and broadenings in polarizable liquids. *J. Chem. Phys.*, 91:340, 1989.

[42] Y. J. Cho, S. R. Vandelinde, L. Zhu, and W. L. Hase. Trajectory studies of S_N2 nucleophilic substitution. II. Nonstatistical central barrier recrossing in the $Cl^- + CH_3Cl$ system. *J. Chem. Phys.*, 96:8275, 1992.

[43] A. Converso, P. L. Saaidi, K. B. Sharpless, and M. G. Finn. Nucleophilic substitution by Grignard reagents on sulfur mustards. *J. Org. Chem.*, 69:7336, 2004.

[44] P. G. Cozzi and L. Zoli. A rational approach towards the nucleophilic substitutions of alcohols "on water". *Angew. Chem.*, 47:4162, 2008.

[45] L. X. Dang and T. Chang. Molecular mechanism of ion binding to the liquid/vapor interface of water. *J. Phys. Chem. B*, 106:235, 2002.

[46] T. E. Dermota, Q. Zhong, and A. W. Castleman. Ultrafast dynamics in cluster systems. *Chem. Rev.*, 104:1861, 2004.

[47] C. A. Eckert, C. L. Liotta, D. Bush, J. S. Brown, and J. P. Hallett. Sustainable reactions in tunable solvents. *J. Phys. Chem. B*, 108:18108, 2004.

[48] K. B. Eisenthal. Liquid interfaces probed by second-harmonic and sum-frequency spectroscopy. *Chem. Rev.*, 96:1343, 1996.

[49] L. W. Flanagin, P. B. Balbuena, K. P. Johnston, and P. J. Rossky. Temperature and density effects on an S_N2 reaction in supercritical water. *J. Phys. Chem.*, 99:5196, 195.

[50] J. L. Gao. *A priori* computation of a solvent-enhanced S_N2 reaction profile in water: The Menshutkin reaction. *J. Am. Chem. Soc.*, 113:7796, 1991.

[51] B. J. Gertner, J. P. Bergsma, K. R. Wilson, S. Lee, and J. T. Hynes. Nonadiabatic solvation model for S_N2 reactions in polar solvents. *J. Chem. Phys.*, 86:1377, 1987.

[52] B. J. Gertner, K. R. Wilson, and J. T. Hynes. Nonequilibrium solvation effects on reaction rates for model S_N2 reactions in water. *J. Chem. Phys.*, 90:3537, 1989.

[53] S. Gonzalez-Lafont and D. G. Truhlar. *Chemical Reactions in Clusters*, page 3. Oxford University Press, Oxford, 1996.

[54] J.P. Hansen and I. R. McDonald. *Theory of Simple Liquids*. Academic, London, 2nd edition, 1986.

[55] K. Harper, B. Minofar, M. R. Sierra-Hernandez, N. N. Casillas-Ituarte, M. Roeselova, and H. C. Allen. Surface residence and uptake of methyl chloride and methyl alcohol at the air/water interface studied by vibrational sum frequency spectroscopy and molecular dynamics. *J. Phys. Chem. A*, 113:2015, 2009.

[56] J. M. Hayes and S. M. Bachrach. Effect of micro and bulk solvation on the mechanism of nucleophilic substitution at sulfur in disulfides. *J. Phys. Chem. A*, 107:7952, 2003.

[57] D. K. Hore, D. S. Walker, L. MacKinnon, and G. L. Richmond. Molecular structure of the chloroform - water and dichloromethane - water interfaces. *J. Phys. Chem. C*, 111:8832, 2007.

[58] W. P. Hu and D. G. Truhlar. Modeling transition state solvation at the single-molecule level: Test of correlated *ab initio* predictions against experiment for the gas-phase S_N2 reaction of microhydrated fluoride with methyl chloride. *J. Am. Chem. Soc.*, 116:7797, 1994.

[59] S. E. Huston, P. J. Rossky, and D. A. Zichi. Hydration effects on S_N2 reactions: an integral equation study of free energy surfaces and corrections to transition-state theory. *J. Am. Chem. Soc.*, 111:5680, 1989.

[60] J.K. Hwang, G. King, S. Creighton, and A. Warshel. Simulation of free energy relationships and dynamics of S_N2 reactions in aqueous solution. *J. Am. Chem. Soc.*, 110:5297, 1988.

[61] J. T. Hynes. *The Theory of Chemical Reactions*, volume 4, page 171. CRC, Boca Raton, FL, 1985.

[62] C. K. Ingold. *Structure and Mechanism in Organic Chemistry, 2nd ed.* Cornell University, Ithaca, NY, 2nd edition, 1969.

[63] M. Jorge and M. N. D. S. Cordeiro. Intrinsic structure and dynamics of the water/nitrobenzene interface. *J. Phys. Chem. C*, 111:17612, 2007.

[64] W. L. Jorgensen and J. K. Buckner. Effect of hydration on the structure of an S_N2 transition state. *J. Phys. Chem.*, 90:4651, 1986.

[65] Y. Jung and R. A. Marcus. Protruding interfacial OH groups and 'on-water' heterogeneous catalysis. *J. Phys.: Condens. Matter*, 22:284117, 2010.

[66] Y.S. Jung and R.A. Marcus. On the theory of organic catalysis "on water". *J. Am. Chem. Soc.*, 129:5492, 2007.

[67] M. J. Kamlet, J. L. Abboud, and R. W. Taft. An examination of linear solvation energy relationships. In *Progress in Physical Organic Chemistry*, volume 13, page 485, New York, 1981. Wiley.

[68] H. J. Kim and J. T. Hynes. Equilibrium and nonequilibrium solvation and solute electronic structure. I. Formulation. *J. Chem. Phys.*, 93:5194, 1990.

[69] H. J. Kim and J. T. Hynes. Equilibrium and nonequilibrium solvation and solute electronic structure. II. Strong coupling limit. *J. Chem. Phys.*, 93:5211, 1990.

[70] Y. Kim, C. J. Cramer, and D. G. Truhlar. Steric effects and solvent effects on S_N2 reactions. *J. Phys. Chem. A*, 113:9109, 2009.

[71] G. King and A. Warshel. Investigation of the free energy functions for electron transfer reactions. *J. Chem. Phys.*, 93:8682, 1990.

[72] J. E. Klijn and J. B. F. N. Engberts. Organic chemistry: Fast reactions 'on water'. *Nature*, 435:746, 2005.

[73] J. E. Klijn and J. B. F. N. Engberts. Vesicular catalysis of an S_N2 reaction: Toward understanding the influence of glycolipids on reactions proceeding at the interface of biological membranes. *Langmuir*, 21:9809, 2005.

[74] R. Kubo. Generalized cumulant expansion method. *J. Phys. Soc. Jpn*, page 1100, 1962.

[75] D. Landini and A. Maia. Phase transfer catalysis (PTC): Search for alternative organic solvents, even environmentally benign. *J. Mol. Catal. A: Chem.*, 204:235, 2003.

[76] D. Landini, A. Maia, and A. Rampoldi. Dramatic effect of the specific solvation on the reactivity of quaternary ammonium fluorides and poly(hydrogen fluorides), $(HF)_n \cdot F^-$, in media of low polarity. *J. Org. Chem.*, 54:328, 1989.

[77] C. Laurence, P. Nicolet, M. T. Dalati, J. M. Abboud, and R. Notario. The empirical treatment of solvent-solute interactions: 15 years of π. *J. Phys. Chem.*, 98:5807, 1994.

[78] R. F. Loring. Statistical mechanical calculation of inhomogeneously broadened absorption line shapes in solution. *J. Phys. Chem.*, 94:513, 1990.

[79] A. Maia. Anion activation by quaternary onium salts and polyether ligands in homogeneous and heterogeneous systems. *Pure Appl. Chem.*, 67:697, 1995.

[80] M. Makosza. Phase-transfer catalysis. A general green methodology in organic synthesis. *Pure Appl. Chem.*, 72:1399, 2000.

[81] R. A. Marcus. On the theory of shifts and broadening of electronic spectra of polar solutes in polar media. *J. Chem. Phys.*, 43:1261, 1965.

[82] N. Mataga and T. Kubota. *Molecular Interactions and Electronic Spectra.* Dekker, New York, 1970.

[83] J. R. Mathis, R. Bianco, and J. T. Hynes. On the activation free energy of the $Cl^- + CH_3Cl$ S_N2 reaction in solution. *J. Mol. Liq.*, 61:81, 1994.

[84] D. V. Matyushov, R. Schmid, and B. M. Ladanyi. A thermodynamic analysis of the π^* and $E_T(30)$ polarity scales. *J. Phys. Chem. B*, 101:1035, 1997.

[85] A. L. McClellan. *Tables of Experimental Dipole Moments.* Freeman, San Francisco, 1963.

[86] J.M. Mestdagh, M.A. Gaveau, C. Gee, O. Sublemontier, and J.P. Visticot. Cluster isolated chemical reactions. *Rev. Phys. Chem*, 16:215, 1997.

[87] D. Michael and I. Benjamin. Electronic spectra of dipolar solutes at liquid/liquid interfaces: Effect of interface structure and polarity. *J. Chem. Phys.*, 107:5684, 1997.

[88] D. Michael and I. Benjamin. Structure, dynamics, and electronic spectrum of n,n′-diethyl-p-nitroaniline at water interfaces. A molecular dynamics study. *J. Phys. Chem. B*, 102:5145, 1998.

[89] D. Michael and I. Benjamin. Molecular dynamics computer simulations of solvation dynamics at liquid/liquid interfaces. *J. Chem. Phys.*, 114:2817, 2001.

[90] L. S. P. Mirashi and S. S. Kunte. Solvent effects on electronic absorption spectra of nitrochlorobenzenes, nitrophenols and nitroanilines — lll.* Excited state dipole moments and specific solute–solvent interaction energies employing Bakhshiev's approach. *Spectrochimica Acta*, 45:1147, 1989.

[91] A. A. Mohamed and F. Jensen. Steric effects in S_N2 reactions. The influence of microsolvation. *J. Phys. Chem. A*, 105:3259, 2001.

[92] S. K. Mondal, S. Yamaguchi, and T. Tahara. Molecules at the air/water interface experience a more inhomogeneous solvation environment than in bulk solvents: A quantitative band shape analysis of interfacial electronic spectra obtained by HD-ESFG. *J. Phys. Chem. C*, 115:3083, 2011.

[93] R. S. Mulliken, C. A. Rieke, D. Orloff, and H. Orloff. Formulas and numerical tables for overlap integrals. *J. Chem. Phys.*, 17:1248, 1949.

[94] I. Nadler, D. Mahgerefteh, H. Reisler, and C. Wittig. The 266 nm photolysis of ICN: Recoil velocity anisotropies and nascent E,V,R,T excitations for the $CN + I(^2P_{3/2})$ and $CN + I(^2P_{1/2})$ channels. *J. Chem. Phys.*, 82:3885, 1985.

[95] S. D. Naik and L. K. Doraiswamy. Phase transfer catalysis: Chemistry and engineering. *AIChE J.*, 44:612, 1998.

[96] S. Narayan, J. Muldoon, M. G. Finn, V. V. Fokin, H. C. Kolb, and K. B. Sharpless. "On water": Unique reactivity of organic compounds in aqueous suspension. *Angew. Chem.*, 44:3275, 2005.

[97] K. V. Nelson and I. Benjamin. Microhydration effects on a model S_N2 reaction in a nonpolar solvent. *J. Chem. Phys.*, 130:194502, 2009.

[98] K. V. Nelson and I. Benjamin. A molecular dynamics–empirical valence bond study of an S_N2 reaction at the water/chloroform interface. *J. Phys. Chem. C*, 114:1154, 2010.

[99] K. V. Nelson and I. Benjamin. A molecular dynamics/EVB study of an S_N2 reaction in water clusters. *Chem. Phys. Lett.*, 492:220, 2010.

[100] K. V. Nelson and I. Benjamin. Effect of a phase transfer catalyst on the dynamics of an S_N2 reaction. A molecular dynamics study. *J. Phys. Chem. C*, 115:2290, 2011.

[101] K. V. Nelson and I. Benjamin. A model S_N2 reaction 'on water' does not show rate enhancement. *Chem. Phys. Lett.*, 508:59, 2011.

[102] K. V. Nelson and I. Benjamin. Electronic absorption line shapes at the water liquid/vapor interface. *J. Phys. Chem. B*, 116:4286, 2012.

[103] D. Nicholson and N. G. Parsonage. *Computer Simulation and the Statistical Mechanics of Adsorption*. Academic Press, New York, 1982.

[104] S. Nosé. Constant-temperature molecular dynamics. *J. Phys.: Condens. Matter*, 2:SA115, 1990.

[105] Y. Okuno. Microscopic description of nonadiabatic, nonequilibrium, and equilibrium solvations for solvated cluster reactions: $(H_2O)_nCl^- + CH_3Cl \rightarrow ClCH_3 + Cl^-(H_2O)_n$. *J. Chem. Phys.*, 105:5817, 1996.

[106] M. H. M. Olsson and A. Warshel. Solute solvent dynamics and energetics in enzyme catalysis: The S_N2 reaction of dehalogenase as a general benchmark. *J. Am. Chem. Soc.*, 126:15167, 2004.

[107] J. R. Pliego. First solvation shell effects on ionic chemical reactions: New insights for supramolecular catalysis. *J. Phys. Chem. B*, 113:505, 2009.

[108] C. S. Pomelli and J. Tomasi. *Ab initio* study of the S_N2 reaction $CH_3Cl + Cl^- \rightarrow Cl^- + CH_3Cl$ in supercritical water with the polarizable continuum model. *J. Phys. Chem. A*, 101:3561, 1997.

[109] Mario Re and Daniel Laria. Solvation effects on a model S_N2 reaction in water clusters. *J. Chem. Phys.*, 105:4584, 1996.

[110] C. Reichardt. *Solvents and Solvent Effects in Organic Chemistry*. Springer-Verlag, Weinheim, 2nd edition, 1988.

[111] C. Reichardt. Solvatochromic dyes as solvent polarity indicators. *Chem. Rev.*, 94:2319, 1994.

[112] R. A. Relph, T. L. Guasco, B. M. Elliott, M. Z. Kamrath, A. B. McCoy, R. P. Steele, D. P. Schofield, K. D. Jordan, A. A. Viggiano, E. E. Ferguson, and M. A. Johnson. How the shape of an H-bonded network controls proton-coupled water activation in HONO formation. *Science*, 327:308, 2010.

[113] D. Rose and I. Benjamin. Free energy of transfer of hydrated ion clusters from water to an immiscible organic solvent. *J. Phys. Chem. B*, 113:9296, 2009.

[114] J. S. Rowlinson and B. Widom. *Molecular Theory of Capillarity*. Clarendon, Oxford, 1982.

[115] J. P. Ryckaert, G. Ciccotti, and H. J. C. Berendsen. Numerical integration of the cartesian equations of motion of a system with constraints: molecular dynamics of n-alkanes. *J. Comput. Phys.*, 23:327, 1977.

[116] M. Sato, H. Yamataka, Y. Komeiji, Y. Mochizuki, T. Ishikawa, and T. Nakano. How does an S_N2 reaction take place in solution? Full *ab initio* MD simulations for the hydrolysis of the methyl diazonium ion. *J. Am. Chem. Soc.*, 130:2396, 2008.

[117] K. Schweighofer and I. Benjamin. Transfer of a tetramethylammonium ion across the water-nitrobenzene interface: Potential of mean force and nonequilibrium dynamics. *J. Phys. Chem. A*, 103:10274, 1999.

[118] H. M. Sevian and J. L. Skinner. Molecular theory of transition energy correlations for pairs of chromophores in liquids or glasses. *J. Chem. Phys.*, 97:8, 1992.

[119] Y. H. Shao, M. V. Mirkin, and J. F. Rusling. Liquid/liquid interface as a model system for studying electrochemical catalysis in microemulsions. reduction of trans-1,2-dibromocyclohexane with vitamin B12. *J. Phys. Chem. B*, 101:3202, 1997.

[120] N. E. Shemetulskis and R. F. Loring. Electronic absorption spectra in a polar fluid: Theory and simulation. *J. Chem. Phys.*, 95:4756, 1991.

[121] Y. R. Shen. *The Principles of Nonlinear Optics*. Wiley, New York, 1984.

[122] A. R. Siler and R. A. Walker. Effects of solvent structure on interfacial polarity at strongly associating silica/alcohol interfaces. *J. Phys. Chem. C*, 115:9637, 2011.

[123] C. M. Starks, C. L. Liotta, and M. Halpern. *Phase Transfer Catalysis*. Chapman and Hall, New York, 1994.

[124] W. H. Steel, C. L. Beildeck, and R. A. Walker. Solvent polarity across strongly associating interfaces. *J. Phys. Chem. B*, 108:16107, 2004.

[125] W. H. Steel, Y. Y. Lau, C. L. Beildeck, and R. A. Walker. Solvent polarity across weakly associating interfaces. *J. Phys. Chem. B*, 108:13370, 2004.

[126] W. H. Steel, R. Nolan, F. Damkaci, and R. A. Walker. Molecular rulers: new families of molecules for measuring interfacial widths. *J. Am. Chem. Soc.*, 124:4824, 2002.

[127] M. D. Stephens, J. G. Saven, and J. L. Skinner. Molecular theory of electronic spectroscopy in nonpolar fluids: Ultrafast solvation dynamics and absorption and emission line shapes. *J. Chem. Phys.*, 106:2129, 1997.

[128] A. A. Tamburello-Luca, P. Hébert, R. Antoine, P. F. Brevet, and H. H. Girault. Optical surface second harmonic generation study of the two acid/base equilibria of Eosin B at the air/water interface. *Langmuir*, 13:4428, 1997.

[129] A. A. Tamburello-Luca, P. Hébert, P. F. Brevet, and H. H. Girault. Resonant-surface second-harmonic generation studies of phenol derivatives at air/water and hexane/water interfaces. *J. Chem. Soc., Faraday Trans.*, 92:3079, 1996.

[130] J. I. Timoneda and J. T. Hynes. Nonequilibrium free energy surfaces for hydrogen-bonded proton-transfer complexes in solution. *J. Phys. Chem.*, 95:10431, 1991.

[131] S. C. Tucker and D. G. Truhlar. A six-body potential energy surface for the S_N2 reaction $Cl^-_{(g)} + CH_3Cl_{(g)}$ and a variational transition-state-theory calculation of the rate constant. *J. Am. Chem. Soc.*, 112:3338, 1990.

[132] Y. Uchiyama, T. Kitamori, and T. Sawada. Role of the liquid/liquid interface in a phase-transfer catalytic reaction as investigated by *in situ* measurements using the quasi-elastic laser scattering method. *Langmuir*, 16:6597, 2000.

[133] G. Vayner and D. G. Truhlar. Steric retardation of S_N2 reactions in the gas phase and solution. *J. Am. Chem. Soc.*, 126:9054, 2004.

[134] J. Villa, J. Bentzien, A. Gonzalez-Lafont, J. M. Lluch, J. Bertran, and A. Warshel. Effective way of modeling chemical catalysis: Empirical va-

lence bond picture of role of solvent and catalyst in alkylation reactions. *J. Comput. Chem.*, 21(8):607, 2000.

[135] A. G. Volkov, editor. *Interfacial Catalysis*. Dekker, New York, 2003.

[136] R. A. Walker W. H. Steel. Measuring dipolar width across liquid–liquid interfaces with 'molecular rulers'. *Nature*, 424:296, 2003.

[137] R. A. Walker W. H. Steel. Solvent polarity at an aqueous/alkane interface: The effect of solute identity. *J. Am. Chem. Soc.*, 125:1132, 2003.

[138] H. Wang, E. Borguet, and K. B. Eisenthal. Polarity of liquid interfaces by second harmonic generation spectroscopy. *J. Phys. Chem. A*, 101:713, 1997.

[139] H. Wang, E. Borguet, and K. B. Eisenthal. Generalized interface polarity scale based on second harmonic spectroscopy. *J. Phys. Chem. B*, 102:4927, 1998.

[140] A. Warshel. *Computer Modeling of Chemical Reactions in Enzymes and Solutions*. Wiley-Interscience, New York, 1997.

[141] A. Warshel and R. M. Weiss. An empirical valence bond approach for comparing reactions in solutions and in enzymes. *J. Am. Chem. Soc.*, 102:6218, 1980.

[142] R. M. Whitnell and K. R. Wilson. *Reviews in Computational Chemistry*. VCH, New York, 1993.

[143] C. T. Williams and David A. Beattie. Probing buried interfaces with non-linear optical spectroscopy. *Surface Science*, 500:545, 2002.

[144] X. Zhang, O Esenturk, and R. A. Walker. Reduced polarity in protic solvents near hydrophobic solid surfaces. *J. Am. Chem. Soc.*, 123:10768, 2001.

[145] X. Zhang, W. H. Steel, and R. A. Walker. Probing solvent polarity across strongly associating solid/liquid interfaces using molecular rulers. *J. Phys. Chem. B*, 107:3829, 2003.

[146] X. G. Zhao, D. H. Lu, Y. P. Liu, G. C. Lynch, and D. G Truhlar. Use of an improved ion–solvent potential-energy function to calculate the reaction rate and α-deuterium and microsolvation kinetic isotope effects for the gas-phase S_N2 reaction of $Cl^-(H_2O)$ with CH_3Cl. *J. Chem. Phys.*, 97:6369, 1992.

[147] X. G. Zhao, S. C. Tucker, and D. G. Truhlar. Solvent and secondary kinetic isotope effects for the microhydrated S_N2 reaction of $Cl^-(H_2O)_n$ with CH_3Cl. *J. Am. Chem. Soc.*, 113:826, 1991.

[148] D. Zimdars and K. B. Eisenthal. Static and dynamic solvation at the air/water interface. *J. Phys. Chem. B*, 105:3993, 2001.